UNIVERSITAT POLITÈCNICA DE VALÈNCIA
I.U.I. CMT - CLEAN MOBILITY & THERMOFLUIDS
PhD pogram in Propulsion Systems for Transport

DOCTORAL THESIS

EVALUATION OF HYDROGEN AS A CARBON-FREE FUEL FOR INTERNAL COMBUSTION ENGINES

UNIVERSITAT
POLITÈCNICA
DE VALÈNCIA

PRESENTED BY

D. Miguel Olcina Girona

SUPERVISED BY

Dr. D. Santiago Alberto Molina Alcaide
Dr. D. Josep Gómez Soriano

FOR THE DEGREE OF

Doctor of Philosophy

MAY 2025

DOCTORAL THESIS

"Evaluation of hydrogen as a carbon-free fuel for internal combustion engines"

Presented by: D. Miguel Olcina Girona
Supervised by: Dr. D. Santiago Alberto Molina Alcaide
Dr. D. Josep Gómez Soriano

THESIS EXAMINERS

Dr. D. Octavio Armas Vergel
Dr. D.ª Blanca Giménez Olavarría

DEFENSE COMITEE

Chairman: Dr. D. Raúl Payri Marín
Secretary: Dr. D. Octavio Armas Vergel
Member: Dr. D.ª Blanca Giménez Olavarría

Valencia, May 2025

A Carmen de la Caridad Bó Nicolás
Murcia, 1926-2024

Abstract

It has been demonstrated that human activities, particularly those responsible for generating greenhouse gases, have caused a rapid increase in global temperatures over the past 200 years. Currently, the Earth's average temperature is 1.1°C higher than during the pre-industrial era, and the last decade has been the warmest on record. Climate change not only results in higher temperatures but also disrupts the planet's balance, leading to droughts, water scarcity, wildfires, rising sea levels, flooding, polar ice melting, extreme storms, and biodiversity loss.

In this context, addressing climate change requires the decarbonization of human activities that emit greenhouse gases, particularly those involving the combustion of fossil fuels such as coal, oil, and gas. Key contributors to these emissions include energy production, industrial processes, transportation, agriculture, land use, and deforestation.

Within road transportation, various alternatives have emerged to reduce dependency on conventional fossil fuels such as gasoline and diesel. Among these options, hydrogen has gained prominence as a carbon-free energy carrier, attracting significant interest for its applications in transportation and industrial processes.

The main goal of this thesis is to study the application of hydrogen in alternative internal combustion engines. Specifically, this research aims to explore the transition to a hydrogen economy by analyzing its effects on propulsion systems and global emissions, as well as investigating different hydrogen injection systems and their impact on the fuel-air mixing process.

The first step in studying the transition to hydrogen involved characterizing the process across various time stages, each defined by the specific availability of green hydrogen. This step was crucial, as the primary goal of implementing hydrogen is to reduce greenhouse gas emissions while avoiding scenarios in which emissions are comparable to or exceed those of fossil fuels. Each stage was characterized by different blends of fossil fuels

and hydrogen, simulating a realistic transition based on available infrastructure. The research included experimental tests with compressed natural gas (CNG) and hydrogen mixtures, as well as simulations to evaluate the impacts of this transition.

Finally, different hydrogen injection configurations were analyzed to assess their influence on combustion dynamics and the efficiency of the fuel-air mixing process. The results provide a comprehensive perspective on the integration of hydrogen into internal combustion engine technologies, offering critical insights to facilitate an efficient and sustainable energy transition.

Resumen

Se ha demostrado que las actividades humanas, responsables de generar gases de efecto invernadero, han causado el rápido aumento de la temperatura global en los últimos 200 años. Actualmente, la temperatura media de la Tierra es 1,1°C más alta que en la época preindustrial, y la última década ha sido la más cálida registrada. El cambio climático no solo implica temperaturas más altas, sino que también afecta al equilibrio del planeta, provocando sequías, escasez de agua, incendios, aumento del nivel del mar, inundaciones, deshielo polar, tormentas extremas y pérdida de biodiversidad.

En este contexto, la lucha contra el cambio climático exige descarbonizar las actividades humanas que generan gases de efecto invernadero, especialmente aquellas relacionadas con la quema de combustibles fósiles, como el carbón, el petróleo y el gas. Entre las fuentes mas notables de emisiones se incluyen la energía, la industria, el transporte, la agricultura, el uso de la tierra y la deforestación.

En el ámbito del transporte por carretera, han surgido distintas alternativas con el objetivo de reducir la dependencia de los combustibles convencionales como la gasolina o el diésel. Entre estas opciones destaca el uso del hidrógeno, un vector energético sin carbono en su composición química que ha despertado gran interés en aplicaciones tanto de transporte como en procesos industriales.

El objetivo principal de esta tesis es analizar la aplicación del hidrógeno a motores de combustión interna alternativos. Concretamente, esta investigación tiene como propósito estudiar la transición a una economía del hidrógeno estudiando los efectos sobre la planta propulsiva, y los efectos en las emisiones globales, así como el estudio sobre los distintos sistemas de inyección de hidrógeno y en el efecto sobre el proceso de mezcla del combustible y aire.

El primer paso en el estudio de la transición hacia el hidrógeno consistió en caracterizar el proceso en distintas etapas temporales, cada una con una disponibilidad específica de hidrógeno verde. Este enfoque resulta crucial para garantizar que el uso del hidrógeno contribuya efectivamente a reducir las emisiones de gases de efecto invernadero, evitando escenarios en los que las emisiones sean equivalentes o incluso superiores a las generadas por los combustibles fósiles. Cada etapa fue representada mediante mezclas específicas de combustibles fósiles e hidrógeno, simulando una transición gradual con limitaciones realistas y considerando la necesidad de desarrollar la infraestructura de producción y distribución de hidrógeno a nivel territorial. La investigación incluyó ensayos experimentales con mezclas de gas natural comprimido (CNG) e hidrógeno, además de simulaciones para evaluar los impactos de esta transición.

Por último, se analizaron distintas configuraciones de inyección de hidrógeno, evaluando su influencia en el proceso de combustión y en la eficiencia de la mezcla aire-combustible. Los resultados ofrecen una perspectiva completa sobre la aplicación del hidrógeno en motores de combustión interna alternativos, proporcionando información clave para una transición energética eficiente y sostenible.

Resum

S'ha demostrat que les activitats humanes, responsables de generar gasos d'efecte hivernacle, han causat l'augment ràpid de la temperatura global en els darrers 200 anys. Actualment, la temperatura mitjana de la Terra és 1,1°C més alta que en l'època preindustrial, i la darrera dècada ha estat la més càlida registrada. El canvi climàtic no només implica temperatures més altes, sinó que també afecta l'equilibri del planeta, provocant sequeres, escassetat d'aigua, incendis, augment del nivell del mar, inundacions, desglaç polar, tempestes extremes i pèrdua de biodiversitat.

En aquest context, la lluita contra el canvi climàtic exigeix descarbonitzar les activitats humanes que generen gasos d'efecte hivernacle, especialment aquelles relacionades amb la crema de combustibles fòssils, com el carbó, el petroli i el gas. Entre les fonts més destacades d'emissions s'inclouen l'energia, la indústria, el transport, l'agricultura, l'ús de la terra i la desforestació.

En l'àmbit del transport per carretera, han sorgit diferents alternatives amb l'objectiu de reduir la dependència dels combustibles convencionals com la gasolina o el dièsel. Entre aquestes opcions destaca l'ús de l'hidrogen, un vector energètic sense carboni en la seva composició química que ha despertat un gran interès tant en aplicacions de transport com en processos industrials.

L'objectiu principal d'aquesta tesi és analitzar l'aplicació de l'hidrogen en motors de combustió interna alternatius. Concretament, aquesta investigació té com a propòsit estudiar la transició cap a una economia de l'hidrogen, analitzant els efectes sobre la planta propulsora i les emissions globals, així com els diferents sistemes d'injecció d'hidrogen i el seu impacte en el procés de barreja entre combustible i aire.

El primer pas en l'estudi de la transició cap a l'hidrogen va consistir a caracteritzar el procés en diferents etapes temporals, cadascuna amb una disponibilitat específica d'hidrogen verd. Aquest enfocament resulta crucial

per garantir que l'ús de l'hidrogen contribueixi efectivament a reduir les emissions de gasos d'efecte hivernacle, evitant escenaris en què les emissions siguin equivalents o fins i tot superiors a les generades pels combustibles fòssils. Cada etapa es va representar mitjançant barreges específiques de combustibles fòssils i hidrogen, simulant una transició gradual amb limitacions realistes i considerant la necessitat de desenvolupar la infraestructura de producció i distribució d'hidrogen a nivell territorial. La investigació va incloure assajos experimentals amb barreges de gas natural comprimit (CNG) i hidrogen, a més de simulacions per avaluar els impactes d'aquesta transició.

Finalment, es van analitzar diferents configuracions d'injecció d'hidrogen, avaluant la seva influència en el procés de combustió i en l'eficiència de la barreja aire-combustible. Els resultats ofereixen una perspectiva completa sobre l'aplicació de l'hidrogen en motors de combustió interna alternatius, proporcionant informació clau per a una transició energètica eficient i sostenible.

List of publications

Following the work performed in the framework of this doctoral thesis and its associated projects, the following journal papers have been published:

[1] S. Molina, R. Novella, J. Gomez-Soriano, and M. Olcina-Girona. "Study on hydrogen substitution in a compressed natural gas spark-ignition passenger car engine". Energy Conversion and Management 291, 2023, p. 117259.

[2] S. Molina, J. Gomez-Soriano, M. Lopez-Juarez, and M. Olcina. "Evaluation of the environmental impact of HCNG light-duty vehicles in the 2020–2050 transition towards the hydrogen economy". Energy Conversion and Management 301, 2024, p. 117968.

[3] S. Molina, R. Novella, J. Gomez-Soriano, and M. Olcina-Girona. "Impact of medium-pressure direct injection in a spark-ignition engine fueled by hydrogen". Fuel 360, 2024, p. 130618.

[4] S. Molina, R. Novella, J. Gomez-Soriano, and M. Olcina-Girona. "New combustion modelling approach for methane-hydrogen fueled engines using machine learning and engine virtualization". Energies 14 (20), 2021, p. 6732.

Additionally, six articles have been published in various journals, presenting work conducted within the scope of the doctoral thesis; however, their content is not explicitly aligned with its primary objectives:

[5] S. Molina, R. Novella, J. Gomez-Soriano, and M. Olcina-Girona. "Experimental evaluation of methane-hydrogen mixtures for enabling stable lean combustion in spark-ignition engines for automotive applications". SAE Technical Paper, 2022.

[6] J. Gomez-Soriano, P. Sapkota, S. Wijeyakulasuriya, M. D'Elia, et al. "Numerical modeling of hydrogen combustion using preferential species diffusion, detailed chemistry and adaptive mesh refinement in internal combustion engines". SAE Technical Paper, 2023.

[7] S. Molina, R. Novella, J. Gomez-Soriano, and M. Olcina-Girona. "Experimental Activities on a Hydrogen-Fueled Spark-Ignition Engine for Light-Duty Applications". Applied Sciences 13 (21), 2023, p. 12055.

[8] S. Molina, S. Ruiz, J. Gomez-Soriano, and M. Olcina-Girona. "Impact of hydrogen substitution for stable lean operation on spark ignition engines fueled by compressed natural gas". Results in Engineering 17, 2023, p. 100799.

[9] M. G. G. Mendoza, A. Garcia, S. Molina, M. Olcina-Girona, et al. "Toy Model: A Naive ML Approach to Hydrogen Combustion Anomalies". SAE Technical Paper, 2024.

[10] V. De Bellis, M. Piras, F. Bozza, E. Malfi, et al. "Development and validation of a phenomenological model for hydrogen fueled PFI internal combustion engines considering Thermo-Diffusive effects on flame speed propagation". Energy Conversion and Management 308, 2024, p. 118395.

Division of work between authors

The work leading up to this thesis was done in collaboration with other researchers. The respondent is the co-author of all papers on which this thesis is based, with author signatures being in order of seniority in the Institute. The respondent implemented the proposed methodology into the different engine set-ups, performed the calculations, processed the numerical results and extracted the presented conclusions. Discussions were also performed in collaboration with supervisors Prof. Molina and Prof. Gómez and the rest of the co-authors.

Funding acknowledgements

The respondent wishes to acknowledge the financial support received through contract CIACIF/2021/437 of the Subvenciones para la contratación de personal investigador predoctoral (ACIF) of Conselleria d'Innovació, Universitats, Ciència i Societat Digital de la Generalitat Valenciana.

Acknowledgements

I would like to begin by expressing my deepest gratitude to CMT for providing all the necessary resources to undertake this thesis. To my supervisors, I am profoundly grateful for the opportunity, your patience, and your guidance. I extend my thanks to Josep for meticulously reviewing the articles with the precision and excellence that define him, and to Santiago for his invaluable advice and insights drawn from his extensive experience. To Ricardo and Marcos, thank you for your constructive support, which pushed me to improve continuously. To Isa, I am grateful for listening to all the thoughts and ideas. To Rodri, thank you for your assistance in overcoming challenges with CALMEC. To Davide, thank you for your time and for every productive meeting. To all the pressure sensors I managed to break.

I also wish to thank to my colleagues Mares, Borja, Juanto, Marc, and Adbeel for the camaraderie, shared moments, and enriching conversations during our almuerzos. I feel fortunate to have had you as companions on this journey.

I am deeply grateful to my family, my parents, Paco and Pilar, and my brothers, Paco and Carlos for their unconditional support and encouragement throughout this journey. To all my friends, specially to Jordi, Pablo, Edu, Masiá, and Adrián, thank you for bringing moments of joy and laughter during challenging times, and to Jorge, for your constant support and positivity. Special thanks to Juanto, I owe special thanks as the one who first inspired and encouraged me to start and complete this thesis. Your support has been pivotal, and for that, I am truly grateful.

Finally, to Inés, thank you for standing by me through the difficult moments and for celebrating the successes along the way.

And last but not least, to myself, for persevering through every challenge and staying committed to this goal.

Valencia, 2025

Contents

List of Figures

List of Tables

List of Symbols

Greek

λ	Air-to-fuel equivalence ratio	–

Acronyms

ANN	Artificial Neural Network
ASC	Ammonia Slip Catalyst
BEV	Battery Electric Vehicle
BME	Brake Mean Effective Pressure
BTE	Brake Thermal Efficiency
BtL	Synthetic Hydrocarbon Fuels Made from Biomass
CH_4	Methane
CNG	Compressed Natural Gas
CO_2	Carbon Dioxide
COP21	Paris Climate Agreement
DI	Direct Injection
DOC	Diesel Oxidation Catalyst
DPF	Diesel Particulate Filter
EGR	Exhaust Gas Recirculation
EHB	European Hydrogen Backbone
EU	European Union
FC	Fuel Cell
FCV	Fuel Cell Vehicle
GHG	Greenhouse Gas
HC	Unburned Hydrocarbons
HCNG	Hydrogen Compressed Natural Gas Blends
H_2	Hydrogen
H_2O	Water
HICE	Hydrogen Internal Combustion Engine
HVO	Hydrotreated Vegetable Oil

ICE	Internal Combustion Engine
IEA	International Energy Agency
ISFC	Indicated Specific Fuel Consumption
LCA	Life Cycle Assessment
N_2	Nitrogen Molecule
N_2O	Nitrous Oxide
NO_x	Nitrogen Oxides
NRMM	Non-Road Mobile Machinery
OME_x	Oxymethylene Dimethyl Ethers
OEMs	Original Equipment Manufacturers
PFI	Port Fuel Injection
PM	Particulate Matter
SCR	Selective Catalytic Reduction
SI	Spark Ignition
SMR	Steam Methane Reforming
TWC	Three-Way Catalyst

CHAPTER 1

Introduction

The Earth's atmospheric composition has been dramatically influenced by anthropogenic activities over the last century. Concentrations of key greenhouse gases (GHGs), such as carbon dioxide (CO_2), methane (CH_4), and nitrous oxide (N_2O), have reached levels unprecedented in recorded history as shown in Fig. 1.1. This increase in GHG concentrations is significantly higher than even the most pessimistic scientific predictions, suggesting that the negative impacts of global warming will become more severe in both the short and medium term [11].

Climate change presents a multifaceted array of intricately interconnected challenges. One of the most pressing concerns is the rise in global temperatures, which has extensive ramifications for natural ecosystems, human health, and agricultural productivity. As temperatures rise, disruptions in oceanic and atmospheric currents have been observed, leading to altered weather patterns and an increase in the frequency and severity of extreme weather events, such as hurricanes, droughts, and heatwaves. These extreme events disproportionately affect vulnerable communities and ecosystems worldwide, exacerbating social inequalities and threatening biodiversity [13–15].

Addressing the challenges presented by climate change requires a dual approach: reducing GHG emissions and enhancing the capacity of natural and engineered systems to act as carbon sinks. Enhancing biological sinks involves protecting and restoring forests, wetlands, and other ecosystems that naturally sequester CO_2. Meanwhile, advances in chemical engineering offer promising solutions for capturing and storing CO_2 from both the atmosphere and industrial processes, contributing to long-term carbon removal.

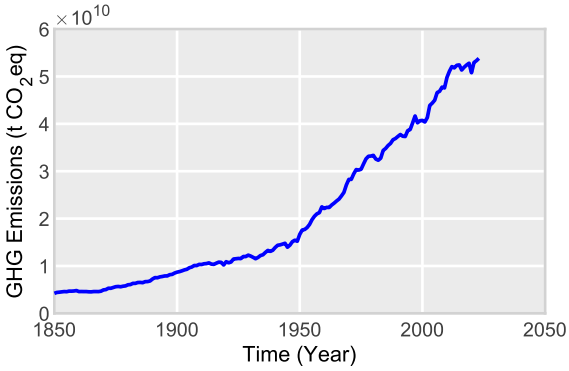

Figure 1.1: Historical greenhouse gases emissions measured in tonnes of carbon dioxide-equivalents over a 100-year timescale [12].

Historical data reveal a significant rise in global surface temperatures since the 1970s, underscoring the urgency of immediate action [16]. The Paris Climate Agreement (COP21) set a critical threshold for temperature increases, aiming to limit global warming to well below 2°C above pre-industrial levels, with efforts to limit the increase to 1.5°C [17]. However, without substantial reductions in GHG emissions, this threshold is at risk of being exceeded, leading to catastrophic environmental, social, and economic consequences.

To combat climate change effectively, robust policy frameworks and stringent regulations are essential. Current projections indicate that if reliance on fossil fuels continues at current levels, GHG emissions will keep rising, exacerbating global warming. Therefore, it is crucial to implement policies that promote the transition to renewable energy sources, improve energy efficiency, and encourage sustainable practices across all sectors of the economy.

The European Union (EU) has set ambitious targets through its Green Deal program, aiming to achieve net-zero GHG emissions by 2050. This long-term goal is supported by an interim target to reduce emissions by 55% by 2030 compared to 1990 levels. Despite these efforts, as of 2020, only a 20% reduction had been realized, highlighting the need for accelerated actions and enhanced policy measures to close the gap and meet the established targets.

Policy initiatives must also focus on supporting the research and development of new technologies, providing financial incentives for green innovation, and ensuring a just transition for communities and workers affected by the

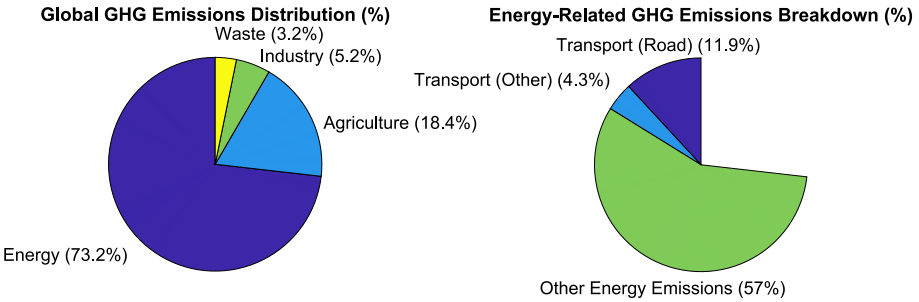

Figure 1.2: Figure 1: Global GHG emissions distribution by sector and global energy-related GHG emissions breakdown.

shift away from fossil fuels. International cooperation and adherence to multilateral agreements are vital to ensure that efforts to combat climate change are coordinated and effective globally.

1.1. Background

Global GHG emissions are predominantly generated by the energy sector, accounting for 73.2% of the total emissions. Agriculture contributes 18.4%, industry 5.2%, and waste 3.2%. Within energy-related emissions, transport alone is responsible for 16.2% of global emissions, with road transport specifically contributing 11.9% (Fig. 1.2). In Europe, road transport-related GHG emissions are even higher, making up 19.4% of the total. Given the substantial contribution of transportation to GHG emissions, it is critical to implement corrective measures to mitigate its environmental impact.

Reducing the environmental footprint of vehicle powertrains requires enhancing their efficiency and identifying alternative fuels to lower CO_2 emissions. Internal combustion engines (ICEs), which heavily rely on carbon-based fuels, need improvements in thermal efficiency and reductions in pollutant emissions to meet global CO_2 emission targets. For instance, European regulations mandate that light-duty vehicles reduce CO_2 emissions to 95 g/km, with even stricter targets anticipated in the future.

Transportation is a major source of CO_2 emissions, particularly in Europe, where it accounts for about 32% of total emissions. Despite the introduction of new environmental regulations and advancements in vehicle technologies, transportation emissions continue to rise. Addressing this issue requires diversifying the types of fuels used in the future and developing CO_2-neutral powertrains that also minimize emissions of other harmful pollutants.

The use of conventional carbon-based fuels in ICEs not only exacerbates global environmental issues but also poses significant health risks by degrading air quality. While complete combustion of hydrocarbons ideally produces CO_2, water (H_2O), and nitrogen (N_2), real-world combustion processes generate additional harmful pollutants, including carbon monoxide (CO), nitrogen oxides (NO_x), unburned hydrocarbons (HC), and particulate matter (PM). These pollutants are detrimental to human health, causing respiratory diseases such as rhinitis, sinusitis, and bronchial asthma, as well as cardiovascular and neurobehavioral effects, and increased cardiopulmonary mortality.

In this scenario, the use of conventional fuels in ICEs are expected to be replaced by carbon-free renewable alternatives. The most attractive option is probably the switch to Battery Electric Vehicles (BEVs). However, the future availability of specific materials (such as lithium, cobalt, or nickel), the low energy density of current batteries, and the fact that their implementation does not necessarily mean a reduction in GHG emissions—since BEV emissions are related to electricity production—make their application to the entire fleet of transport vehicles less optimal. In this sense, a massive BEV implementation may lead to an undesired rise in GHG emissions if non-renewable energy sources are used to feed the grid. In addition, the overall efficiency of the system could be reduced, increasing energy demand and resulting in higher energy prices.

The use of current ICE powertrains still represents one of the most realistic options for achieving efficient and effective decarbonization of transportation when combined intelligently with alternative fuels, electrification, and the use of renewable energy sources. A multitude of new fuel options are being evaluated, such as hydrotreated vegetable oil (HVO), synthetic hydrocarbon fuels made from biomass (BtL), dimethyl ether (DME), oxymethylene dimethyl ethers (OMEx), and alcohols (ethanol, methanol, or butanol), among others. All of these are promising from the perspective of a low GHG footprint, considering both their production and use in energy generation.

In particular, Compressed Natural Gas (CNG), produced by compressing conventional natural gas at high pressure, emerges as a potential solution due to its lower carbon content per molecule compared with conventional fuels like gasoline or diesel. The absence of C-C bonds in the fuel and the use of lean combustion strategies may reduce particulate matter by about 75%. Additionally, CNG could be obtained from renewable sources (e.g., animal

waste, landfills, food industry waste, aquatic biomass, or agricultural waste). In European countries, the existing infrastructure for natural gas reduces the cost of implementing this technology for fueling transport purposes.

In internal combustion engine research, increasing efficiency while reducing pollutants are common objectives. The widespread strategy to control pollutant emissions in spark ignition (SI) engines consists of combining a Three-Way Catalyst (TWC) with stoichiometric air-fuel mixtures. However, efficiency levels are compromised due to this requirement. Lean combustion strategies emerged in the past as a potential solution to improve efficiency while reducing pollutant emissions. In this combustion concept, fuel is burned in diluted conditions, increasing the air-to-fuel equivalence ratio (λ) well above 1. In these conditions, heat transfer losses are reduced, and thermal efficiency increases, especially at partial loads, where increasing air dilution is one of the main strategies to reduce pumping losses.

However, there are some drawbacks to consider. The primary issue is the effective operating or dilution limit. Beyond a certain point, increasing the excess air is not feasible. When this limit is reached, combustion stability is compromised, leading to partial burning and increased emissions of carbon monoxide and hydrocarbons.

Another common strategy, the use of exhaust gas recirculation (EGR), involves introducing hot burned gases from the previous combustion cycle into the intake. This reduces pumping losses, the specific heat ratio, and combustion temperature, leading to higher thermal efficiency and reduced NO_x. However, similar to the lean burn concept, there is a dilution limit with EGR; introducing too much EGR can decrease combustion efficiency and increase CO and HC emissions.

1.2. The role of hydrogen in decarbonization

The increased public awareness of climate change has led countries to establish GHG emission reduction targets. In this context, hydrogen (H_2) is a potential energy vector for decarbonizing the economy and society. The theoretical absence of CO_2 emissions during hydrogen combustion and its high heating value make it an attractive option as a future fuel substitute. Additionally, hydrogen has the potential to enhance energy independence for countries, reducing their vulnerability in diplomatic relations caused by the unequal distribution of fossil fuel reserves worldwide.

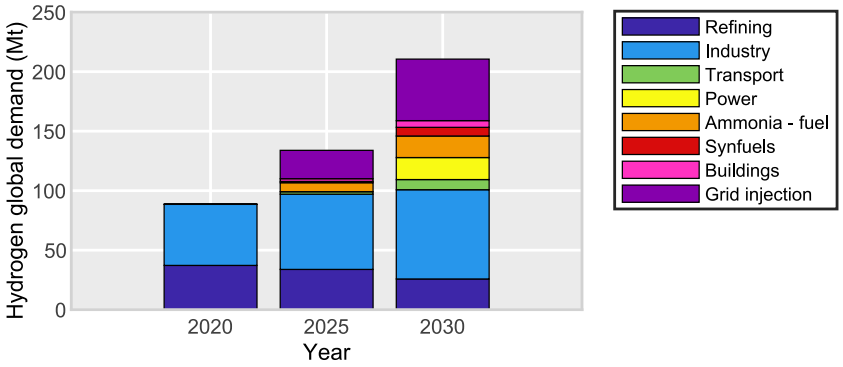

Figure 1.3: Global hydrogen demand by sector in the Net Zero Scenario, 2020-2030 [18]

.

Figure 1.3 illustrates the main sectors of global hydrogen consumption, along with current demand and projections according to the International Energy Agency (IEA) [18]. As shown, hydrogen plays a crucial role in industrial processes. It serves as a significant feedstock across various industries, with about one-third of global hydrogen production dedicated to oil refining. In this sector, hydrogen is used for hydrotreating, hydrocracking, and hydroconversion of crude oil, and also plays a direct role in synthetic and rocket fuel production cycles. The chemical industry also heavily relies on hydrogen, primarily for synthesizing ammonia and methanol. Furthermore, the metallurgical sector uses hydrogen in the reduction of metal-containing ores.

1.2.1. Hydrogen production

Hydrogen can be produced using a variety of different processes. Thermochemical processes use heat and chemical reactions to release hydrogen from organic materials, such as fossil fuels and biomass, or from materials like water. Water can also be split into hydrogen and oxygen through electrolysis or solar energy. Microorganisms such as bacteria and algae can produce hydrogen through biological processes [19].

The methods of hydrogen production can be categorized based on their source:

- Fossil Resources: Production from natural gas, coal, and other fossil fuels.

- Water: Production through processes like electrolysis, often powered by renewable energy.
- Organic Matter: Production from biomass, biogas, and other organic materials.

The growing implementation of renewable energies is also evident across all industries, including the use of solar panels and wind turbines for electricity production, renewable energy sources to supply heating systems in buildings, and biofuels to substitute conventional fossil fuels. This available energy could be used for hydrogen production.

Various methods exist for hydrogen production, with green hydrogen being a noteworthy example. Green hydrogen is generated through electrolysis powered by renewable energy and is considered a crucial component of the broader effort to decarbonize the economy [20, 21]. Beyond its role as a potential fuel for the automotive sector, hydrogen is also being explored as an energy vector to manage the variable energy outputs from renewable sources [22]. However, it is important to note that the majority of hydrogen currently originates from fossil resources. The predominant method of production is steam methane reforming (SMR) [23], a process that contributes to GHG emissions by releasing carbon in the form of CO_2 into the atmosphere. To mitigate this environmental impact, efforts are underway to integrate carbon capture mechanisms into SMR production [24]. Nevertheless, carbon capture technology remains an ongoing subject of research and development.

1.2.2. Hydrogen distribution challenges

The global distribution and bulk storage of hydrogen present significant logistical and economic challenges that are critical to its future as a major energy carrier. Regions such as the Middle East and North Africa are well-positioned to produce hydrogen at lower costs, potentially driving substantial international trade. However, transporting hydrogen—whether as a gas via pipelines, as a cryogenic liquid by ship, or through conversion to ammonia—incurs considerable costs and energy losses. For example, it is estimated that the infrastructure required for hydrogen distribution, including refueling stations, pipelines, storage, and import/export terminals, could account for 14% to 18% of global cumulative investments by 2050, depending on the scenario considered [25].

Projects like the European Hydrogen Backbone (EHB) aim to repurpose existing natural gas networks to transport hydrogen across 21 countries. However, the energy-intensive process of hydrogen liquefaction and the need

for specialized, costly storage solutions highlight the significant infrastructure demands. Ammonia emerges as a promising carrier for long-distance hydrogen transport, due to its higher energy density and established infrastructure, despite the energy conversion losses and handling risks associated with it [26, 27]. Additionally, geological storage in salt caverns offers a cost-effective solution for long-term and seasonal energy storage, which is essential for balancing the intermittent supply from renewable sources [28, 29].

These complexities underscore the critical need for strategic investments and technological advancements to make hydrogen a viable and competitive element in the global energy landscape.

1.2.3. Hydrogen as a fuel for automotive applications

Hydrogen is emerging as a promising alternative in the quest to decarbonize the automotive sector, owing to its carbon-free composition, which makes it an effective option for reducing GHG emissions [30]. The forthcoming EURO VII regulation aims not only to decrease NO_x emissions but also to significantly reduce CO_2 emissions from vehicle fleets. Specifically, the regulation sets ambitious targets: a 15% reduction from 2021 levels by 2025 and a 37.5% reduction by 2030 for all vehicles, with slightly lower targets of 15% and 31% for light-duty vehicles [31].

Within the automotive industry, hydrogen can be utilized in two primary ways: through fuel cells (FCs) or ICEs. Fuel cell vehicles (FCVs) offer high tank-to-wheel efficiencies, approximately 50% [32], and emit only H_2O, eliminating NO_x emissions entirely. However, despite these advantages, the dynamic behavior of FC systems in automotive applications presents challenges, particularly the reduced durability of FC stacks due to factors such as catalyst corrosion [33]. Leading manufacturers like Toyota, Honda, and Hyundai have already introduced commercial FCVs, but high production costs, driven by limited economies of scale, remain a significant barrier [32]. Moreover, FCVs rely on batteries to distribute the energy generated by the FC stack, which brings concerns similar to those associated with BEVs, such as the use of rare-earth elements and battery degradation.

This thesis reviews recent publications, focusing on the technical aspects of hydrogen engines and exploring their potential applications in areas where they may offer competitive advantages. Notably, the recent EU legislation targets heavy-duty vehicles, where hydrogen combustion engines could present a viable alternative to fuel cells. Applications such as long-haul trucking and off-road vehicles, which are difficult to electrify, may benefit more from hy-

drogen combustion engines than from FCs. Additionally, there is significant momentum toward achieving ultra-low emissions in the non-road mobile machinery (NRMM) sector. In these cases, battery-electric solutions may not be feasible due to limited autonomy, particularly in remote work sites or in urban environments, where machines operate under continuous high loads that local grids may struggle to support.

Hydrogen combustion engines present distinct advantages in such scenarios. First, ICEs achieve their highest efficiencies under high-load conditions, whereas fuel cells tend to perform least efficiently under similar conditions. For medium- and heavy-duty applications, especially those requiring power outputs over 200 kW, hydrogen engines can match or even exceed the efficiency of fuel cells at around 80% of nominal power. Second, both ICEs and fuel cells generate substantial waste heat, but ICEs carry a large portion of this heat away via exhaust gases. Even the heat rejected into the coolant remains at relatively high temperatures. In contrast, fuel cells operate with cooler coolant temperatures (80°C versus 110°C for ICEs) and produce less heat in their exhaust, necessitating larger radiator surfaces. This presents a particular challenge for NRMM applications, which often operate in dusty environments at low speeds, requiring significant power for radiator fan drives, and where machine size must be limited for access and visibility reasons. MAN [34] identifies a market for hydrogen engines in environments requiring robust powertrains, while BorgWarner [35] highlights the durability concerns for fuel cells, noting that ICEs do not suffer from efficiency loss over time. Furthermore, when hydrogen is used in ICEs [36], it offers higher tolerance for fuel purity, reduces reliance on rare-earth materials, and allows for the relatively straightforward adaptation of existing engine designs to replace conventional carbon-based fuels [37]. This adaptability positions hydrogen combustion technology as a promising contender in the future of carbon-free automotive propulsion [38]. Additionally, the absence of carbon in hydrogen virtually eliminates the emission of HC, CO, and CO_2, with these pollutants being produced only in minimal amounts due to the combustion of lubricants within the engine [39].

The review papers by Verhelst and Wallner [39, 40] have listed most hydrogen internal combustion engine (HICE) vehicle demonstrators up to 2008 and 2013, respectively. All these vehicles used either carbureted or port fuel-injected engines, resulting in reduced power densities compared to the original, mostly gasoline-powered versions. They met contemporary pollutant emissions limits, and in the monofuel cases where the engine was

optimized for hydrogen use, they could have higher overall engine efficiency than the gasoline version (due to lean operation, higher compression ratios, reduced pumping losses at part load, etc.).

In recent years, technological developments have enabled significant advances for hydrogen engines, as outlined by Keppy [41]:

- Turbocharger systems have developed strongly, with e-boost systems now available (electrically driven compressors that enable power-density-optimized turbochargers by providing transient boost).
- Hydrogen storage systems have been further developed, with on-board vehicle storage now reaching 700 bar hydrogen pressure.
- Direct injection (DI) equipment is becoming available for hydrogen (though currently limited to low pressure, as will be discussed below).
- NO_x after-treatment technology has progressed significantly for diesel engines.

Recent research efforts are concentrating on adapting engine designs to leverage the unique properties of hydrogen. This entails modifications in fuel supply, combustion chambers, and ignition systems to ensure safety and efficiency. Safety concerns stemming from hydrogen's low ignition energy and wide flammability range have prompted research into secure handling and storage, especially in vehicle applications [42]. Beyond engine adjustments, efforts have been directed towards broader infrastructure considerations, including hydrogen production, transportation, and distribution for widespread use [43]. Ongoing research is also focused on advancements in materials science, catalyst development, and general engine technology to enhance hydrogen compatibility as a fuel in spark-ignition engines.

Recent studies have demonstrated the potential of hydrogen DI in achieving high performance and efficiency. By controlling the timing of the intake valve closing and exhaust valve opening, researchers achieved an impressive 42.2% brake thermal efficiency (BTE). However, retrofitting conventional internal combustion engines with port fuel injection (PFI) is more straightforward and less expensive than converting them to direct injection. A review of the literature reveals that research on the conversion of existing gasoline engines to HICE prototypes is commonly found. Additionally, hydrogen PFI offers other advantages, including longer mixing time and optimized injection angles, which prevent abnormal combustion and NO_x formation.

In this context, the primary focus in HICEs is on reducing NO_x emissions [44]. The formation of nitrogen oxides can be attributed to thermal, prompt, and fuel mechanisms. The thermal NO_x mechanism develops under high temperatures, the prompt NO_x mechanism is activated at low temperatures in the early combustion stages, and the fuel NO_x mechanism depends on fuel composition [45]. In the case of hydrogen, the absence of nitrogen renders the fuel NO_x mechanism irrelevant, with the thermal path being the most pertinent one [46–48].

The properties of hydrogen facilitate stable combustion with high dilution, leading to a decrease in the concentration of generated NO_x [49]. It is widely acknowledged that when the air-to-fuel equivalence ratio exceeds 2 [50], NO_x emissions are notably diminished. Nevertheless, challenges associated with NO_x emissions during transient operating conditions (e.g., dynamic torque build-up phases) become evident in several investigations [51]. During these transitional periods, it is common for the air path system to experience delays in boost pressure, resulting in a reduced air-to-fuel ratio and, consequently, brief NO_x emission spikes. Consequently, Selective Catalytic Reduction (SCR) must be implemented to mitigate these emissions [40]. Recent research has explored the use of hydrogen as a reducing agent in SCR systems. The availability of onboard hydrogen represents an innovative and convenient approach to NO_x reduction, eliminating the need for urea/NH_3 storage in tanks and reducing the potential for ammonia slip at the tailpipe. The results of using H_2-deNO_x catalysts are promising in reducing NO_2 at low temperatures under lean combustion conditions [52].

Thus, capabilities for treating NO_x in an oxygen-rich environment have expanded, and their conversion efficiencies have increased. At the time of the review papers mentioned above [40], SCR systems were just being introduced for heavy-duty vehicles. Now, they have become commonplace for light-duty vehicles as well, complemented by NO_x storage catalysts.

In the following, we review recent publications from Original Equipment Manufacturers (OEMs), presenting hydrogen engine prototypes; engine suppliers, presenting engine components; and those considering market factors. The goal is to illustrate the key concepts outlined in the previous sections to improve understanding of the design challenges and opportunities for hydrogen SI engines.

1.2.4. Current prototype hydrogen engines

The development of hydrogen engines by leading companies such as Deutz AG, MAN Truck and Bus SE, and Keyou GmbH represents a significant advancement in adapting diesel engine technology for hydrogen fuel applications. Each company has pursued distinct strategies to overcome the inherent challenges of this adaptation, focusing on modifications to engine design, fuel delivery systems, and emissions control.

Deutz AG's hydrogen engine development, as reported in [53], is centered on a 7.8 L diesel engine platform, modified to meet the specific requirements of mobile machinery. The key changes include reducing the compression ratio to 10:1, replacing diesel injectors with spark plugs, and introducing hydrogen through a PFI system. The engine features turbocharging, an intercooler, and a cooled high-pressure EGR system to manage emissions and performance. A significant challenge identified is balancing transient response with NO_x emissions during dynamic optimization. Current development indicates that achieving the desired power density will necessitate a shift from PFI to DI, highlighting the limitations of PFI in predicting and preventing backfire using 0D/1D engine simulations.

In parallel, MAN Truck and Bus SE has presented a hydrogen engine concept designed for long-haul trucking, based on a 16.8 L engine with a target power output of 368 kW and 2300 Nm peak torque [34]. The design incorporates a low-pressure direct injection system, maintaining a compression ratio between 11 and 13 to eliminate the risk of backfire. The modifications include new piston rings, a "cold" spark plug, and adaptations to the cooling circuit to prevent abnormal combustion. MAN's approach has demonstrated a 37% increase in power density compared to earlier hydrogen engines, primarily due to the switch from PFI to DI. However, this improvement has also led to increased NO_x emissions, necessitating the retention of the diesel aftertreatment system, minus the diesel oxidation catalyst (DOC) and diesel particulate filter (DPF), while adding an ammonia slip catalyst (ASC) to convert unburned hydrogen into water.

Finally, Keyou GmbH has developed a retrofit concept for converting existing diesel engines into hydrogen engines, closely collaborating with Deutz AG on this initiative [54]. The retrofit involves replacing diesel injectors with spark plugs, reducing the compression ratio, and implementing a PFI system to introduce hydrogen during the intake valve's open period, thereby reducing the likelihood of backfire. Turbocharging plays a critical role in compensating for reduced volumetric efficiency, with various control strategies—such as adjusting the equivalence ratio, ignition timing, and EGR valve

position—being employed to optimize transient response and manage NO_x emissions. The study also explores methods to enhance exhaust enthalpy, such as insulating the exhaust manifold, though the results on engine dynamics remain inconclusive. Earlier findings indicated that high-pressure cooled EGR not only reduces NO_x emissions but also mitigates knock [55].

In summary, the ongoing research and development of hydrogen engines involve extensive modifications to traditional diesel engines, with a significant emphasis on managing NO_x emissions, optimizing power density, and ensuring rapid transient response. These efforts represent a critical step toward the commercialization of hydrogen-fueled internal combustion engines that can meet stringent environmental regulations while delivering the performance required for their intended applications.

1.3. Hydrogen-CNG fuel blends

The addition of hydrogen as a fuel component has shown significant promise in enhancing combustion performance and reducing tailpipe CO_2 emissions. Hydrogen-compressed natural gas (HCNG) blends, in particular, have emerged as a viable alternative fuel for ICEs, offering improved efficiency compared to engines running solely on CNG [56] or hydrogen. Moreover, HCNG blends have demonstrated the potential to reduce emissions of CO and HC [57]. By enabling higher air dilution ratios, these blends lower combustion chamber temperatures, effectively reducing NO_x emissions. Studies evaluating the emission performance of HCNG-powered vehicles have consistently reported significant improvements over conventional fuels.

Some studies have adopted a comprehensive approach by assessing not only vehicle operation but also fuel production and refinement processes. Research comparing conventional and alternative single-fuel sources has provided valuable insights. For instance, Karman et al. [58] compared CNG and diesel fuels, while other studies have focused on liquefied biomethane as a sustainable option for heavy-duty transport [59–61]. For passenger vehicles, Desantes et al. [32] assessed GHG and NO_x emissions across various fuel types, including hydrogen-powered vehicles (fuel cells and ICEs), BEVs, CNG-powered ICEs, and traditional fossil fuel-powered vehicles.

However, these analyses often rely on scenarios that may not reflect current realities, potentially introducing biases. For example, studies on hydrogen frequently assume its exclusive production from renewable energy sources or biomass [62, 63], while research on natural gas explores its sourcing from both conventional and renewable origins, such as sugarcane bagasse or waste

hydrogen [64–67]. While such research underscores the environmental benefits of hydrogen and natural gas, it often overlooks the challenges of large-scale implementation under present conditions. Many technologies required for widespread adoption are still under development, and their short-term feasibility is limited.

Focusing exclusively on single-fuel solutions also restricts flexibility in minimizing environmental impacts. In contrast, HCNG blends allow for leveraging both hydrogen's low-emission potential and natural gas's widespread availability. This adaptability makes HCNG blends a practical short-term solution, as they require minimal modifications to existing propulsion systems while supporting gradual hydrogen integration.

In this context, Gupta et al. [68] conducted a comprehensive life cycle analysis of a heavy-duty vehicle powered by HCNG, focusing on a 20% hydrogen blend. The study assessed net energy ratios, GHG emissions, and cost-effectiveness over the entire well-to-wheel cycle. In a separate study, Gupta et al. [69] evaluated the well-to-wheel performance of a light-duty truck using HCNG blends with varying hydrogen content (0%, 15%, and 30%).

Similarly, Candelaresi et al. [70] explored the use of Hythane (a blend of 20% hydrogen and 80% methane) in ICE and hybrid-electric vehicles, identifying vehicle infrastructure as a major contributor to environmental impact. Their findings indicated that hydrogen-natural gas blends could significantly reduce emissions compared to conventional fuels, promoting hydrogen adoption in the short term. Another study by the same authors [71] compared the environmental life cycle of passenger car fleets powered by renewable hydrogen and conventional fuels. The results showed carbon footprint reductions of 7% to 35%, depending on the hydrogen-to-mixture energy ratio. However, these studies did not optimize hydrogen content in HCNG blends to minimize environmental impact while balancing production and tailpipe emissions.

Future research should focus on optimizing HCNG blend compositions to achieve the best balance between environmental benefits, engine performance, and system compatibility. Long-term studies are also needed to evaluate the impacts of these blends on engine durability and infrastructure requirements.

1.4. Knowledge gaps

Building upon the findings of previous studies, the literature highlights several knowledge gaps, as summarized below:

1. Research on fuel blends is limited: The majority of studies projecting the future environmental impact of fuels primarily concentrate on single, unmixed compositions [32, 58–61]. There is a notable absence of extensive literature dedicated to investigating the effects of fuel blends, especially in the case of HCNG, across a broad spectrum of mixtures.

2. Heavy-duty Application Focus: The majority of studies on HCNG predominantly center around heavy-duty applications [68, 69]. There is a scarcity of research exploring the potential of HCNG in other sectors or applications.

3. Relying on Literature-Based Estimations: A few of the identified studies rely on experimental results when estimating fuel consumption and emissions in the operational phase of the life cycle assessment. Instead, estimations are predominantly based on existing literature, indicating a need for more empirical data in this aspect [70, 71].

4. Despite significant advancements in the study of hydrogen-fueled engines, a notable gap exists in understanding the integration of modern engine platforms with innovative hydrogen-based technologies and operating strategies.

5. A key challenge in advancing HCNG-fueled engines is the lack of reliable low-order combustion models tailored to HCNG blends, as most existing models are designed for traditional hydrocarbons. This gap limits the accurate prediction of combustion under varying hydrogen-to-methane ratios and operating conditions. Developing dedicated HCNG models is essential for efficient engine simulation, optimizing performance and emissions, and supporting real-time control systems.

1.5. Objectives

Building on the previous considerations, it becomes clear that combining engine experiments with numerical modeling and life cycle assessments is crucial to predict realistic scenarios where HCNG-powered engines for

automotive applications could play a significant role in global decarbonization. Therefore, the primary objective (PO) of this thesis is to evaluate the environmental impact of light-duty vehicle fleet using realistic scenarios to identify optimal transition strategies for decarbonizing the transportation sector with HCNG, hydrogen, and CNG-fueled vehicles. Additionally, several specific objectives (SOs) will be pursued to support this goal:

- SO-1: Conduct an experimental evaluation of the performance and emission levels of an engine fueled by HCNG blends for a light-duty vehicle, considering a transition towards a fully developed hydrogen economy. This transition will involve different scenarios based on the availability of green hydrogen, with the aim of establishing an optimized roadmap for adopting hydrogen as a sustainable fuel for future internal combustion engines.

- SO-2: Perform an environmental impact assessment of HCNG-powered light-duty vehicles in realistic scenarios transitioning to a fully developed hydrogen economy. This will include evaluating potential cradle-to-grave emissions based on the evolution of the energy mix, natural gas, and hydrogen. The objective is to determine the optimal HCNG blend for minimizing cradle-to-grave emissions between 2020 and 2050 and to identify the biogas requirements needed to achieve zero cradle-to-grave emissions.

- SO-3: Investigate the effects of various operating strategies and technologies on air-fuel mixture formation in engines using gaseous fuels, such as CNG and hydrogen. Focus on technologies like port fuel injection and direct injection systems to analyze performance, combustion characteristics, and emissions across different injection techniques and air dilution levels. The aim is to identify the most efficient and sustainable approaches.

- SO-4: Develop a flexible fuel composition model (encompassing hydrogen, HCNG blends, and CNG) capable of predicting engine performance and estimating the burning rate of air-fuel mixtures within the combustion chamber. The goal is to improve the accuracy of combustion modeling across a wide range of operating conditions, air-fuel dilutions, and fuel types, while maintaining computational efficiency.

1.6. Thesis outline

This thesis is structured into seven chapters. Following the introduction, which is Chapter 1, there is a sequence of four chapters corresponding to the articles published by the author. These chapters focus on the research results obtained within the framework of this thesis.

Chapter 2 explores the impact of HCNG blends on engine emissions and efficiency, offering a strategy for reducing emissions in the transportation sector as part of the broader transition to a hydrogen economy.

Building on this, Chapter 3 analyzes the potential of HCNG blends to reduce emissions more comprehensively during this transition. It identifies optimal HCNG blends for minimizing emissions over time and demonstrates how increasing the hydrogen content can enhance overall greenhouse gas reductions.

Once it is established that hydrogen is a viable fuel for ICE by 2050, Chapter 4 examines the effectiveness of various operating strategies and technologies aimed at enhancing the performance of hydrogen-fueled engines. For instance, it compares the performance of port fuel injection and direct injection systems in modern spark-ignition engines running on hydrogen, emphasizing differences in efficiency and emissions.

Chapter 5 introduces a new combustion model for HCNG blends in spark-ignition engines, developed using the experimental database generated as part of this thesis. This model leverages machine learning techniques to enhance accuracy, flexibility, and computational efficiency.

In Chapter 6, a detailed discussion of the results obtained during the experimental and computational investigations is presented, highlighting key findings and their implications.

Lastly, Chapter 7 will present the main conclusions derived from this research and propose future work to further explore this field. These recommendations aim to advance the development and implementation of HCNG engines as a viable solution for road transport decarbonization.

CHAPTER 2

Study on hydrogen substitution in a compressed natural gas spark-ignition passenger car engine

[1] S. Molina, R. Novella, J. Gomez-Soriano, and M. Olcina-Girona. "Study on hydrogen substitution in a compressed natural gas spark-ignition passenger car engine". Energy Conversion and Management 291, 2023, p. 117259.

2.1. Introduction

Concentrations of carbon dioxide (CO_2), methane (CH_4), and dinitrogen oxide (N_2O) in the atmosphere have reached the highest values recorded to date. The increase of these greenhouse gases (GHG) compared to the most pessimistic predictions suggests that the harmful consequences of global warming will increase in the medium and also in the short term. Historical records evince a significant global surface temperature increment since 1970 [16]. As a consequence, the temperature increase threshold established at the Paris Climate Conference (COP21) [17], will be exceeded if no drastic measures to reduce GHG emissions are taken in the next few years.

Around 73.2% of worldwide GHG emissions are related to energy production. This percentage considers the contribution of transportation (including road, rail, air, and marine applications), which represents 16.2% of the total. The global road transport emissions account for 11.9% [72], whereas this value increases 19.4% in Europe [31].

In this scenario, conventional fuels such as gasoline and diesel are expected to be replaced by carbon-free renewable alternatives. The most attractive option is probably the switch to Battery Electric Vehicles (BEVs). However,

the future availability of specific materials (such as lithium, cobalt, or nickel), the low energy density of current batteries, and the fact that their implementation does not strictly mean a reduction in GHG emissions —BEVs emissions are related to electricity production— make their application to the entire fleet of transport vehicles not optimal. In this sense, a massive BEV implementation may lead to an undesired rise in GHG emissions if non-renewable energy sources are used to feed the grid. In addition, the overall efficiency of the system could be reduced, increasing the energy demand and resulting in higher energy prices [73].

The use of current internal combustion engine (ICE) power plants still represents one of the most realistic options to achieve an efficient and effective decarbonization of transportation if combined intelligently with alternative fuels, electrification, and the use of renewable energy sources. A multitude of new fuel options are being evaluated, such as hydrotreated vegetable oil (HVO), synthetic hydrocarbon fuels made from biomass (BtL), dimethyl ether (DME), oxymethylene dimethyl ethers (OMEx), alcohols (ethanol, methanol, or butanol), among others [74]. All of them are interesting from the point of view of low GHG footprint considering both their production and use in energy generation.

The Environmental Protection Agency (EPA) believes that methane or its commercial surrogate, compressed natural gas (CNG), could be a viable fuel in the near future. The high hydrogen-carbon ratio (H/C) of CNG reduces CO_2 and particulate matter (PM) emissions during combustion [75]. Moreover, the higher octane number of CNG compared to gasoline allows for the use of higher compression ratios, resulting in improved thermal efficiency. CNG can be obtained from renewable sources, such as anaerobic digestion (AD), where organic materials like food waste, sewage sludge, livestock waste, crop residues, or sequential crops are decomposed into biogas containing 50% to 70% of CH_4, with the remaining percentage being CO_2. Additionally, the organic waste used in this process can be utilized to generate bio-fertilizers, contributing to the development of a circular economy. Lee et al. [76] analyzed the environmental impacts of different anaerobic digestion technologies applied to sludge for energy production, and found that renewable CNG production could reduce GHG emissions by 39% in the worst-case scenario. Although the share of biogas is still small in most developed countries, it is expected to increase in the future [77]. When applied to road transport applications, CNG vehicles are considered a

better option for passenger transport, both in urban and intercity settings, compared to diesel vehicles in terms of equivalent CO_2 emissions and total cost of ownership (TCO) [78].

Hydrogen (H_2) is a potential alternative to current fossil fuels. Recent studies have demonstrated the potential of hydrogen direct injection (H2-DI) in achieving high performance and efficiency. By controlling the timing of the intake valve closing and exhaust valve opening, researchers achieved an impressive 42.2% brake thermal efficiency (BTE) [79]. However, retrofitting conventional internal combustion engines with port fuel injection (PFI) is more straightforward and less expensive than converting them to direct injection. A review of the literature reveals that research on the conversion of existing gasoline engines to hydrogen internal combustion engine (HICE) prototypes is commonly found [36]. In addition, hydrogen PFI offers other advantages, including longer mixing time and optimized injection parameters.

Despite its excellent combustion properties, hydrogen-powered engines face similar disadvantages as BEVs. If water electrolysis is used to split water into hydrogen and oxygen (O_2), the bottleneck to achieving a complete CO_2-free energy production chain is electricity. Therefore, a largely GHG-free grid production is necessary to ensure a real GHG-free H_2 fuel (green hydrogen) with a low environmental footprint. Despite this huge challenge, hydrogen is expected to play a key role in future decarbonization plans in Europe. For example, in the European Union (EU), 40% of the total natural gas-based heating systems will be adapted to use 7% (in volume) of hydrogen-compressed natural gas (HCNG) fuel blends by 2030, and 32% HCNG by 2040 [80].

Due to the evident synergy between both fuels, several researchers have investigated the use of HCNG blends as an alternative fuel for internal combustion engines. Adding hydrogen to CNG has been shown to extend dilution limits and improve combustion stability [81]. Duan et al. [82] proposed an improved particle swarm algorithm optimized back propagation neural network method to study HCNG flame propagation. Du et al. [83] studied the effects of turbulent intensities and equivalence ratios on the flame structure of outwardly propagating HCNG-premixed flames. Kosmadakis [84] examined the cyclic variability in a spark-ignition (SI) engine fueled with CH_4/H_2 blends using a computational fluid dynamics (CFD) code. Mehra et al. [85] summarized the expected benefits of HCNG in terms of performance, emissions, and other relevant parameters in a review. Furthermore, Pandey et al. [86] found that smaller amounts of hydrogen in CNG could avoid

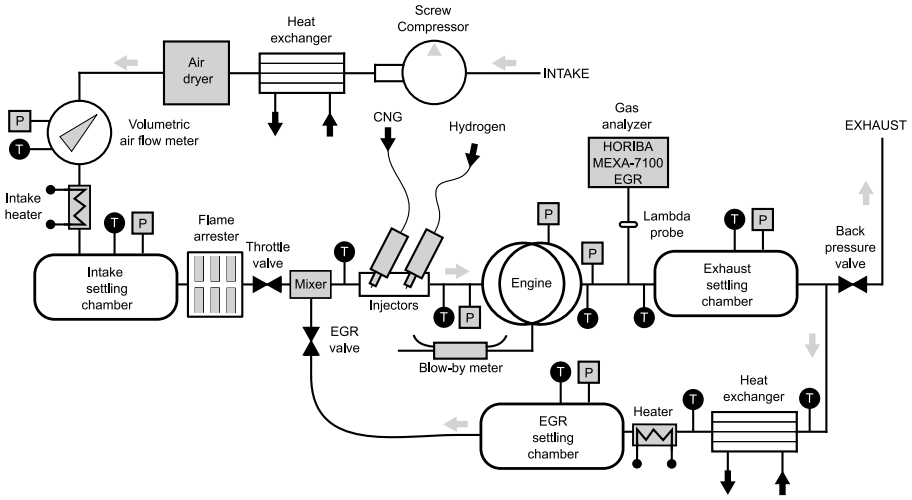

Figure 2.1: Test bench layout.

costly and complex engine modifications required to achieve maximum brake torque ignition timing, making the conversion to HCNG a more viable option for vehicles [87]. Additionally, Gupta et al. [88] demonstrated the reduced environmental impact of HCNG-fueled vehicles throughout their life cycle, highlighting its potential as a promising alternative fuel. In a study conducted by Sagar et al. [89], the knocking characteristics of a single cylinder port fuel injected SI engine were examined using different fuels, including hydrogen and HCNG mixtures. The study found that hydrogen-enriched natural gas led to reduced emissions of CO_2, hydrocarbons (HC), and carbon monoxide (CO), but resulted in increased nitrogen oxides (NO_x) emissions.

The production of NO_x is a major concern associated with high-hydrogen content fuels. Numerous studies have been conducted to address this issue in HCNG-fueled engines. Park et al. [49] evaluated two dilution methods and found that the lowest engine-out NO_x emissions were observed under lean combustion. Similarly, Rao et al. [90] developed a quasi-dimensional combustion model with exhaust gas recirculation (EGR) [91] to predict NO_x emissions. Prasad et al. [92] investigated the combustion, performance, and emission characteristics of different HCNG mixtures under identical maximum brake torque timing using laser-induced ignition and spark ignition techniques. Laser ignition reduced the kernel flame formation and propagation time and produced less NO_x than conventional spark ignition [93].

The various investigations conducted so far highlight the complexity of achieving GHG-free mobility. Fuel production, costs, and availability, as well as vehicle manufacturing and operational requirements, are some of the key aspects that need to be considered for a progressive and realistic decarbonization of transportation. HCNG fuel blends may offer an intermediate and flexible solution to adapt propulsion requirements while optimizing the transition to a fully-developed hydrogen economy. In this sense, natural gas can partially meet the energy demand until green hydrogen becomes more widely available. Despite the large number of investigations, almost all of them focus on giving a very specific view of a particular situation which is difficult to extrapolate to other cases (i.e. focusing on a specific technology, operating strategy...). However, the current situation demands a more general vision that allows a quick adaptation to the changing conditions of the environment, such as the economy, socio-political interests and environmental factors.

The objective of this investigation is to evaluate the performance and emission levels of a single-cylinder spark-ignition (SI) engine fueled by HCNG blends, considering different scenarios based on the availability of green hydrogen. This method will help establish an optimized roadmap towards the use of hydrogen as a sustainable fuel for the future. As a result, the optimal share of hydrogen in the fuel blend to be targeted in further development steps (i.e. at a multi-cylinder or vehicle levels) can be defined based on the current situation in each region, significantly reducing the global warming footprint of transportation during the transition process. This strategy represents a significant step forward, as it not only focuses on the ultimate goal of a fully-developed hydrogen economy, but also allows for flexible adaptation during the transition. In this sense, the study brings together current technologies and strategies to be applied and re-adapted to the external factors, contributing to the current knowledge gap.

2.2. Materials and Methods

This section presents a detailed description of the tools and methods employed in the investigation, with the aim of providing a clear and concise picture of the experimental techniques and procedures.

Number of cylinders	1
Displaced volume	454.2 cm^3
Stroke	86.0 mm
Injection systems	PFI
Ignition system	Spark plug
Cylinder diameter	82.0 mm
Compression ratio	10.7
Connecting rod length	144.0 mm
Valves per cylinder	2 intake, 2 exhaust
Engine management system	AVL PREMS GDI
Combustion system	4-valve pent roof GDI
IVO	-135 CAD
IVC	340 CAD
EVO	120 CAD
EVC	-338 CAD

Table 2.1: Engine specifications

2.2.1. Experimental tools

The experimental campaign was carried out on a single-cylinder SI research engine equipped with a port fuel injection system. The main engine specifications listed in Table 4.1 were the same as those used in a previous investigations [5, 8]. The fuel blend, which was injected using two different injectors, allowed enhanced control over the mixing and injection processes. Both injectors utilized in the study were Zavoli JET Injectors specifically designed for gaseous fuels. These devices are capable of operating at a maximum pressure of 4.5 bar and within a temperature range of -40 ^oC to 120 ^oC. The discharge nozzle of each injector has a diameter of 3 mm.

Figure 4.1 depicts the schematic of the test cell used in this research. The original test bench layout was modified to accommodate dual gaseous fuel strategies. In-cylinder pressure was measured using a piezoelectric sensor, while exhaust emissions were recorded using a HORIBA MEXA-7100EGR device. The mass flow rate of both fuels was controlled by two flowmeters: Bronkhorst F-113AC-1M0-AAD-55-V for hydrogen, and F-113AC-M50-AAD-55-V for CNG. The experimental facilities provided comprehensive control over all relevant parameters. Boost conditions were achieved using an external compressor, and the exhaust back pressure was regulated by a knife-gate

Signal (High frequency)	Sensor	Specification
In-cylinder pressure	Piezoelectric sensor	0 to 250 bar ± 0.3% linearity
Intake pressure	Piezoresistive sensor	0 to 10 ± 0.001 bar
Exhaust pressure	Piezoresistive sensor	0 to 10 ± 0.001 bar
Variable (Low frequency)	**Sensor**	**Specification**
Engine Speed	Optical angular encoder	1 to 6000 ± 1 rpm
Engine Torque	Strain-gauges torque-meter	-200 to 200 ± 1 N m
Intake pressure	Piezoresistive transducer	0 to 10 bar ± 1%
Exhaust pressure	Piezoresistive transducer	0 to 10 bar ± 0.3%
Intake temperature	Thermocouple type K	0 to 1000 ± 0.5 °C
Exhaust temperature	Thermocouple type K	0 to 1000 ± 0.5 °C
Fluid temperature	Pt100 thermoresistance	-200 to 850 ± 0.3°C
Air mass flow	Air flow meter	0.6-100 m^3/h ± 1%
Hydrogen mass flow	Thermal mass flow meter	200-1600 l/min (based on N_2) ± 0.5 %
CNG mass flow	Thermal mass flow meter	200-1600 l/min (based on N_2) ± 0.5 %

Table 2.2: Instrumentation accuracy.

valve located on the exhaust line. The accuracy of the instrumentation is presented in Table 4.2, and the precision of the gaseous pollutant measurements is shown in Table 4.3.

In terms of fuel definition, CNG was obtained directly from the Spanish natural gas network and compressed. Its composition consisted of 89.95% methane, 6.27% ethane, and other impurities. On the other hand, hydrogen was supplied in pressurized tanks. Further details about both fuels are summarized in Table 3.4.

Engine and combustion-related output parameters, such as Indicated Mean Effective Pressure (IMEP), cycle-to-cycle variability expressed by the IMEP covariance (COV_{IMEP}), emissions levels, and indicated efficiency, were computed using an in-house combustion diagnostics tool [94]. The tool was adapted for hydrogen, CNG, and HCNG fuel blends.

The referred combustion diagnosis tool estimates the energy released during combustion by resolving the energy equation with the measured in-cylinder pressure, and assuming several simplifications. For instance, it considers uniform pressure and temperature fields throughout the whole combustion chamber and several simplifications for estimating the heat transferred to the cylinder walls among others. It has been improved during some modifications [95] to reduce errors in the calculations.

Pollutant	Analyzer	Range	Accuracy
HC	FID	min. 0 to 10 ppm C max. 0 to 50 kppm C	± 4%
NO_x	CLD	min. 0 to 10 ppm max. 0 to 10 kppm C	± 4%
CO	NDIR	min. 0 to 3 kppm C max. 0 to 12 vol%	± 4%
CO_2	NDIR	min. 0 to 5 kppm C max. 0 to 20 vol%	± 4%
O_2	PMA	min. 0 to 5 vol% max. 0 to 25 vol%	± 4%

Table 2.3: Accuracy levels of HORIBA MEXA 7100 DEGR for measurements of gaseous pollutants.

Properties	CNG	H_2
RON	120	> 130
AF_{st}	16.00	34.3
LHV	46.87 MJ/kg	119.9 MJ/kg
H/C	3.79	-
O/C	0.026	-
Molar mass	17.77 g/mol	2.01 g/mol
Purity	-	$\geq$ 99.9%

Table 2.4: Specifications of CNG and H_2 fuels.

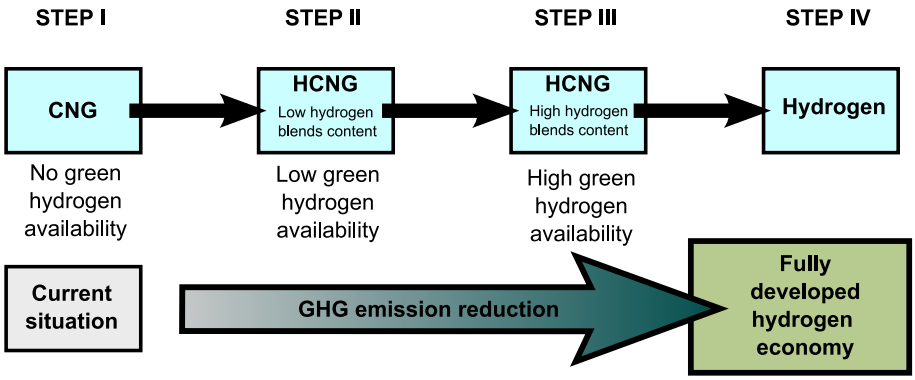

Figure 2.2: Diagram of the proposed method based on the different scenarios to mimic the fuel transition.

The model originally considered three different components: air, fuel, and combustion products. The fuel component is now considered a single hydrocarbon ($C_xH_yO_z$) with equivalent properties of the real fuel mixture. The properties of this fuel element are weighted by the fuel composition used in each test as:

$$Y^{\mathrm{i}}_{\mathrm{fuel}} = \frac{\dot{m}^{\mathrm{i}}_{\mathrm{fuel}}}{\dot{m}^{1}_{\mathrm{fuel}} + \dot{m}^{2}_{\mathrm{fuel}}} \tag{2.2.1}$$

$$X^{\mathrm{i}}_{\mathrm{fuel}} = \frac{Y^{\mathrm{i}}_{\mathrm{fuel}}/M^{\mathrm{i}}_{\mathrm{fuel}}}{Y^{1}_{\mathrm{fuel}}/M^{1}_{\mathrm{fuel}} + (1-Y^{1}_{\mathrm{fuel}})/M^{2}_{\mathrm{fuel}}} \tag{2.2.2}$$

Here, $Y^{\mathrm{i}}_{\mathrm{fuel}}$ and $X^{\mathrm{i}}_{\mathrm{fuel}}$ represent the fuel mass and molar fraction of each fuel element ($\mathrm{i} \rightarrow \{\mathrm{CNG}, \mathrm{H_2}\}$), $\dot{m}^{\mathrm{i}}_{\mathrm{fuel}}$ is the mass flow rate and $M^{\mathrm{i}}{}_{\mathrm{fuel}}$ the molar mass of fuel$^{\mathrm{i}}$.

Therefore, the most relevant properties such as Lower Heating Value ($\mathrm{LHV}^{\mathrm{avg}}$), molar mass ($\mathrm{M}^{\mathrm{avg}}$) and density ($\rho^{\mathrm{avg}}$) of the equivalent fuel can be computed as:

$$\mathrm{LHV}^{\mathrm{avg}} = \mathrm{LHV}^{1}_{\mathrm{fuel}} \cdot Y^{1}_{\mathrm{fuel}} + \mathrm{LHV}^{2}_{\mathrm{fuel}} \cdot Y^{2}_{\mathrm{fuel}} \tag{2.2.3}$$

$$M^{\mathrm{avg}} = X^{1}_{\mathrm{fuel}} \cdot M^{1}_{\mathrm{fuel}} + X^{2}_{\mathrm{fuel}} \cdot M^{2}_{\mathrm{fuel}} \tag{2.2.4}$$

$$\rho^{\mathrm{avg}} = Y^{1}_{\mathrm{fuel}} \cdot \rho^{1}_{\mathrm{fuel}} + Y^{2}_{\mathrm{fuel}} \cdot \rho^{2}_{\mathrm{fuel}} \tag{2.2.5}$$

$$Y^{\mathrm{avg}}_{\mathrm{C}} = Y^{1}_{\mathrm{fuel}} \cdot Y^{1}_{\mathrm{C}} + Y^{2}_{\mathrm{fuel}} \cdot Y^{2}_{\mathrm{C}} \tag{2.2.6}$$

$$Y^{\mathrm{avg}}_{\mathrm{H}} = Y^{1}_{\mathrm{fuel}} \cdot Y^{1}_{\mathrm{H}} + Y^{2}_{\mathrm{fuel}} \cdot Y^{2}_{\mathrm{H}} \tag{2.2.7}$$

Operating point	Step I	Step II	Step III	Step IV
1500@4	$\lambda = [1,\lambda_{max}^{CNG}]$	λ_{max}^{CNG}	-	λ sweep
1500@7	$\lambda = [1,\lambda_{max}^{CNG}]$, EGR_{max}^{CNG}	λ_{max}^{CNG}	λ sweep	λ sweep
1500@10	$\lambda = [1,\lambda_{max}^{CNG}]$	λ_{max}^{CNG}	-	-
3000@10	$\lambda = [1,\lambda_{max}^{CNG}]$	λ_{max}^{CNG}	-	-

Table 2.5: Test matrix definition.

$$Y_O^{avg} = Y_{fuel}^1 \cdot Y_O^1 + Y_{fuel}^2 \cdot Y_O^2 \tag{2.2.8}$$

2.2.2. Definition of scenarios

This section describes the basis of the method used to simulate the transition to a fully-developed hydrogen economy, considering different scenarios based on the availability of green hydrogen. The assessment of the complete decarbonization of the transport sector, particularly from a tank-to-wheel perspective, is conducted through four different situations that progress from the use of a current fossil fuel (CNG) to the ultimate scenario of using H_2 as fuel. Accordingly, it should be possible to define the optimal fuel composition that ensures a substantial reduction in GHG emissions. Figure 2.2 provides a summary of the key aspects of each scenario, including the transition from CNG (Step I), low hydrogen substitution (Step II), high hydrogen substitution (Step III), and finally hydrogen (Step IV).

In the current situation (Step I), where there is limited infrastructure for green hydrogen production, CNG could serve as an alternative to conventional fuels. With anticipated advancements in biogas production and improvements in CNG-powered engines, it may be possible to achieve a reduction in GHG emissions without changing the fuel composition. This initial scenario is thus centered on enhancing the CNG combustion process, reducing NO_x emissions, and minimizing thermal losses through the implementation of a dilution strategy.

Disadvantages of lean combustion, such as high cycle-to-cycle dispersion that limits engine performance, will be attempted to be overcome in the second scenario (Step II). In this scenario, a small amount of H_2 will be required to improve CNG combustion features. Combining Steam Methane Reforming (SMR) with Carbon Capture and Storage (CCS) techniques could

help introduce enough hydrogen to control CNG combustion instabilities at the beginning of the transition process. Additionally, these quantities of hydrogen can be obtained through an onboard reforming system [96]. In this way, the hydrogen line can be removed from the vehicle, avoiding the need for large amounts of H_2 storage and subsequently minimizing the range distance penalties associated with low hydrogen density. This approach can be initially implemented in niche fleets and later extended to other vehicle types as local hydrogen grids are established.

As the distribution, production, and storage challenges associated with H_2 are solved, green hydrogen will reduce energy costs, boost industrial competitiveness, and also diversify energy sources. In this scenario (Step III), an extensive refueling station network and pipeline infrastructure will be built. The focus is no longer on improving CNG combustion, but rather on reducing the carbon content of the fuel. Additionally, a wider dilution range can be achieved thanks to hydrogen combustion properties, which is expected to result in efficiency gains.

In the final scenario (Step IV), only hydrogen is used as a fuel for ICEs. This scenario represents a fully-developed hydrogen economy where fossil fuels are completely replaced. Decoupling the demand for resources from access to highly efficient energy production can help achieve zero effective emissions. Similar to the previous scenario, the objective is to identify the optimal dilution conditions for achieving the lowest fuel consumption.

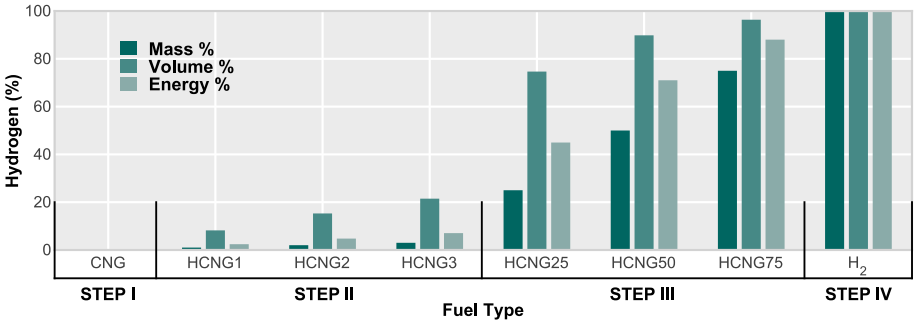

Figure 2.3: Characterization of fuel blends as a function of hydrogen percentage on mass, volume, and energy content.

2.2.3. Definition of operating conditions

An experimental campaign was conducted to compare the engine performance and emission levels (including pollutants and greenhouse gases) under the scenarios defined above. The engine operating conditions used for each scenario are summarized in Table 2.5.

As it can be seen, two engine speeds (1500 and 3000 rpm) and three engine loads (4, 7 and 10 bar of IMEP) are studied, being enough representative of real driving conditions. The operating conditions are referred by a pair of numbers ([rpm]@[bar]) representing the engine speed and engine load (IMEP). The IMEP targets were established by operating the engine with a stoichiometric CNG mixture without the use of external EGR. Once the desired load level was achieved, the fuel energy was calculated based on the injected mass of CNG and its LHV. Subsequently, the injected fuel mass was adjusted to maintain the same energy available for combustion at that particular load level. As a result, the amount of injected fuel mass is reduced as the hydrogen percentage is increased in the fuel blend due to its higher LHV. Specifically, for an equivalent CNG condition, the amount of H_2 is 60% lower. Furthermore, it should be noted that under these conditions, the IMEP level may vary if the thermal efficiency changes due to modifications in other parameters, such as the dilution ratio or combustion phasing. Therefore, the target values of engine load, which are used to designate the operating points, should be viewed as qualitative references that simply indicate whether the engine load is low, medium, or high.

In most research works, the hydrogen content in the fuel blend is expressed in volumetric fraction. However, the authors chose the mass fraction as the characterization parameter because it facilitates discussion in the scenarios considered. Figure 2.3 illustrates the equivalences between different ways of characterizing mixtures in terms of hydrogen content.

The energy deposition provided by the spark plug was maintained in all tests. The intake temperature measured at the surge tank was fixed at 308.15 K, and oil and coolant temperatures were kept constant at 363.15 K. The dilution ratio (air-to-fuel ratio) was controlled through the intake pressure. Three repetitions of each test were recorded to reduce the uncertainty of the measurements. The results presented in the following sections correspond to the average value of these three repetitions.

Depending on the scenario considered, some aspects of the methodology have been adapted according to:

- In Step I, four operation conditions (1500@4, 1500@7, 1500@10, and 3000@10) were studied. The spark timing (ST) was case-by-case optimized to reach the maximum brake torque (MBT) limit at stoichiometric and maximum-diluted conditions. The latter situation is achieved when 5% of COV_{IMEP} is exceeded. Also, the impact of diluent composition —air-fuel ratio (λ) vs. exhaust gas recirculation— was analysed through an ST sweep comparison.

- In the second scenario (Step II) low hydrogen content fuels with 1% of H_2 by mass (HCNG1), 2% (HCNG2), and 3% (HCNG3) were analysed. This upper limit was fixed to avoid high volumetric losses and abnormal combustion phenomena such as pre-ignition or backfire. The same operation conditions used for Step I were considered in the analysis. The air-to-fuel ratio was obtained also from the previous scenario, being stabilised by the maximum dilution achieved in each operating condition.

- The third scenario (Step III) focuses on evaluating high hydrogen content fuels. Since the amount of H_2 in the fuel blend increased significantly, the effect of higher dilution was also studied. Sweeps of λ were measured at the MBT limit from close stoichiometric ($\lambda \approx 1.2$) to ultra-lean conditions ($\lambda > 2$). The analysis was focused only on the operating condition 1500@7. The fuel composition was defined by increasing the hydrogen amount in 25% steps (HCNG25, HCNG50, and HCNG75).

- Finally, hydrogen combustion was assessed at two operation conditions (1500@4 and 1500@7) in Step IV. The idea is to give an overview of the main limitations when operating a PFI SI engine with hydrogen fuel. The analysis was focused on the same boundary conditions considered for the previous scenario.

2.3. Results

Results are divided into four sections, analyzing in detail the performance and emission levels under each of the proposed scenarios.

2.3.1. No hydrogen fuel availability

The target of this first study is to establish an initial reference for future comparisons, giving an overview of a situation similar to the current one. First, Fig. 2.4 shows a comparison of diluent compositions under the operating condition 1500@7. In general, the stable ST window is reduced with respect to the stoichiometric case when considering any type of dilution. This is particularly evident in the case of air dilution ($\lambda_{\max} = 1.47$) where the stable ST window is reduced from 14 to 12 CAD. In addition, this window is systematically advanced, moving the MBT point from -14 CAD aTDC to -26 CAD aTDC for the air dilution case, and to -34 CAD aTDC for the EGR dilution case ($EGR_{\max} = 21\%$).

The MBT case for λ_{max} conditions reports approximately 15% more IMEP than the stoichiometric case ($\lambda = 1$). This gain decreases up to 3% when considering EGR dilution. Trends of Gross Indicated Efficiency (GIE) are analogous to the IMEP profiles. As expected, the highest values of GIE are achieved for the air dilution cases, reaching almost 37%. Using EGR dilution is possible to achieve slightly higher levels compared with the non-diluted case (35% from 33%). Cycle-to-cycle variation (CCV) is analyzed through COV_{IMEP} parameter. Results show how combustion stability is strongly compromised when delaying the ST in diluted conditions. While the non-dilution tests are able to burn properly even at delayed ST (around -10 CAD aTDC), dilution tests experience a significant combustion instability at a given ST. This point is around -22 CAD aTDC for the air dilution and around -28 CAD aTDC for the EGR dilution. Regarding fuel consumption, dilution strategies reduce ISFC achieving an optimal point of 198 g/kWh at maximum air dilution conditions.

Trends of main pollutant and GHG emissions are plotted in Fig. 2.5. Since methane has 25 times more greenhouse effect than CO_2, unburned HC should be considered in the GHG analysis. In this investigation, it was not possible to discretize the HC measurement into methane and other intermediate species. However, the chemical characteristics of methane (dissociation energy, chain length, etc.) make the amount of HC intermediate species at the exhaust tailpipe negligible. Therefore, the unburned HC measurement included in Fig. 2.5 can be qualitative, and to some extent quantitative, indicator of CH_4 emissions. In this case, unburned HC increased respect to non-diluted cases when using air dilution, especially at delayed ST. Similarly, HC emissions due to EGR dilution also increase at delayed ST.

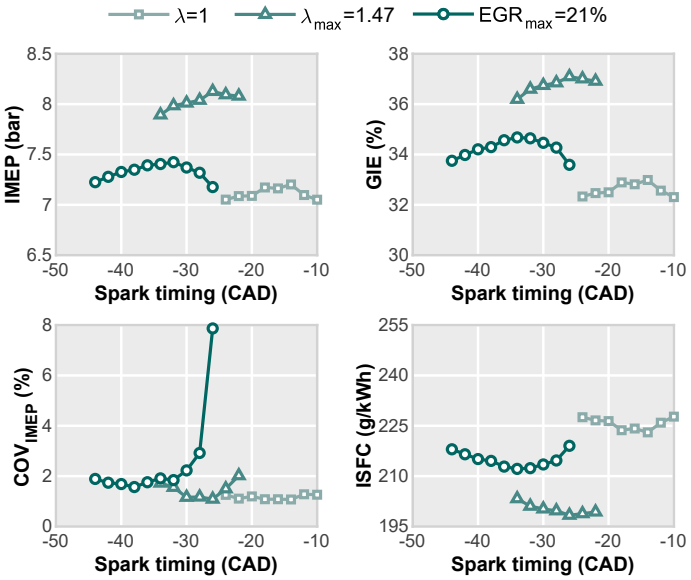

Figure 2.4: Performance levels comparison. Different dilution strategies (no dilution, air and EGR) are considered at 1500 rpm and 7 bar of IMEP.

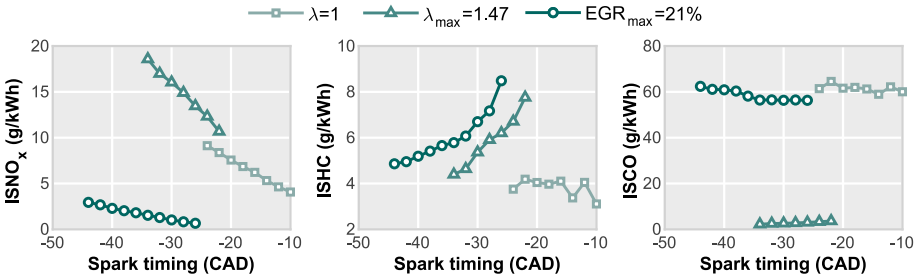

Figure 2.5: Emission levels comparison. Different dilution strategies (no dilution, air, and EGR) are considered at 1500 rpm and 7 bar of IMEP.

Regarding pollutant emissions, NO_x are drastically reduced when diluting by EGR. Contrarily, air dilution shows comparable values to those of the non-diluted stoichiometric case, being higher for cases with larger ignition advance. The effect of the spark timing is higher for air-diluted conditions than for the non-diluted case. EGR dilution is less sensitive to ignition timing. CO emissions are comparable between the non-diluted and EGR-diluted cases, whereas they are significantly reduced in the case of air-dilution since the higher oxygen availability promotes CO oxidation to CO_2.

In view of the better results obtained with air dilution, the extension of the analysis to all operating points is carried out only considering this type of dilution. The study, presented in Figs. 2.6 and 2.7, is focused on the MBT case of the non-diluted stoichiometric and maximum λ tests at each operating point. A general improvement is observed in GIE and therefore in IMEP levels. This significantly improves the fuel consumption in all operating points, while maintaining combustion stability.

As far as emissions are concerned, due to the fact that part of the fuel is not completely oxidized in stoichiometric conditions, a NO_x emission increase due to a higher temperature and improved combustion performance at maximum λ is observed. Note that although HC levels are maintained, the amount of CO is drastically reduced.

2.3.2. Low hydrogen content in the fuel

This scenario was deeply analyzed by the authors in a previous publication [5]. Focusing almost exclusively on the combustion process analysis, the authors show the effect of small hydrogen substitution percentages. Results showed that combustion was enhanced by increasing the percentage of hydrogen in the fuel. The high flame speed and wide ignition limits of hydrogen accelerate the combustion process, improving combustion stability at high dilution conditions [97]. The HRR is systematically advanced to the compression stroke and significantly shortened under equivalent conditions.

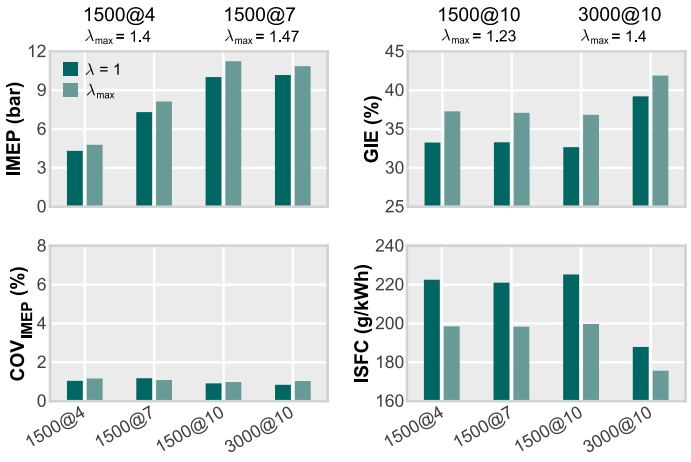

Figure 2.6: Performance levels comparison at the MBT limit of all operating points.

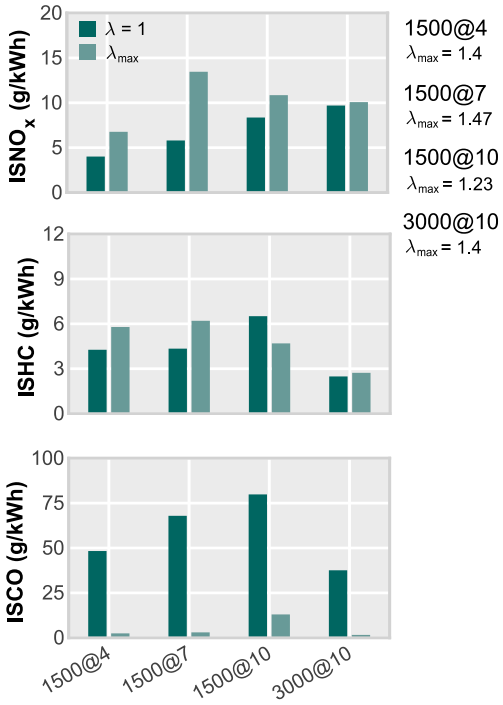

Figure 2.7: Emission levels comparison at the MBT limit of all operating points.

This causes an increment in the maximum in-cylinder pressure peak: around 10 bar when comparing the CNG and HCNG with 3% hydrogen concepts in the 3000@10 test. This faster combustion leads to a CCV reduction, and it also widens the stable operating range determined by the spark timing.

To see the impact of these effects on engine performance and emissions, the analysis performed is complemented by the results in Figs. 2.8 and 2.9. Here, the performance levels, emissions and other relevant parameter es are plotted for the four operating points considered so far at the MBT limit. Figure 2.8 shows an optimum point around 2% of hydrogen substitution. IMEP and GIE parameters evince the highest values at this hydrogen content in all operating points. As revealed in [5], combustion stability is improved especially at low load (1500@4) and high load-speed (3000@10). Requirements of the boosting system can be estimated through the intake pressure inspection. This is especially relevant in the case of HCNG fuel blends due to the low density of hydrogen that may compromise the volumetric efficiency in a PFI

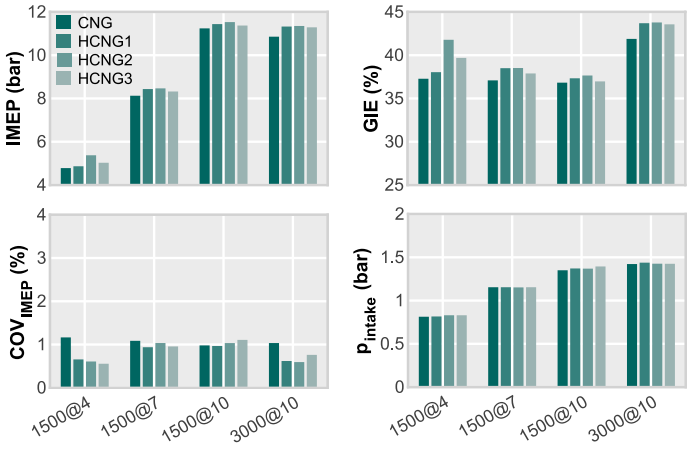

Figure 2.8: Performance levels comparison. Different fuel compositions (CNG, HCNG1, HCNG2, and HCNG3) are considered at the MBT limit of 1500@4, 1500@7, 1500@10, and 3000@10.

system. Results do not show a critical rise in intake pressure due to the small amounts of H_2 present in the fuel, suggesting that volumetric losses are not relevant.

Regarding GHG emissions, Fig. 2.9 show an improvement in terms of both CO_2 and CH_4 (quantified through the unburned HCs) as the hydrogen content increase. This enhancement is a consequence of better GIE and combustion stability. NO_x emissions are not significantly affected by the increase of the H_2 percentage. As Fig. 2.9 shows, there is no clear relationship between hydrogen content and these emissions. The only substantial difference is that in general, HCNG cases have slightly higher values than CNG cases, probably due to the higher local temperatures achieved due to H_2 addition. CO emissions depend on the operating point studied. Hydrogen helps to slightly reduce CO in the products at 1500@4, 1500@7 and 3000@10, whereas trends are not so clear at 1500@10.

In summary, low hydrogen substitution results in better performance outputs when small amounts of H_2 are considered. Higher combustion stability leads to enhanced control over combustion which extends the operating range. The higher thermal efficiency, the carbon substitution by hydrogen, and enhanced combustion stability help to reduce GHG emissions. CO emissions remain at the same level of CNG combustion while NO_x levels highlight the need for catalytic converters to deal with pollutant regulations.

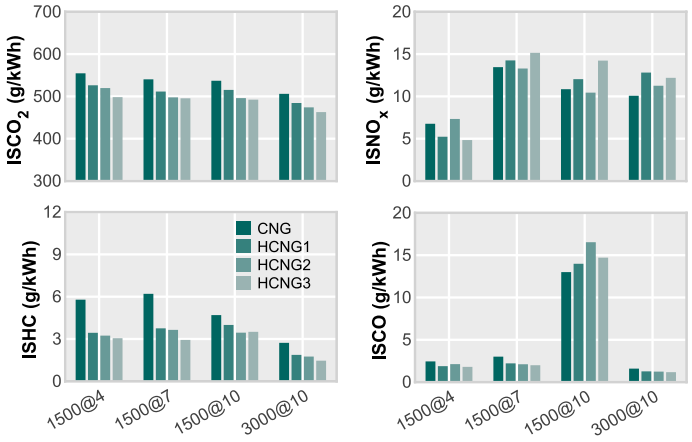

Figure 2.9: Emission levels comparison. Different fuel compositions (CNG, HCNG1, HCNG2, and HCNG3) are considered at the MBT limit of 1500@4, 1500@7, 1500@10, and 3000@10.

2.3.3. High hydrogen content in the fuel

In this scenario, the operating point 1500@7 was chosen as the representative condition to continue with the investigation. Results of increasing hydrogen share to 25, 50, and 75% (in mass) are analyzed at different λ conditions.

Figure 2.10 shows the performance level of each fuel composition and dilution condition. Again, IMEP and GIE values follow an equivalent behavior due to the testing method used in this investigation (same fuel energy per test). Therefore, the engine performance output is directly related to efficiency. There are two regions characterized by how λ affects these parameters. From stoichiometric conditions to $\lambda = 2$, each 0.2 λ increment grows efficiency by approximately 1%. Then, the efficiency-performance growth ratio is reduced for higher dilution rates. In this study, the maximum measured λ was determined by the drop in efficiency, never reaching the point where the COV_{IMEP} exceeds 5%. Thus, the CCV remains bounded at all measured points, even at the highest diluted points.

Focusing on the effect of fuel composition, HCNG25 results show the highest values of GIE at the same λ above HCNG50 and HCNG75. As the hydrogen content increases the IMEP and GIE levels decrease whereas the maximum value is reached at a higher dilution ratio. This peak value is achieved at $\lambda = 2$ for HCNG25, $\lambda = 2.2$ for HCNG50 and $\lambda = 2.4$ for HCNG75. Since the combustion stability is not excessively altered in

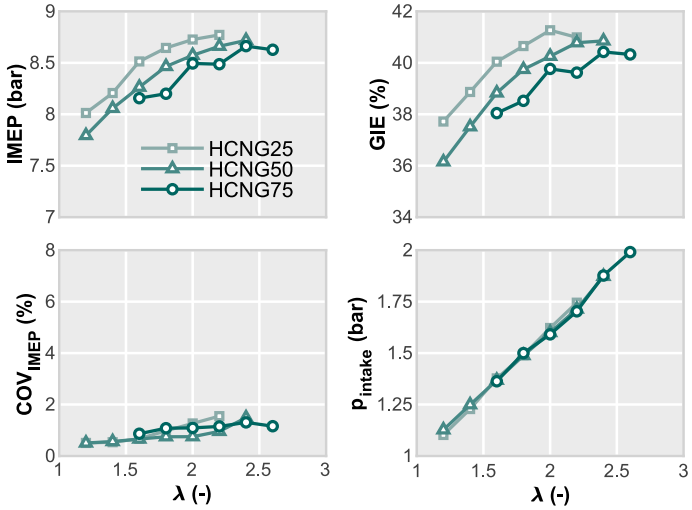

Figure 2.10: Performance levels comparison. Different fuel compositions (HCNG25, HCNG50, and HCNG75) are considered at 1500 rpm and 7 bar of IMEP.

any of the conditions measured, the efficiency drop observed due to the hydrogen increase in the fuel should be directly related to the wall heat transfer. The high burning rate of hydrogen incites heat transfer losses by increasing convection while reducing the quenching distance. Shudo et al. [98] investigated the cooling losses in SI engines using CNG and H_2, showing higher cooling losses for hydrogen. Nieminen [99] studied the potential of hydrogen compared to gasoline as a fuel for ICE at the same air dilution. They demonstrated that hydrogen reduces heat rejection and blowdown

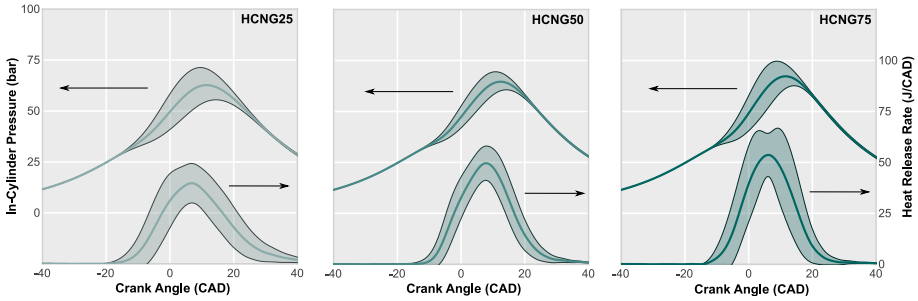

Figure 2.11: In-cylinder pressure and HRR profiles for different fuel compositions (HCNG25, HCNG50, and HCNG75) operating at 1500@7 $\lambda = 2$ MBT conditions.

during the exhaust stroke. In another work by Nieminen et al. [100] an exergy analysis pointed out that a HICE improves thermodynamic efficiency and reduces combustion irreversibilities. Nevertheless, less indicated work was obtained in comparison with gasoline because of the high thermal losses. Demuynck et al. [101] presented instantaneous heat flux measurements in a SI engine fueled with hydrogen and other relevant fuels. Results also indicated the negative effect of higher heat losses on engine efficiency. As a consequence, to maintain a high engine efficiency high dilution strategies (air dilution and/or EGR) should be applied to HICE port fuel injection engines.

Examination of intake pressure values reveals a direct relationship with the target dilution ratio. Moreover, there is no significant effect due to the fuel composition since all lines practically overlap. This makes sense if considering that volumetric percentages of hydrogen are between 75% (HCNG25), and 95% (HCNG75).

The combustion stability is remarkable even at the leanest conditions where flammability is typically considered unstable for conventional fuels. It should be noted that the hydrogen concentration is notably high, with levels above 25% by mass and 75% by volume, resulting in flammability limits that are closer to those of hydrogen rather than CNG. Most of the studies referenced in the bibliography focus on lower hydrogen content within the ranges considered in our investigation. Nevertheless, Ma and Wang [102] reported stable combustion levels at a lambda value of 2.1 when using a 50% H_2 content (by volume) in a HCNG blend. Therefore, reaching a maximum lambda value of 2.2 when using HCNG25 with a 75% hydrogen volume content seems reasonable to conclude that the values obtained are realistic.

To better understand these trends, Fig. 2.11 shows the in-cylinder pressure and the HRR profile for thee hydrogen content levels (HCNG25, HCNG50, and HCNG75) when operating at 1500@7 $\lambda = 2$ MBT conditions. An examination of these signals reveals that an increase in H_2 substitution has a pronounced effect on HRR, leading to sharper profiles and higher peak values. Furthermore, the cycle-to-cycle variability, as indicated by the shadow area, decreases to a certain extent with increasing hydrogen substitution.

The effect of air dilution on the combustion process is illustrated in Fig. 2.12. As evident from the figure, hydrogen accelerates combustion, resulting in a shorter combustion duration. Specifically, when switching from 25% to 75% of H_2 substitution, the CA90-10 is reduced by approximately 10 CAD. Consequently, the ST must be advanced to maintain the

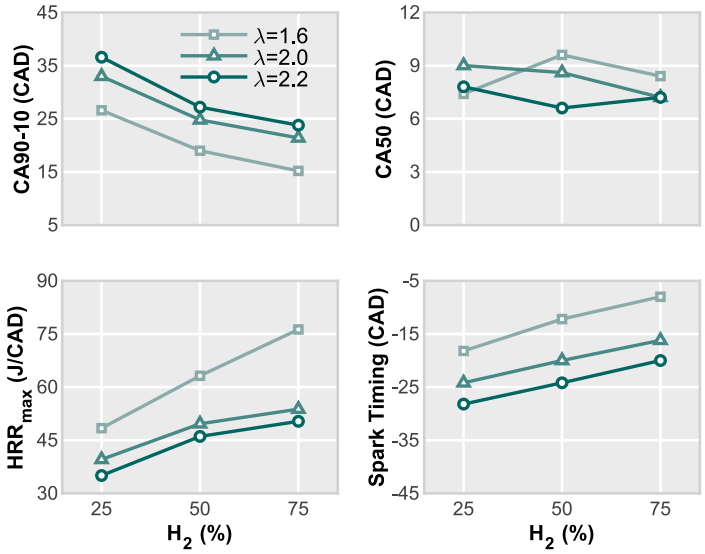

Figure 2.12: Combustion parameters for different fuel compositions (HCNG25, HCNG50, and HCNG75) and dilution ratios operating at 1500@7 MBT conditions.

optimum combustion phasing (CA50). Furthermore, the maximum peak of heat release rate (HRR) also increases with the hydrogen content. These trends are consistent across all λ values considered in this study.

As in the previous sections, the emission levels measured for the three fuel blends are plotted in Fig. 2.13. Focusing on specific CO_2 emission values ($ISCO_2$), it is evident how they are related to the fuel composition. Obviously, the more H_2 in the fuel, the less CO_2 produced by combustion. In this way, HCNG25 made approximately 300 g/kWh of $ISCO_2$ whereas HCNG50 and HCNG75 reduced this level up to 170 g/kWh and 70 g/kWh, respectively. Increasing the degree of dilution (λ slightly reduces $ISCO_2$ emission due to thermal efficiency gains observed in Fig. 2.10. However, the effect of dilution is not comparable to that of fuel composition. Emissions of unburned HC (mostly CH_4) and CO follow a similar trend. They are notably reduced as the amount of hydrogen is increased in the fuel blend and the number of carbon atoms is progressively reduced. Because of this, the effect of λ is also different as the fuel shifts toward less carbon content. While unburned HC increase by almost 0.5 g/kWh with 25% of H_2 content (from $\lambda = 1.2$ to λ

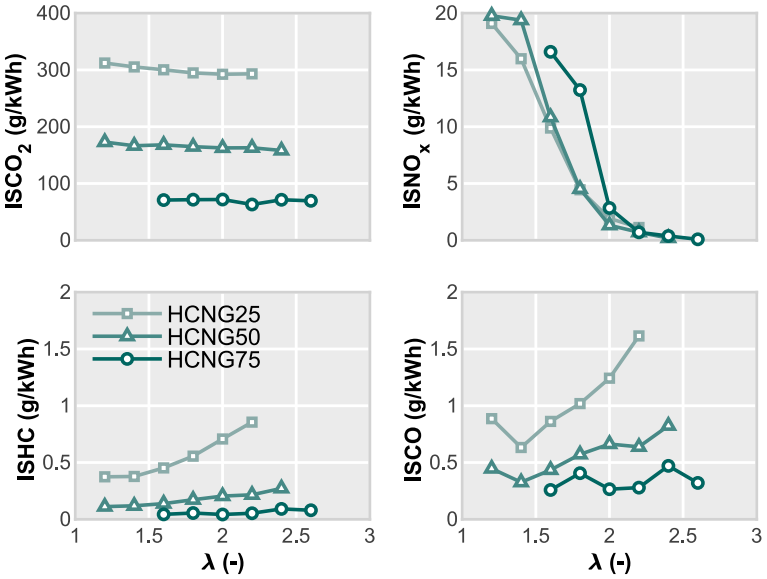

Figure 2.13: Emission levels comparison. Different fuel compositions (HCNG25, HCNG50, and HCNG75) are considered at 1500 rpm and 7 bar of IMEP.

$= 2.2$), in the case of 75% this increase is around 0.01 g/kWh (from $\lambda = 1.6$ to $\lambda = 2.6$). Similarly, CO emissions rise from 1 to 1.6 with HCNG25 whereas they roughly remain constant around 0.35 g/kWh.

NO_x emissions show a completely different pattern. The reduction is a consequence of the dilution increasing rather than the fuel composition. Data evince an inflection point between $\lambda = 1.5$ and $\lambda = 2$. In this range, NO_x emissions are reduced from 20 g/kWh to nearly zero levels for all assumed fuels. It seems the maximum local temperatures as a result of combustion do not change excessively with fuel composition. This is to some extent to be expected since both fuel components have similar adiabatic flame temperatures: $T^{ad}_{CH_4} = 2226$K vs. $T^{ad}_{H_2} = 2254$K (for stoichiometric combustion with standard air).

In summary, the application of these high-content H_2 fuels to transportation could be inferred a strong reduction on CO_2 emissions as the hydrogen percentage is increased. Moreover, the use of catalytic converters for NO_x control could be avoided with the operation with the correct dilution ratio.

2.3.4. Hydrogen fuel

This section analyzes the application of hydrogen as fuel, considering two representative conditions: 1500 rpm with 4 and 7 bar of IMEP. A air dilution sweep was performed under both operating conditions. The limits of the sweeps were conditioned by combustion abnormalities due to knock and maximum thermal efficiency. These values range from 1.4 to 4 for the low-load case and, 2.4 to 3.4 for the high-load case.

Results of the main performance outputs are presented in Fig. 2.14. In both operating points, the maximum efficiency and performance values are found around $\lambda = 3$. Increasing air dilution from this point on deteriorates the engine performance due to CCV. In these leaner conditions, combustion instabilities result in higher losses than gains in efficiency. The main difference between the two operating points lies in the effective dilution range. While at low load (1500@4) there is almost no knock limitation and combustion stability over a wide λ range (1.4 - 4), this range is much narrower as the load increases (2.4 - 3.4). This results in a reduced range of efficiency variation: ∼4% to ∼1%.

Only unburned hydrogen, NO_x and water are the awaited HICE exhaust gasses. No carbon dioxide or carbon monoxide are expected to be emitted due to H_2 combustion. However, small amounts of these elements were recorded during the experimental campaign as a consequence of the interaction of H_2 with the lubricant [103]. Figure 2.15 will focus on the analysis of nitrogen oxides as the main pollutant of HICE.

At low load conditions, the maximum NO_x emission values are recorded at $\lambda = 1.4$, being the lower dilution conditions tested. Increasing air dilution reduces combustion temperatures, inhibiting the thermal NO_x formation mechanism, leading to considerably low values for λ around 2 (< 1 g/kWh).

2.4. Discussion

Results of previous section demonstrate the potential of hydrogen as a carbon-neutral fuel if its production is based on renewable energy sources. However, they have also shown that the way in which society transition to this scenario can have a significant effect on CHG and pollutant emission levels. The objective of this section is to provide a set of guidelines to help identify the best operating strategy for HCNG-ICEs based on the availability of green hydrogen.

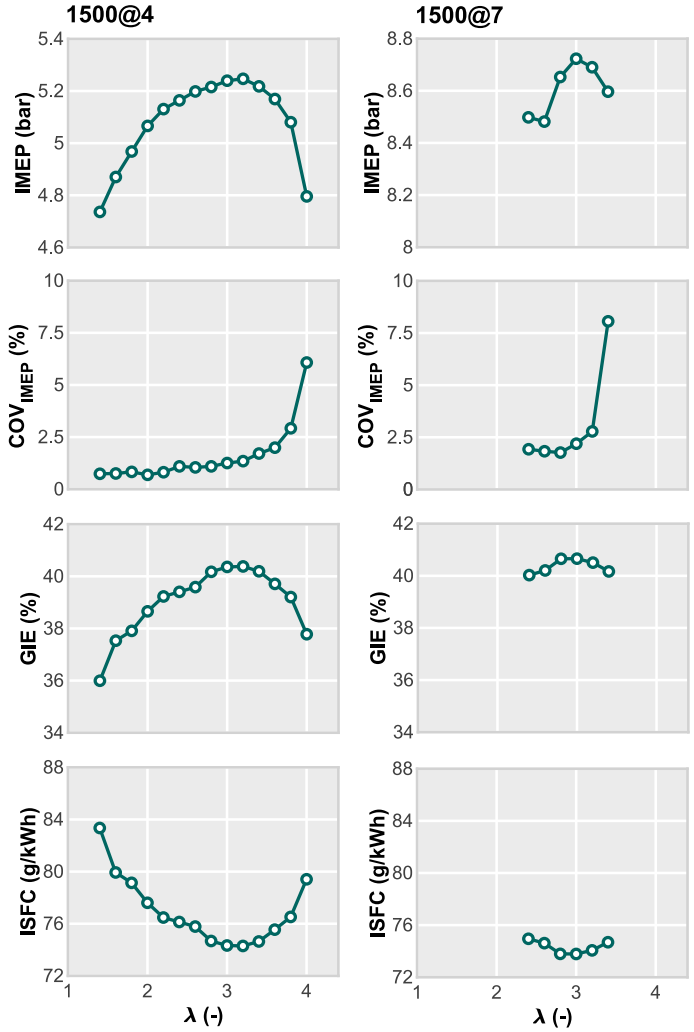

Figure 2.14: Performance and efficiency results for H_2 combustion considering two operating points.

The operation point 1500@7 was selected to be the reference due to the wide range of conditions measured. Figure 2.16 summarizes the emission levels registered considering all the situations studied throughout the four scenarios.

Inspection of $ISCO_2$ reveals the relationship between the amount of H_2 in the fuel and the CO_2 reduction. However, the gain in thermal efficiency also results in CO_2 reduction without the need for carbon-based fuel substitution.

Results of the second scenario (Step II), in which small amounts of hydrogen were studied, evince a significant reduction compared to the CNG case (see left in-zoom view of Fig. 2.16). In this situation, the mechanism responsible for the improvement in CO_2 emissions is not evident, since the percentage of substitution is small and the gain in efficiency is considerable. In contrast, the improvement in thermal efficiency as dilution increases for larger amounts of H_2 (Step III) does not seem to have an impact comparable to that produced by H_2 substitution. These effects can be better appreciated in Fig. 2.17, where the specific CO_2 emissions are drawn against the GIE. From Step I to Step II, the indicated efficiency increases almost 1.5%, lessen the CO_2 by 45 g/kWh. In Step III, these increments of GIE are notably higher (2.5% - 5%) but with lower CO_2 reductions (15-20 g/kWh).

The results from Step IV reveal non-zero emissions of CO_2 and CO even considering the fact that the fuel is carbon free. Previous research works [103] have indicated that CO and CO_2 can be present in the exhaust gases of SI engines fueled with pure hydrogen. These carbon-bearing species are formed due to the oxidation of lubricating oil and can serve as natural tracers for indicating oil consumption through combustion. Hydrogen, with its small quenching distance, has the ability to extend combustion into narrow gaps and crevices, potentially leading to higher consumption of lubricating oil compared to conventional fuels. However, it remains uncertain to what extent the presence of hydrogen in the cylinder mixture chemically contributes to the observed oil consumption. The temperature of the engine surface and the bulk temperature of burnt products are strongly influenced by thermal loading, which is a contributing factor to increased rates of oil consumption.

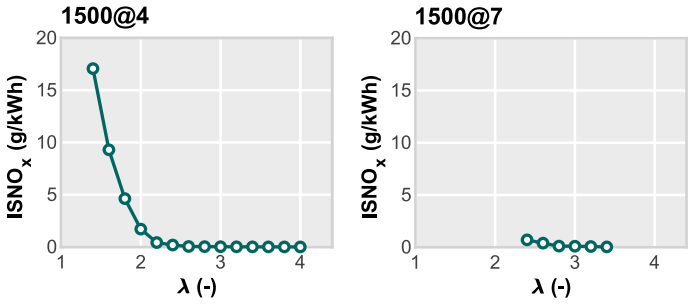

Figure 2.15: NO_x emission levels registered for H_2 combustion considering two operating points.

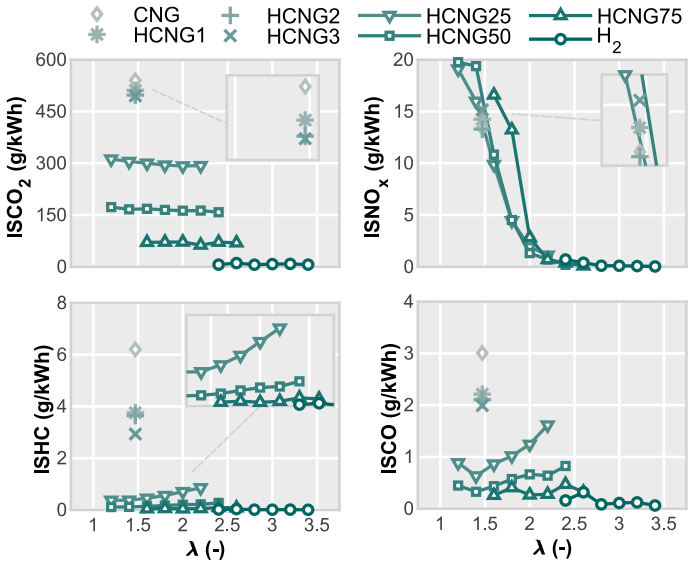

Figure 2.16: Summary of exhaust emissions for the operation point 1500@7 considering all fuel compositions.

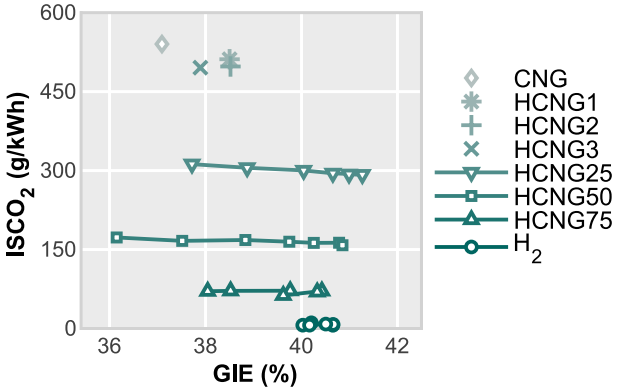

Figure 2.17: ISCO$_2$ vs. GIE for the operation point 1500@7 considering all fuel compositions.

A numerical study was performed in order to shed some light on the influence of these two parameters on CO_2 removal. This study uses an energy balance to convert the amount of fuel used into specific CO_2 emissions, allowing both effects (H_2 substitution and thermal efficiency gain) to be decoupled when considering a single-step complete combustion. Results are presented in Fig. 2.18, showing a CO_2 reduction map as a function of the

hydrogen content in the fuel and thermal efficiency variables. An increase of 2.5% of hydrogen causes a 5% reduction in CO_2, which is comparable to the reduction achieved by 2% of thermal efficiency gain. Both numbers being in range with the first and second scenario. With higher increments of hydrogen, the reduction in CO_2 emissions is remarkably larger than any reasonable gain in thermal efficiency. For example, for a mixture of 12% H_2, the CO_2 reduction is comparable to a 10% gain in thermal efficiency. Therefore, the performance improvement of HCNG-ICEs is more relevant in the first scenarios (Step I and II) where the amount of hydrogen is small. This relevance is diluted as hydrogen from renewable sources increases its presence, as it becomes a mere economic aspect due to the higher or lower fuel consumption.

Regarding NO_x emissions, it can be observed from Fig. 2.16 that it is a problem directly related to the dilution ratio. In this sense, the natural transition to a high hydrogen content is going in the right direction due to the properties of hydrogen, since it allows operating at sufficiently high air-to-fuel ratios to minimize this type of emissions. The issues with NO_x are expected in the early stages of this transition (Step II), where the low-hydrogen content in the fuel hinders the combustion stability at high dilution rates. This trend is clearly observed in Fig. 2.19. Here, the specific NO_x emissions are plotted against the percentage of hydrogen in the fuel and the λ. The highest levels of NO_x agglutinate at low λ whereas the lowest values correspond to the highest GIE levels. In terms of maximum performance, it is possible to distinguish an optimum region with values above 41% for fuel blends with 25% of H_2.

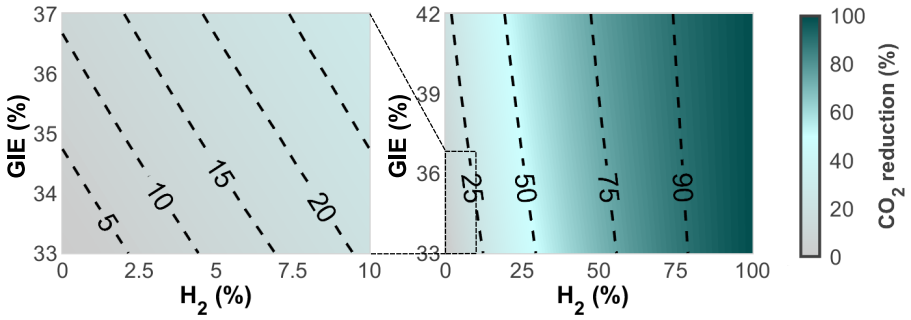

Figure 2.18: CO_2 reduction map considering hydrogen percentage content and indicated efficiency.

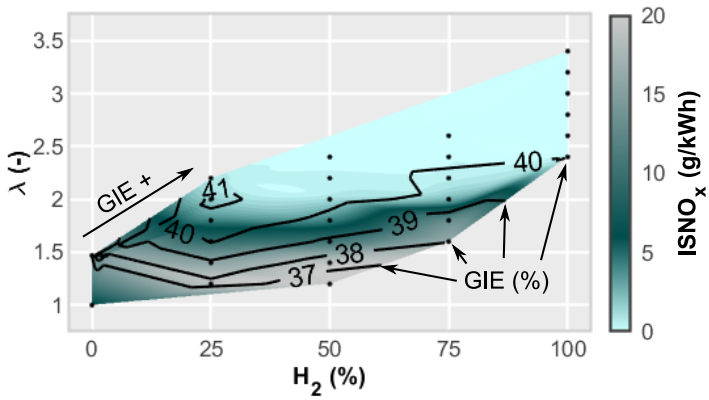

Figure 2.19: NO_x emissions for the operation point 1500@7 considering all fuel compositions.

Finally, recalling the unburned HC and CO trends depicted in Fig. 2.16, a substantial reduction in ISHC (Indicated specific HC) as hydrogen percentage increases is observed. The two reasons for this reduction are the improvement in combustion efficiency and the reduction of carbon in the fuel composition. Including small hydrogen amounts allows reducing these emissions significantly in Step II. Nevertheless, the highest reduction occurs when a higher content of hydrogen is used in Step III. CO emissions have the same effect as for unburned hydrocarbons; the carbon reduction in the fuel composition and the improvement in combustion stability reduce them. However, the sensitivity to dilution is higher.

2.5. Conclusions

This paper proposes a new approach to mitigating the problem of greenhouse gas emissions. The investigation focuses on analyzing the effects of different scenarios with varying fuel compositions and dilution conditions on emissions and efficiency levels, aiming to establish the first step towards a flexible roadmap for a hydrogen-based economy. These scenarios are based on the availability of green hydrogen, which is crucial for achieving GHG emission-free transport. To this end, an extensive experimental campaign was conducted in a single-cylinder spark-ignition engine powered by HCNG blends at several representative operating points.

Experiments with low hydrogen content revealed that adding small amounts of hydrogen to the fuel (1-3% by mass) helps stabilize combustion at moderate dilution ratios ($\lambda \approx 1.4$), resulting in an improvement in thermal efficiency by approximately 1.5%, and a reduction in CO_2 and CH_4 emissions.

The use of larger quantities of hydrogen (25-75% by mass) results in a significant reduction in both GHG and pollutant emissions (HC and CO), leading to very low levels. However, thermal efficiency is conditioned as the percentage of H_2 increases, with increased heat transfer to the chamber walls being a key parameter that controls this trend. There is an optimum point that offers the best performance based on a specific quantity of hydrogen (25%) and dilution condition (λ 2).

Further studies reveal that the loss of thermal efficiency as hydrogen increases in the fuel is compensated by the percentage of substitution of carbon elements, making it practically the only factor controlling CO_2 emissions for fuel blends with a H_2 content higher than 5% (by mass).

In the case of pure hydrogen combustion, where GHG emissions are not a relevant issue if fuel production is based on renewable sources, the problem seems simpler, at least initially. The solution is to find an engine platform that allows for operation with a reasonable thermal efficiency and minimizes NO_x generation as much as possible. In these conditions, small amounts of CO and CO_2 are measured due to the oxidation of lubricating oil.

The issue of NO_x emissions is a recurring problem in all scenarios. However, it is less critical in scenarios III and IV, where the higher presence of H_2 in the fuel allows for reaching higher dilution values that reduce these emissions below 1g/kWh. In this sense, NO_x emissions are a problem that is directly linked to the dilution degree used in engine operation, regardless of the level of H_2 in the fuel. Therefore, the three-way catalyst is the most feasible solution for scenarios I and II in order to meet emissions standards, necessitating stoichiometric combustion.

In later stages, it is possible to further increase dilution, which can significantly lower NO_x levels in the exhaust and improve thermal efficiency. However, limitations in the boosting system to achieve the required dilution rate or misalignments during engine transients suggest that the use of aftertreatment systems, such as hydrogen-selective catalytic reduction devices, will continue to be required.

Finally, these findings illustrate a flexible roadmap that can be readjusted by the current regional situation, and which has the potential to significantly reduce the global warming footprint of transportation during the transition towards a hydrogen-based economy.

However, this study is based on very specific experiments that may not fully reflect the actual operation of a vehicle-mounted engine in certain circumstances. Therefore, further studies conducted under conditions closer to real driving conditions should be performed in subsequent research steps, in order to verify the attainability of the values indicated by the proposed method in more realistic situations.

CHAPTER 3

Evaluation of the environmental impact of HCNG light-duty vehicles in the 2020–2050 transition towards the hydrogen economy

[2] S. Molina, J. Gomez-Soriano, M. Lopez-Juarez, and M. Olcina. "Evaluation of the environmental impact of HCNG light-duty vehicles in the 2020–2050 transition towards the hydrogen economy". Energy Conversion and Management 301, 2024, p. 117968.

3.1. Introduction

The current issue of climate change presents a complex array of interconnected problems. One of the primary concerns is the escalating local temperatures, which have far-reaching implications for ecosystems, human health, and agricultural productivity [13]. Rising temperatures also contribute to the disruption of oceanic and atmospheric currents, leading to altered weather patterns and increased occurrences of extreme events such as hurricanes, droughts, and heat waves. These changes pose significant threats to vulnerable communities [14] and ecosystems [15] worldwide.

Addressing the multifaceted challenges of climate change requires comprehensive strategies and significant investments [104]. A crucial initial step is to curb our reliance on fossil fuels, which are the primary contributors to greenhouse gas emissions. Transitioning towards renewable energy sources, such as solar, wind, or hydroelectric power, can help reduce carbon emissions and mitigate the adverse impacts of climate change. This transition

necessitates a shift towards sustainable transportation systems, increased energy efficiency measures, and the promotion of clean technologies. This interest in reducing fossil fuel consumption has led to the exploration of various solutions for the energy-intensive road transportation sector [105]. Electric vehicles (EVs) are considered a promising option due to their high efficiency in energy utilization. However, the widespread adoption of EVs poses challenges related to the availability of charging infrastructure, the demand for rare-earth elements, less fossil fuels dependent electricity mix [106], and the environmental impact of their production and disposal [107].

Hydrogen (H_2) has emerged as a promising alternative fuel, offering the potential to reduce the material requirements in vehicles. As a carbon-free fuel, it can be seamlessly integrated with renewable energy [108, 109], resulting in significantly lower emissions during its production. However, the current state of hydrogen production is not yet fully environmentally friendly, as the industry is still in the process of scaling up renewable energy sources. Consequently, the availability of green hydrogen remains limited, suggesting that its widespread use may be constrained due to the current low supply. To overcome this challenge, the concept of blending hydrogen with fossil fuels has gained attention, aiming at ensuring equitable and accessible energy while transitioning towards a hydrogen-based economy. Recent research has focused on studying fuel blends of hydrogen with gasoline, diesel, ammonia, and compressed natural gas (CNG) [8, 110].

The addition of hydrogen has shown promising results in improving combustion performance and mitigating carbon dioxide (CO_2) tailpipe emissions. For instance, H_2 and CNG blends (HCNG) have demonstrated significant potential as an alternative fuel for internal combustion engines (ICE), delivering notable improvements in efficiency levels compared to pure CNG engines [56]. Furthermore, these blends offer the opportunity to reduce carbon monoxide (CO) and hydrocarbons (HC) emissions [57]. By enabling higher air dilution ratios, HCNG blends facilitate lower combustion chamber temperatures, thereby reducing nitrogen oxides (NO_X) emissions. Extensive research has also been conducted to evaluate the overall emission performance of vehicles running on HCNG blends, revealing substantial improvements compared to conventional fuels. In a previous study, Molina et al. [1] investigated the performance and emission implications of an engine fuelled with HCNG blends and pure hydrogen. This investigation simulates the hydrogen transition across various stages of infrastructure and green hydrogen production deployment by varying the percentage of

hydrogen in the fuel blend. Results show an improvement in performance and emissions as the hydrogen substitution percentage increases, especially in terms of efficiency and NO_x.

However, this study only considers the effects caused by vehicle operation whereas other relevant aspects such as vehicle and fuel production are not pondered. In this sense, other studies evaluated the problem including vehicle operation, production, and fuel refinement processes. Numerous studies have been conducted to compare single fuels, whether they are conventional or unmixed, in the realm of alternative energy sources. For example, Karman et al. [58] conducted a comparative analysis between CNG and diesel fuels. Additionally, liquefied natural gas (LNG) has garnered significant attention in recent years, with several researchers examining the specific case of liquefied biomethane for heavy-duty transport [59–61]. Regarding passenger car applications, Desantes et al. [32] estimated greenhouse gas (GHG) and NO_x emissions for various fuel types, including hydrogen-fueled vehicles (both fuel cells and internal combustion engines), battery electric vehicles (BEVs), compressed natural gas internal combustion engine vehicles, and conventional fuel vehicles.

These studies often involve scenarios that may not reflect long-term realities, potentially introducing bias into the results. For instance, in the case of hydrogen fuel, these scenarios frequently assume its exclusive production from biomass or biowaste [62] or from renewable energy sources [63]. Regarding natural gas (NG) based fuels, current studies aim to evaluate the environmental benefits of sourcing this fuel from various origins, including conventional extraction [64], natural resources such as sugar cane bagasse [65], or renewable hydrogen and waste sources [66, 67]. While this research is undoubtedly valuable for understanding the potential of hydrogen and natural gas to reduce the environmental impact of transportation technologies, it may not adequately represent short-term conditions. Some of these technologies may not yet be available at the scale required to supply the existing vehicle fleet. Therefore, they cannot be used to assess the environmental impact of current vehicle technologies without considering a realistic evolution of the hydrogen and CNG mixtures over time in a specific geographical area.

Limiting consideration to a single fuel neglects a degree of freedom necessary to minimize the environmental impact of a particular vehicle application, as it restricts the ability to leverage fuel availability. For instance, in the case of HCNG fuel blends, the current limited availability of hydrogen can be offset by excess natural gas production. Moreover, because both fuels

are gaseous, they can be utilized with relatively minor modifications to the propulsion system. Consequently, the adoption of HCNG blends offers a promising avenue to enhance vehicle performance and mitigate environmental impact.

In this field, Gupta et al. [68] conducted a comprehensive life cycle analysis of a heavy-duty vehicle powered by HCNG. The study focused on evaluating a 20% gaseous hydrogen blend in terms of net energy ratio, GHG emissions, and cost-effectiveness throughout the entire well-to-wheel cycle. Additionally, in their study [69], Gupta et al. analyzed the well-to-wheel performance of a light-duty truck, considering different blends of hydrogen (0%, 15%, and 30%) within the HCNG mixture.

In the research conducted by Candelaresi et al. [70], they investigate the use of Hythane blends (20% hydrogen and 80% methane by volume) in ICE vehicles (ICEV) and hybrid-EV vehicles. The findings highlight vehicle infrastructure as the primary contributor to the environmental impact. However, vehicles using hydrogen blends with natural gas or gasoline show promise in promoting short-term hydrogen use with emissions reductions compared to conventional vehicles. In another study [71], they compare the environmental life cycle assessment (LCA) of eight-passenger car fleets. These fleets utilize renewable hydrogen and a conventional fuel (natural gas or gasoline) under the same total energy input and hydrogen-to-mixture energy ratio. The proposed strategies achieve a reduction in carbon footprint ranging from 7% to 35% compared to conventional fleets. Nevertheless, none of these studies optimized the hydrogen content in the fuel to minimize the environmental impact of HCNG vehicles by simultaneously considering both fuel production and tailpipe emissions. Therefore, future research and development efforts should focus on optimizing blend compositions and investigating their long-term effects on engine performance, emissions, and overall system compatibility.

3.1.1. Knowledge gaps

Building upon the findings of previous studies, the literature highlights several knowledge gaps, as summarized below:

1. Research on fuel blends is limited: The majority of studies projecting the future environmental impact of fuels primarily concentrate on single, unmixed compositions [32, 58–61]. There is a notable absence

of extensive literature dedicated to investigating the effects of fuel blends, especially in the case of HCNG, across a broad spectrum of mixtures.

2. Heavy-duty Application Focus: The majority of studies on HCNG predominantly center around heavy-duty applications [68, 69]. There is a scarcity of research exploring the potential of HCNG in other sectors or applications.

3. Relying on Literature-Based Estimations: A few of the identified studies rely on experimental results when estimating fuel consumption and emissions in the operational phase of the life cycle assessment. Instead, estimations are predominantly based on existing literature, indicating a need for more empirical data in this aspect [70, 71].

Based on the previous considerations, it becomes evident that combining engine experiments with life cycle assessment is essential to predict a realistic scenario where HCNG-powered engines for automotive applications could play a significant role in global decarbonization. For this reason, this study aims to evaluate the environmental impact of HCNG light-duty vehicles from 2020 to 2050, using realistic scenarios that can indicate the optimal transition strategy for decarbonizing the transportation sector with HCNG, hydrogen, and CNG-fueled vehicles.

3.1.2. Contribution and objectives

The motivation behind this study is to assess the environmental impact of HCNG-powered vehicles in realistic scenarios and to optimize this technology for the purpose of decarbonizing the transportation sector during the transition towards a hydrogen-based economy. The specific contributions aimed at achieving this objective include:

- Quantifying the impact of using different blends of Hydrogen-Compressed Natural Gas (HCNG) on fuel consumption and emissions in a light-duty vehicle's internal combustion engine (ICE).
- Analyzing the potential cradle-to-grave emissions of HCNG vehicles depending on the energy, NG and H_2 mix evolution.
- Determining the optimal HCNG blend for minimizing cradle-to-grave emissions between 2020 and 2050 and provide recommendations regarding the optimal transition from CNG to H_2.

- Identifying the biogas requirements for achieving zero cradle-to-grave emissions, if feasible.

3.2. Methodology

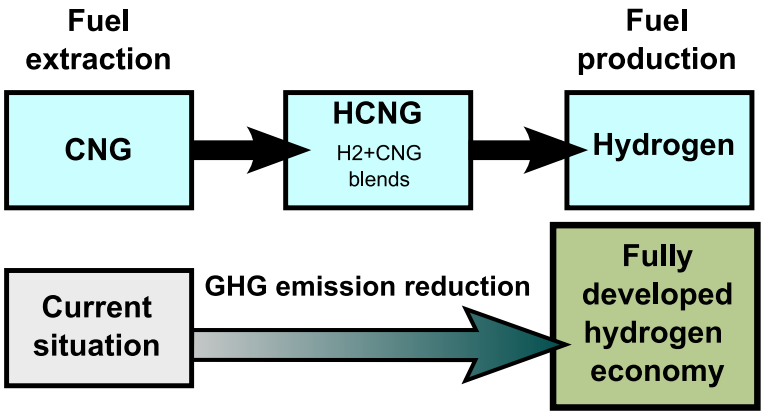

Figure 3.1: Diagram of the proposed method based on the fuel transition.

Recognizing the imperative of transitioning from fossil fuels to hydrogen, it is essential to underscore the gradual nature of this process, emphasizing that such a transformation cannot be instantaneous. A noteworthy challenge lies in the absence of a dedicated hydrogen infrastructure; however, the existing natural gas infrastructure holds promise as a viable interim solution. Particularly noteworthy is the capability of the natural gas grid in the European Union to transport up to 12% of the hydrogen volume and, in the United States, up to 15% [111]. Given these considerations, strategic utilization of the current natural gas infrastructure emerges as a prudent approach to expedite the shift away from fossil fuels towards a hydrogen-based energy paradigm. A gradual approach is sought through blends with fossil fuels, with CNG acting as the representative fossil fuel, as presented in figure 3.1.

Observations have indicated that HCNG offers advantages in terms of reducing typical emissions such as CO, NO_x, and unburned hydrocarbons. However, the performance of HCNG varies depending on specific circumstances, engine types, and operational modes.

Five scenarios are proposed to characterize this transition: pure CNG, a blend of 75% CNG and 25% H_2, a blend of 50% CNG and 50% H_2, a blend of 25% CNG and 75% H_2 by mass, and finally, pure H_2. These scenarios aim to define a gradual progression towards hydrogen economy.

3.2.1. Experimental tools

The experimental study was conducted on a research engine with a single cylinder and a spark ignition system. The engine was equipped with a port fuel injection system. The specifications of the engine used in this campaign were identical to those employed in previous research works [1, 8]. The most relevant data are listed in Table 4.1 for reference. The test cell used in this research is illustrated in Fig. 4.1, which features a modified layout to accommodate the implementation of dual gaseous fuel strategies.

To enhance precision in the injection and mixing procedures, a pair of Zavoli JET Injectors were utilized to separately inject the fuels into the intake manifold. These injectors boast a maximum pressure of 4.5 bar and have been engineered to operate within a temperature range of -40 ºC to 120 ºC. The discharge nozzle of each injector measures 3 mm in diameter.

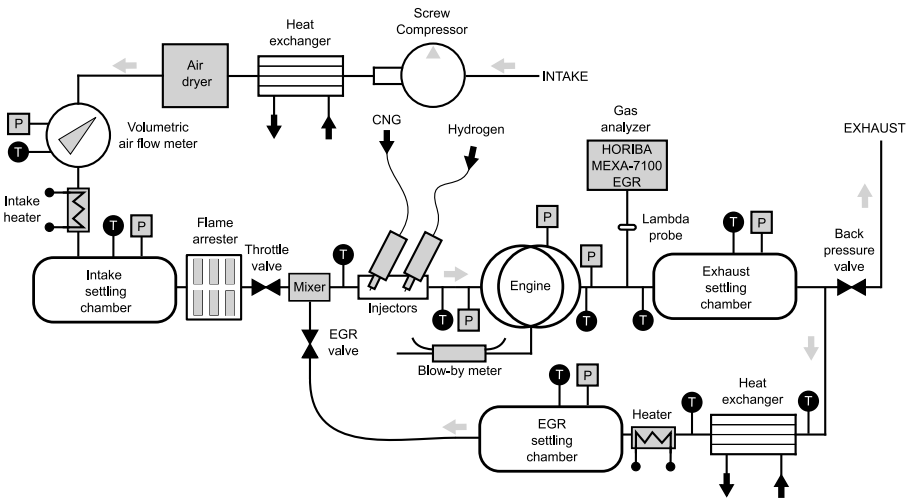

Figure 3.2: Test bench layout.

Exhaust gas composition measurements, including O_2, CO, CO_2, HC, and NO_x, were conducted using a gas analyzer HORIBA MEZA 7100 DEGR. To facilitate the analysis, a sample of exhaust gases from the settling chamber was directed through a pre-heated pipe maintained at 150°C to the gas

Number of cylinders	1
Displaced volume	454.2 cm^3
Stroke	86.0 mm
Injection systems	PFI
Ignition system	Spark plug
Cylinder diameter	82.0 mm
Compression ratio	10.7
Connecting rod length	144.0 mm
Valves per cylinder	2 intake, 2 exhaust
Engine management system	AVL PREMS GDI
Combustion system	4-valve pent roof GDI
IVO*	-380 CAD
IVC*	-135 CAD
EVO*	-600 CAD
EVC*	-338 CAD

*with respect to the firing TDC (0 CAD)

Table 3.1: Main engine specifications

analyzer. For the measurement of instantaneous in-cylinder pressure, a piezoelectric sensor was used. Piezoresistive sensors, on the other hand, were employed to measure intake and exhaust pressures. To control the mass flow rate of both fuels, two flowmeters were employed: the Bronkhorst F-113AC-1M0-AAD-55-V for hydrogen and the F-113AC-M50-AAD-55-V for CNG. The experimental facilities provided comprehensive control over all relevant parameters. Boost conditions were achieved through an external compressor, and exhaust back pressure was regulated by a knife-gate valve positioned in the exhaust line.

The accuracy of the instrumentation used in the study can be found in Table 4.2. Table 4.3 presents the precision of the gaseous pollutant measurements using the HORIBA device.

Compressed natural gas used in this study was sourced directly from the Spanish natural gas network. The composition of CNG consisted of 89.95% methane, 6.27% ethane, and other impurities. On the other hand, hydrogen was provided in pressurized tanks. Additional information regarding the characteristics of both fuels can be found in Table 3.4.

Engine and combustion-related output parameters, such as indicated mean effective pressure (IMEP), cycle-to-cycle variability expressed by the IMEP covariance (COV_{IMEP}), emission levels, and indicated efficiency, were computed using an in-house combustion diagnostics tool [94]. The tool was adapted for hydrogen, CNG, and HCNG fuel blends. The combustion diagnosis tool referenced in this study employs an estimation approach to

Signal (High frequency)	Sensor	Specification
In-cylinder pressure	Piezoelectric sensor	0 to 250 bar ± 0.3% linearity
Intake pressure	Piezoresistive sensor	0 to 10 ± 0.001 bar
Exhaust pressure	Piezoresistive sensor	0 to 10 ± 0.001 bar
Variable (Low frequency)	**Sensor**	**Specification**
Engine Speed	Optical angular encoder	1 to 6000 ± 1 rpm
Engine Torque	Strain-gauges torque-meter	-200 to 200 ± 1 N m
Intake pressure	Piezoresistive transducer	0 to 10 bar ± 1%
Exhaust pressure	Piezoresistive transducer	0 to 10 bar ± 0.3%
Intake temperature	Thermocouple type K	0 to 1000 ± 0.5 °C
Exhaust temperature	Thermocouple type K	0 to 1000 ± 0.5 °C
Fluid temperature	Pt100 thermoresistance	-200 to 850 ± 0.3°C
Air mass flow	Air flow meter	0.6-100 m^3/h ± 1%
Hydrogen mass flow	Thermal mass flow meter	200-1600 l/min (based on N_2) ± 0.5 %
CNG mass flow	Thermal mass flow meter	200-1600 l/min (based on N_2) ± 0.5 %

Table 3.2: Instrumentation accuracy.

Pollutant	Analyzer	Range	Accuracy
HC	FID	min. 0 to 10 ppm C max. 0 to 50 kppm C	± 3%
NO_x	CLD	min. 0 to 10 ppm max. 0 to 10 kppm C	± 3%
CO	NDIR	min. 0 to 3 kppm C max. 0 to 12 vol%	± 3%
CO_2	NDIR	min. 0 to 5 kppm C max. 0 to 20 vol%	± 3%
O_2	PMA	min. 0 to 5 vol% max. 0 to 25 vol%	± 3%

Table 3.3: Accuracy levels of HORIBA MEXA 7100 DEGR for measurements of gaseous pollutants.

Properties	CNG	H_2
RON	120	130
AF_{st}	16.00	34.3
LHV	46.87 MJ/kg	119.9 MJ/kg
H/C	3.79	-
O/C	0.026	-
Molar mass	17.77 g/mol	2.01 g/mol
Purity	-	≥ 99.9%

Table 3.4: Specifications of CNG and H_2 fuels.

calculate the energy released during combustion. This estimation is achieved by solving the energy equation using the measured in-cylinder pressure while making certain simplifying assumptions. One such assumption is the consideration of uniform pressure and temperature distributions throughout the entire combustion chamber. Additionally, simplifications are made to estimate the heat transfer to the cylinder walls and other related factors. To enhance accuracy in the calculations, the combustion diagnosis tool has undergone modifications, as described in previous work by Benajes et al. [95]. These modifications were implemented to reduce errors associated with the estimation process. Originally, the model considered three distinct components: air, fuel, and combustion products. However, the current version of the model treats the fuel component as a single hydrocarbon entity ($C_xH_yO_z$) with equivalent properties to those of the actual fuel mixture.

3.2.2. Life cycle assessment

The environmental impact of HCNG vehicles according to their H_2-CNG mixture is evaluated by means of a life cycle assessment (LCA). An LCA consists of evaluating the environmental impact of a given technology by including the emissions produced during its operation, its manufacturing and the production of the fuel required for its operation or any combinations of these processes. This methodology can be applied in different scenarios to understand how a given technology would perform depending on factors such as the carbon intensity in the energy mix of a given country. In the case of the automotive industry, a cradle-to-grave LCA implies calculating the emissions associated with the manufacturing of all the components of the vehicle, quantifying/measuring the emissions produced during its operation and those generated during the production of the energy carrier used in the vehicle, be it electricity, H_2 or any other fuel. Therefore, cradle-to-grave LCAs provide a fair basis for comparison of transportation technologies fuelled with alternative fuels by avoiding any bias coming from the omission of a given stage of the life cycle.

The first step of an LCA is to define the scenarios under study in terms of the fuel mixtures, time, and geographic location since these factors influence vehicle manufacturing and fuel production emissions. Then, the boundaries and environmental flows are selected since they define the processes included in the LCA which emissions are to be considered as part of the life cycle of the vehicle as well as the inputs and outputs that are taken from and released to the environment. Then, the functional unit is selected as the unit corresponding to the amount of emissions provided in the study. For

instance, if the functional unit is 1 vehicle and 150000 km, then it means that for the overall LCA all the emissions results will correspond to the manufacturing of 1 vehicle and its operation during 150000 km. The impact categories are then defined as the type of environmental impact quantified in the study. Finally, the life cycle inventory, which defines the data and its source used for the LCA, is presented.

In this study, this methodology is only applied to evaluate the global warming impact of the technology since the main purpose of transitioning towards these vehicles is to mitigate the GHG. And, since considering other impact categories in the numerous scenarios considered would result in an incomprehensible amount of information with unclear conclusions.

3.2.2.1. Scenarios definition

The scenarios considered in this study comprise a set of possibilities whose impact on the LCA is sometimes grouped in error bars and sometimes differentiated clearly. These scenarios and their impact on the environmental flows and production pathways are:

- Geographic: Europe.
- Temporal: 2020, 2030, 2040 and 2050.
  - Impact 1: Electricity mix evolution.
  - Impact 2: H_2 mix evolution [112].
  - Impact 3: Natural gas composition evolution [113].
- Strategic towards the use of natural gas: SDS and STEPS.
  - Impact: biogas fraction in the natural gas mix (Fig. 3.3). [113]
- Strategic towards the H_2 economy: Steam methane reforming (SMR) and Electrolysis dominant.
  - Impact: dominant technologies in the H_2 production pathway (Fig. 3.4) [112].

The evolution of the electricity mix together with its uncertainty was obtained from the Sphera professional database according to the energy trends, the NI (no improvements) and the SI (significant improvements) scenarios. In the NI scenario, there is no improvement in the sustainability policies with time while the SI scenario implies a significant improvement

in the sustainability policies compared to the current policies. The carbon intensity in the electricity mix, i.e., the GHG emissions per kWh of consumed electrical energy, was used as an input for all the processes in the CNG, H_2 and vehicle components production. An average value from the energy trends, NI and SI scenarios was considered while the highest and lowest values were used to compute the emissions uncertainty on such processes.

The source of the natural gas has a significant impact on the well-to-tank emissions. If the source of the natural gas is a byproduct or waste from other chemical processes (water sludge, for example), then its environmental impact is computed as the emissions produced in the process of capturing and processing it minus the hypothetical impact of releasing it to the environment, since that would be representative of an "inaction" scenario. Therefore, since the global warming potential (GWP) of CH_4, which is the major gas in NG mixtures, is significantly higher than that of CO_2, it is possible to find negative emissions in the well-to-tank and even in the well-to-wheel processes. Nonetheless, it is imperative to develop a careful analysis of these negative emissions to avoid any undesirable bias towards biogas.

Given the relevance of accounting for these negative emissions, it is imperative to identify the fraction of the natural gas that comes from conventional gas (extraction from natural resources) and from biogas (from processes of natural origin that otherwise would be released to the environment). This was considered in this study by means of two potential scenarios, defined as STEPS and SDS, following the report issued by the International Energy Agency about the prospects for the evolution of the natural gas and biogas mix worldwide [113]. The natural gas mix and its expected evolution with time is presented in Fig. 3.3. As with the energy mix, the average natural gas mix between these scenarios is used as an input for the H_2 and CNG production pathways while the upper and lower values in terms of emissions are considered as the uncertainties.

The H_2 mix evolution depending on whether the electrolysis-dominant or SMR-dominant scenarios are considered was obtained from the Hydrogen Roadmap for Europe [112]. The breakdown in the H_2 production pathway source is presented in Fig. 3.4.

The combination of this set of scenarios implies that the final results in terms of cradle-to-grave emissions account for the uncertainty of the environmental impact to the energy, natural gas and H_2 mixes in the major pathways, thus providing a clear picture about the future trends and the expected uncertainty. This is expected to permit the identification of the

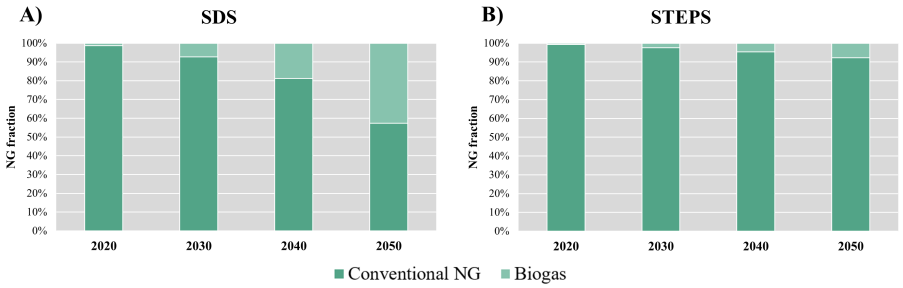

Figure 3.3: Time evolution of the natural gas fraction obtained from conventional gas and biogas in the SDS (A) and STEPS (B) scenarios.

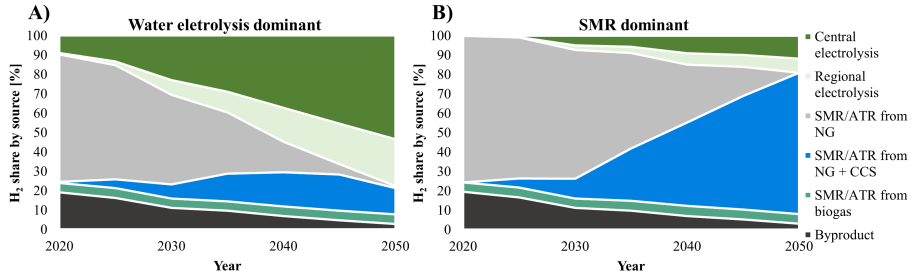

Figure 3.4: Evolution of the H_2 production pathway breakdown from 2020 to 2050 following the electrolysis-dominant (A) and SMR-dominant (B) scenarios proposed by the EU [112].

optimal HCNG mixture and provide recommendations about how the HCNG vehicles should evolve in the coming decades to imply lower emissions than CNG and H_2 ICEV if possible.

3.2.2.2. Boundaries and environmental flows

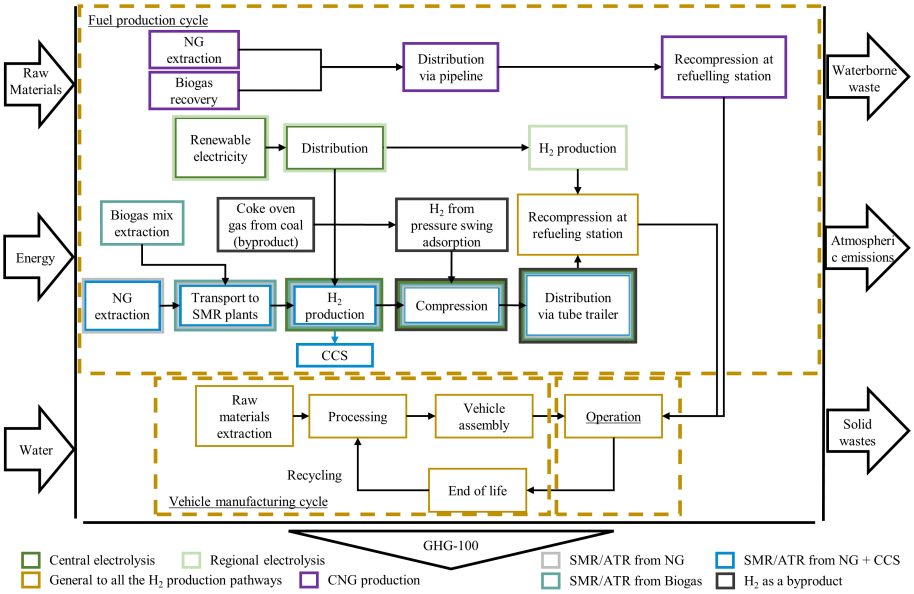

Figure 3.5: System boundaries and environmental flows.

The boundaries of an LCA define the processes involved in the production pathways that contribute to the environmental impact under study. The inputs and outputs that come directly from the environment are called environmental flows and can be raw materials, water, or pollutants, among others. The boundaries and environmental flows considered in this study are presented in Fig. 3.5. As it can be seen, the boundaries comprise the extraction of raw materials, their processing, and their use in the vehicle during the operation phase. In Fig. 3.5, it is possible to differentiate the different processes associated with the H_2 production pathways attending to the colors. The reader should note that in this study there are several H_2 production pathways according to the mixes in Fig. 3.4. One of the key novelties of this study is that, despite not proposing any novel hydrogen production method, a combination of hydrogen production pathways that is representative of the current and future scenarios, following the hydrogen

roadmap in Europe, was proposed. Furthermore, these production pathways are combined with different electricity mix and natural gas mix scenarios, thus providing an integral LCA framework that can be used to identify the potential cradle-to-grave emissions of HCNG vehicles in the 2020-2050 period and the uncertainty associated with the evolution of such mixes. The processes included in this study are presented in Fig. 3.5, the hydrogen mix scenarios in Fig. 3.4, the natural gas mix scenarios in Fig. 3.3 and the electricity mix scenarios were extracted from LCA for experts (Sphera professional) database and described in section 3.2.2.1.

3.2.2.3. Functional unit

The functional unit of this study depends on the part of the life cycle under analysis. For the well-to-tank part, the functional unit is 1 kWh of energy contained in the fuel, considering its lower heating value. In the cradle-to-gate, the functional unit is 1 vehicle produced. For the tank-to-wheel and well-to-wheel phases the functional unit is a lifetime of 150000 km. Finally, for the cradle-to-grave process, all the emissions are referred to 1 vehicle produced and a lifetime of 150000 km.

3.2.2.4. Impact categories

The impact category considered is global warming by means of greenhouse gases and their effect in a 100-year horizon (GHG-100). Other impact categories were not considered since an extensive analysis of this pollutant is explored in so many dimensions and scenarios that including further impact categories may affect the readability of this study. Furthermore, GHG were considered since mitigating the global warming impact is the main motivation behind transitioning towards the Hydrogen Economy and more sustainable fuels. Therefore, considering this impact category is completely in line with the objectives of this study.

3.2.2.5. Life cycle inventory

The life cycle inventory used in this study is based on the databases of GREET® v2022 and Sphera Professional. First, the software Sphera Professional (LCA for experts) together with the professional database was used to obtain the carbon intensity of the EU scenarios from 2020 to 2050. The carbon intensities considered in each of the timeframes are three: those predicted from the energy trends report (ETS) according to the European

Commission forecasts [114], those in a scenario where there are no improvements in the sustainability policies, and those in the scenario where there are significant improvements in the sustainability policies as defined in the Sphera Professional database.

Then, the electricity from these mixes and their associated carbon intensity was used as an input for the GREET® model in all the production pathways, including those for CNG, H_2, and the vehicle components. The combination of both tools enabled obtaining the cradle-to-gate and well-to-tank emissions of the HCNG vehicles and the associated uncertainty caused by the variability in future scenarios.

3.2.2.6. Limitations and hypotheses

The main scope of the paper is to understand the environmental impact of HCNG vehicles and its uncertainties in the long term with the scenarios proposed by the EU in terms of the electricity, NG, and H_2 mixes. This will provide an understanding of which HCNG mixture should be used as time goes by to minimize the environmental impact of light-duty vehicles and what these scenarios mean in terms of actual GHG emissions. Nonetheless, this study comprises the same hypothesis and assumptions behind these scenarios. The main assumption is that there is enough energy, natural gas, biogas, and H_2 to cover the fuel demand of the HCNG vehicle fleet, be it because the production is increased or because the fuel demand of the fleet is small. Therefore, it is not within the scope of the paper to indicate whether the considered scenarios are realistic, but rather to identify the implications of environmental impact for the HCNG vehicles in case they are fulfilled. Furthermore, the analysis is mainly focused on the environmental impact of HCNG vehicles, so there is no cost analysis depending on the blend. This is out of the scope of this study and is left for future work.

Other relevant hypotheses included in the LCA are:

- The investigation primarily centers on mid-size passenger vehicles, given their predominant representation within the contemporary vehicular fleet.
- The constancy of fuel production and engine technologies over time is assumed, notwithstanding fluctuations in the significance of individual production pathways. Consequently, the emissions projections associated with these factors in the EU 2050 scenario may exhibit slight under or overestimation.

- The emissions stemming from the manufacturing processes of the machinery and devices employed in energy source generation and vehicle production are omitted from consideration. The emissions generated during the transportation of materials between factories for the vehicle manufacturing cycle are neglected as well. These omissions are deemed inconsequential in the context of the overall vehicle life cycle emissions, as the machinery in question is consistently utilized in the industry for the production of alternative vehicles or the generation of H_2.

3.3. Fuel consumption of HCNG vehicles

This section shows the process of obtaining the fuel consumption of CNG, HCNG blends, and H_2 vehicles, starting from the experimental data to the derivation of the fuel consumption values.

3.3.1. Engine fuel consumption and emissions

To evaluate the fuel consumption and performance of a representative engine, the authors referred to previous investigations that utilized a contemporary engine platform designed for light-duty applications. The experimental database was constructed using a single-cylinder version of a turbocharged spark-ignition engine equipped with port fuel injection and a variable valve timing (VVT) system [8]. The engine fuel consumption was measured across various conditions, including different fuel compositions, air-based dilutions, ignition timings, and engine loads. Specifically, the study in [1] measured HCNG fuel blends containing 25%, 50%, and 75% hydrogen (by mass percentage), along with CNG and hydrogen fuels. The operating conditions, determined by engine speed and load, were set at 1500 rpm and loads ranging from 4 to 10 bar of IMEP.

Within the entire measured range, operating settings were optimized to minimize fuel consumption. In this context, air dilution and ignition timing were fine-tuned for each combination of fuel composition and operating conditions. This approach enabled the estimation of optimal fuel consumption for each HCNG fuel under varying operating conditions.

For CNG, only stoichiometric conditions (no dilution) were employed to operate a three-way catalyst (TWC) in the vehicle, a state-of-the-art technology for pollutant reduction and regulatory compliance. Blends containing hydrogen necessitated higher dilution ratios due to the unique combustion characteristics of hydrogen. This phenomenon has been previously noted by

several researchers [98, 100, 101], who argued that thermal losses are the primary contributors to reduced efficiency and performance when comparing hydrogen to other fuels. To maintain high engine efficiency, significant dilution, whether with air or exhaust gas recirculation, is essential. Consequently, an alternative after-treatment technology is required instead of the traditional TWC. Here, an oxidizer catalyst should be employed to reduce unburned fuel, accompanied by a selective catalytic reduction (SCR) system to mitigate NO_x emissions, as illustrated in Fig. 3.6. Recent studies suggest that these catalysts can be supplied with H_2 [115, 116], potentially eliminating the need for liquid urea refueling and addressing ammonia slip issues.

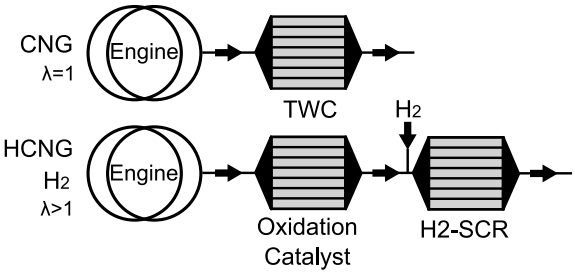

Figure 3.6: Schematic representation of the after-treatment systems.

A sample from the referenced database is presented in Figs. 3.7 and 3.8. These graphs illustrate the impact of hydrogen blending on CNG, revealing an enhancement in IMEP and GIE as hydrogen content increases in the fuel blend. This improvement primarily stems from the higher λ achieved due to the combustion properties of hydrogen, enabling ultra-lean, stable combustion ($COV_{IMEP} > 3\%$). For pure hydrogen fuel, the optimal air dilution reaches $\lambda = 3$, resulting in a reduction in thermal losses. Similar optimal λ values are reached for 25%, 50%, and 75% H_2. However, efficiency gains are slightly reduced for 50% and 75% HCNG blends, and the performance is diminished compared to the 25% HCNG blend.

Increased air dilution also has a positive impact on pollutant emissions, diminishing levels of CO and NO_x emissions. Carbon monoxide undergoes oxidation and transformation into carbon dioxide, while lower combustion temperatures impede the formation of NO_x due to thermal generation mechanisms. Specific carbon monoxide (ISCO) emission levels decrease from approximately 70 g/kWh with pure CNG to around 1 g/kWh at 25%

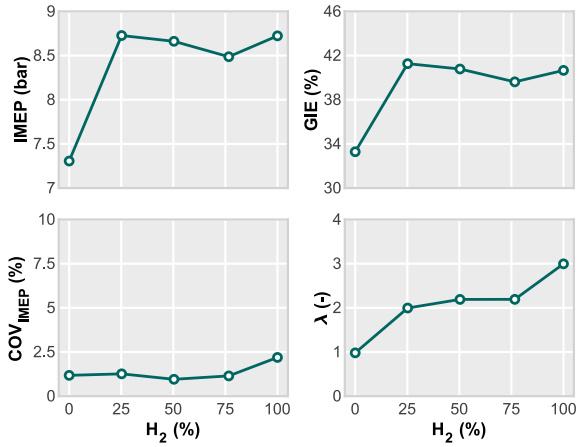

Figure 3.7: Impact of hydrogen substitution percentage on engine performance.

HCNG, while NO_x emissions exhibit a reduction of approximately 35% under these conditions. This effect is evident in Fig. 3.8, where both CO and NO_x emission values decrease due to the higher optimal dilution.

Furthermore, the substitution of CNG with hydrogen results in a reduction in all carbon-based emissions (CO, CO_2, and HC). However, even in the case of pure hydrogen, the net CO_2 emission is not zero due to the combustion of lubricant, as highlighted in a previous study [103].

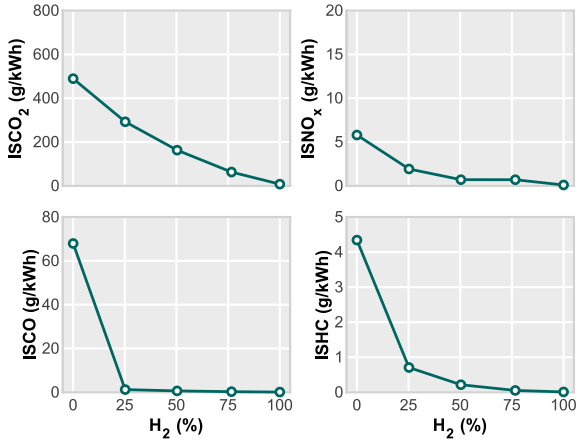

Figure 3.8: Impact of hydrogen substitution percentage on exhaust gas emissions.

3.3.2. Vehicle fuel consumption and emissions

The vehicle utilized for the overall fuel consumption estimation was the FIAT Panda Natural Power, and the World Harmonized Light-duty Vehicle Test Procedure (WLTP) was employed to represent real driving conditions. This vehicle is equipped with an engine platform designed for CNG operation, sharing similar geometrical characteristics with those used in the preceding section to characterize the engine fuel consumption under steady bench conditions.

The estimation of vehicle fuel consumption took into account the engine database described in the previous section and the stoichiometric CNG operation reference point obtained from [117]. Consequently, the vehicle fuel consumption, considering both fuel components (CNG and H_2), under realistic conditions was scaled based on the difference obtained from this reference point to the conditions measured for each fuel blend composition. The summarized results are presented in Table 3.5.

Design Nº	1	2	3	4	5
% H_2	0	25	50	75	100
% CNG	100	75	50	25	0
H_2 (kg/100 km)	0	0.52	0.83	1.06	1.17
CNG (kg/100 km)	3.5	1.55	0.83	0.35	0

Table 3.5: WLTP Fuel consumption of the H_2 and CNG

Moreover, a correlation was established between the quantity of hydrogen present in the fuel and the amount of CO_2 emitted during the process. This data is depicted in Fig. 3.9, enabling a rapid estimation of CO_2 emissions as a function of the hydrogen content. Additionally, the relationship between the consumed CNG and the generated CO_2 was also established, revealing a clear linear trend.

3.4. Environmental impact of HCNG vehicles

This section is aimed at presenting the results related to the environmental impact of HCNG vehicles in each phase of the life cycle: cradle-to-gate (section 3.4.1), well-to-tank (section 3.4.2), tank-to-wheel (section 3.4.3), well-to-wheel (section 3.4.4) and cradle-to-gate (section 3.4.5).

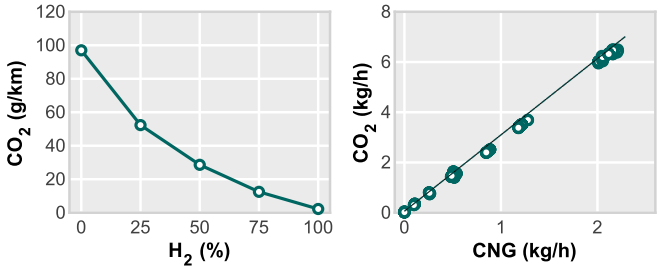

Figure 3.9: Correlation obtained for CO_2 emissions estimation as a function of H_2 percentage in the fuel and consumed amount of CNG.

Design N°	1	2	3	4	5
% H_2	0	25	50	75	100
% CNG	100	75	50	25	0
H_2 capacity [kg]	0	2.07	3.31	4.42	4.67
CNG capacity [kg]	14	6.21	3.31	1.41	0

Table 3.6: Capacity of the H_2 and CNG tanks for a range of 400 km.

3.4.1. Cradle-to-gate emissions

The cradle-to-gate emissions are those associated with the manufacturing phase of the life cycle. In the case of the HCNG vehicles considered in this study, they are expected to operate with the same CNG-H_2 mixture during the whole operation. Therefore, the capacity of their CNG and H_2 tanks should be fixed for each mixture. Considering the fuel consumption results derived from the experimental data in section 3.3 and a target range of 400 km the capacity of the tanks was estimated as in Table 3.6.

These capacities were used to calculate the mass of the tanks to estimate the emissions associated with their production. For the CNG tanks, their mass was correlated to their capacity following the database in [118] for CNG cylinders of type 2. For the H_2 the mass was calculated considering a gravimetric capacity of 0.055 kg H_2/kg system for type IV tanks that store gas at 700 bar based on the technical targets provided by the Department of Energy [119].

Figure 3.10 shows the GHG emissions and how they would evolve with the expected energy mix decarbonization from 2020 to 2050 for the CNG-pure and the H_2-pure vehicles. The emissions associated with the production of 1 vehicle powered only with CNG (Fig. 3.10A) are lower in all the time scenarios than those associated with the production of a vehicle running purely on H_2 (Fig. 3.10B). This is due to the additional materials required

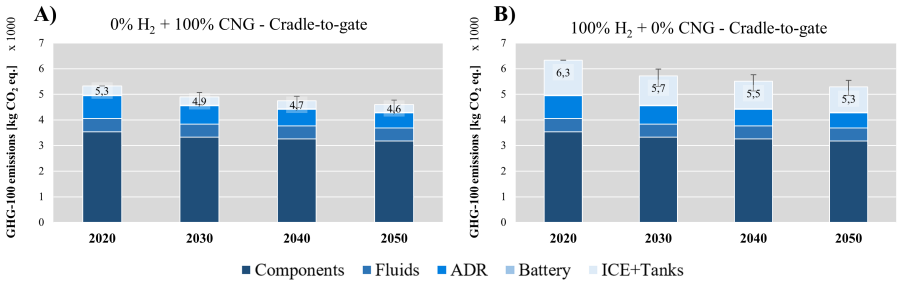

Figure 3.10: Cradle-to-gate emissions of the target vehicle only with 0% H_2 and 100% CNG (A) and with 100% H_2 and 0% CNG (B). Evolution from 2020 to 2050.

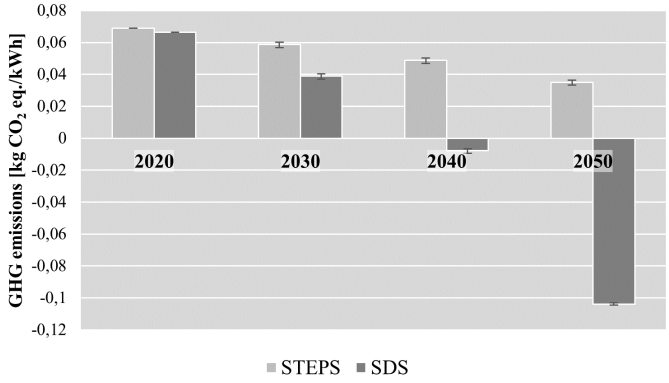

Figure 3.11: Well-to-tank emissions of CNG production from 2020 to 2050 in the SDS and STEPS scenarios.

by the H_2 tanks since they need to resist higher gas pressures. Between these two vehicle concepts, the cradle-to-gate emissions of the H_2-fueled vehicle compared to the CNG vehicle are 18.9% higher in 2020 while they are only 15.2% higher in 2050, meaning that the production of H_2 tanks is more energy-consuming than the production of CNG tanks since they are more affected by the energy mix carbon intensity.

In the case of pure CNG vehicles, the emissions in the manufacturing phase range from 5.3 tonnes of CO_2 eq. in 2020 to 4.6 tonnes in 2050 while for H_2-pure vehicles this phase implies 6.3 tonnes in 2020 and 5.3 tonnes in 2050. As explained previously, the carbon intensity has a greater impact on the H_2-powered vehicles (1 tonne of CO_2 of difference against 0.7 tonnes for the CNG vehicle) since the manufacturing of the storage system requires more energy.

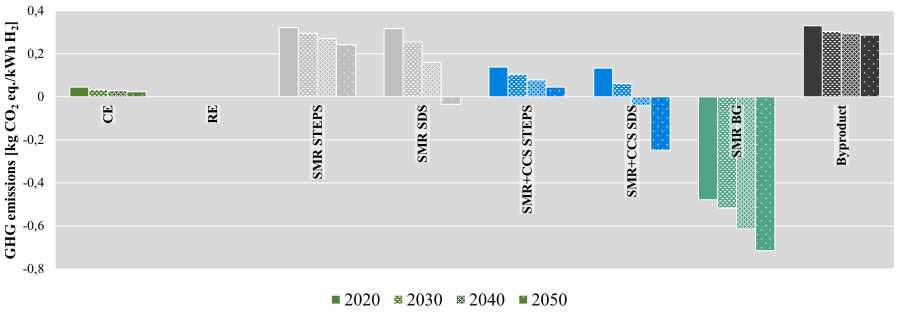

Figure 3.12: Well-to-tank emissions the different H_2 production pathways proposed by the EC from 2020 to 2050

3.4.2. Well-to-tank emissions

The well-to-tank emissions are those related to the processes in the "fuel production cycle" box in Fig. 3.5. They involve all the processes required to produce either H_2 or CNG, treat them, and distribute them to the refueling station. In this case, since the H_2 comes from a mix of production pathways it is necessary to consider all the production strategies independently and estimate the well-to-tank emissions as a weighted average.

In this study, CNG and H_2 are considered as different fuels for different reasons. The first reason is that NG is used as an input for SMR processes in the H_2 production. Therefore, if any modification should be added to the NG mix used in the vehicle, it should consistently be considered in any other process as well. The second reason is that it provides a higher degree of flexibility to generate mixes of each fuel according to the production pathways and mixes of both fuels combined (HCNG).

Regarding the CNG production, the well-to-tank GHG emissions per kWh of CNG are presented in Fig. 3.11 for the SDS and the STEPS scenarios. These two scenarios were defined in Fig. 3.3A and Fig. 3.3B, being the former the scenario representing a higher share of biogas in the natural gas mix. As a consequence, the well-to-tank emissions in the SDS scenario are always lower than in the STEPS scenario. From 2040, the biogas percentage in the natural gas mix reaches 19% and the well-to-tank emissions turn negative, reaching a value close to -0.1 kg CO_2/kWh in 2050. The reader should note that, despite the negative emissions in the well-to-tank process, consuming CNG during the operation phase implies releasing CO_2 emissions. Therefore, it does not mean that the well-to-wheel nor the cradle-to-grave

emissions are negative. The small uncertainty in this figure comes from the energy mix. These uncertainties are low since CNG production requires relatively low electricity.

The well-to-tank GHG emissions of each H_2 production pathway and how they change with the time scenarios that include changes in the electric and NG mixes are found in Fig. 3.12. In this figure, the negative emissions when producing H_2 are only achieved when it is produced from biogas, either partially or totally. In this sense, the lowest emissions are found when the H_2 is produced from SMR fed with biogas since it is considered that a significant amount of biogas is consumed instead of released to the atmosphere. The SMR pathways are classified as grey (without carbon capture and storage or CCS) or blue (with CCS) and are evaluated in the STEPS and SDS scenarios. In the case of grey H_2, the well-to-tank emissions are higher than for most of the production pathways except in the 2050 SDS scenario, in which the amount of biogas in the NG mix reaches 43%. The reader should note that these scenarios are those proposed in the different roadmaps to improve the sustainability of the current and alternative fuels, but they may not be realistic unless significant investment is produced while the technology is widely integrated into all the processes where biogas can be retrieved.

Blue H_2, i.e., produced from SMR with CCS, implies less than half the amount of GHG emissions than SMR in the 2020 scenario and far more negative emissions than grey H_2 since around 90% of the CO_2 released in the reforming process is captured.

Green H_2 is divided into H_2 produced from central electrolysis (CE) or regional electrolysis (RE). In both pathways, since the axiom of green H_2 is that it is produced from renewable energy, it is assumed that there is any amount of energy where the H_2 is produced and all the on-site processes are powered with renewable energy are. Therefore, in the case of CE, the H_2 production, treatment and compression to be loaded into the tube trailers for distribution is powered with renewable energy while there are CO_2 emissions produced by the truck transporting the fuel and the recompression at the refueling station is powered with the electricity mix. In contrast, in this study, RE implies the production of H_2 at the refueling station. Hence, all the processes, including the total compression of the fuel can be covered with renewable energy since there should be a renewable energy production facility nearby for it to be green. Hence, the environmental impact of H_2 produced from RE is nearly zero. Again, the reader must note that this is

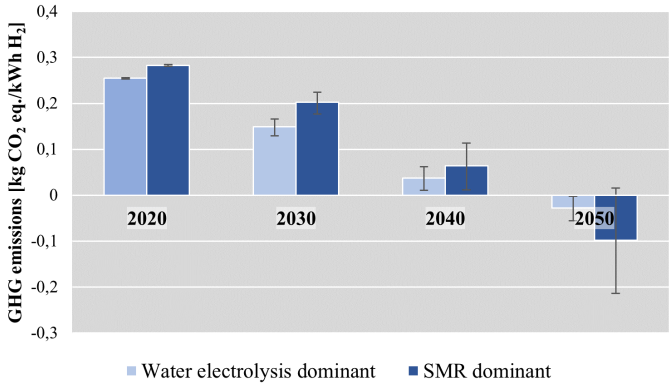

Figure 3.13: Well-to-tank emissions of H_2 production from 2020 to 2050 in the electrolysis-dominant and SMR-dominant scenarios

only due to the fact that the manufacturing of the equipment to produce the H_2 is left out of the boundaries as in Fig. 3.5, which is the usual approach for cradle-to-grave LCA for transport applications.

Among all the production pathways, that in which the H_2 is produced as a byproduct implies the highest emissions since its production implies the release of emissions from the same source it is produced. Such is the case when it is produced from coke oven gas, captured and then purified.

The information in Fig. 3.12 combined with the evolution of the H_2 mixes in the water electrolysis and SMR dominant scenarios (Fig. 3.4) is then used to estimate the well-to-tank emissions per kWh of H_2 produced in Fig. 3.13. As it can be noted, here the STEPS and SDS scenarios for the NG mix are condensed into average values and error bars to identify the variability in the actual well-to-tank emissions for H_2 production. The results in Fig. 3.13 show how in the early stages of the transition towards the Hydrogen Economy (2020-2040), the water electrolysis dominant scenario implies on average lower emissions than the SMR-dominant since the use of green H_2 implies lower emissions than considering a higher share of H_2 coming from SMR with or without CCS. Nonetheless, in the 2040 scenario, the combination of the SMR pathway together with the SDS scenario, implying a high content of biogas in the NG mix, makes that the SMR-dominant scenario could offer lower emissions than the water electrolysis dominant scenario, provided that they are not negative yet. It is not until 2050 that the well-to-tank emissions coming from the production of H_2 turn negative for both scenarios, being them lower in the SMR-dominant one due to the high use of the SMR production pathway together with the high share of biogas in the NG mix.

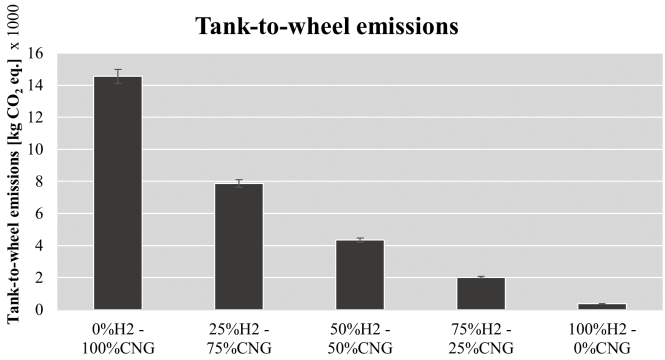

Figure 3.14: Tank-to-wheel emissions for the different HCNG mixtures for a lifetime of 150000 km

Nevertheless, the error bars indicate that depending on the evolution of the electricity mix and the biogas share, the well-to-tank emission of both scenarios could be either similar and lower than zero or the SMR-dominant could provide significantly lower emissions. The negative results in emissions are only possible due to the use of biogas to produce H_2. Therefore, even though green H_2 could imply close-to-zero emissions, the use of biogas and SMR technology must be considered to achieve negative emissions in the well-to-wheel phase and zero emissions in the cradle-to-grave cycle. However, the use of biogas and NG depends on the natural resources availability and on the amount of waste and processes that can be used to retrieve biogas. Despite the increased attention towards green H_2 and the urgent need to enhance its application to reduce the emissions emanating from its production, the energy production sector must shift its focus towards the production and utilization of biogas, provided that there are abundant natural resources available for such production. This shift is critical in pursuit of the ultimate goal of achieving zero-emission vehicles.

Finally, if Fig. 3.11 and Fig. 3.13 are compared, it is possible to identify how in 2020-2040, the well-to-tank emissions per kWh for H_2 are higher than for CNG, and this trend changes from 2040, depending on the NG mix scenario. This will be critical to compute the well-to-wheel emissions, since it may influence the optimal HCNG mixture as a trade-off between the well-to-tank and the tank-to-wheel emissions.

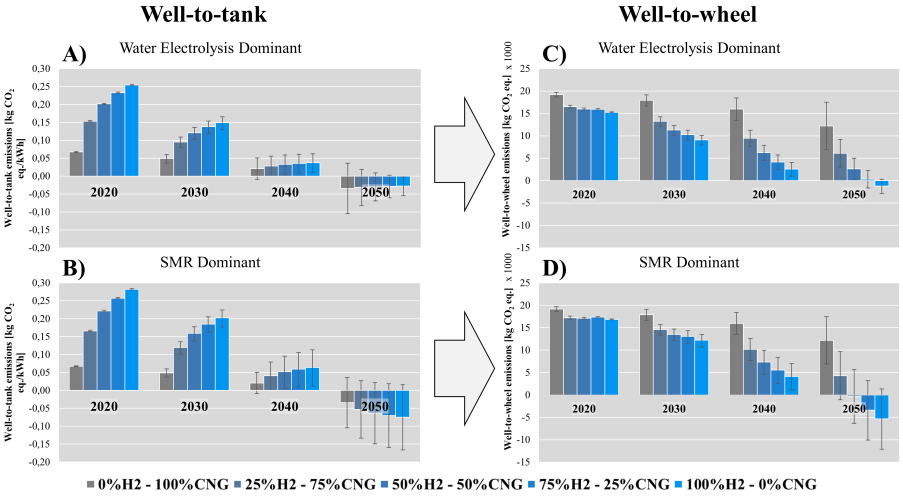

Figure 3.15: Well-to-wheel and well-to-tank emissions of HCNG mixtures from 2020 to 2050 according to both the electrolysis-dominant and the SMR-dominant scenarios. The functional unit for the well-to-tank phase (graphs A-B) is 1 kWh of fuel referenced to their lower heating value while for the well-to-wheel results (graphs C-S) the functional unit is 150000 km of lifetime

3.4.3. Tank-to-wheel emissions

The tank-to-wheel emissions are mainly derived from the experimental results by applying the process described in section 3.3. These GHG emissions are presented in Fig. 3.14 for different HCNG mixtures considering a lifetime of 150000 km. As it is expected, there is a direct correlation between the CO_2 emissions and the carbon content of the fuel. In this sense, the highest change in the tailpipe GHG emissions occurs when comparing pure CNG with the mixture containing 75% of CNG and 25% of H_2 for two reasons. On one hand, although the percentages are in mass terms, the criteria for the mixtures in the experimental campaign was to introduce the same amount of energy at each operating condition so that all the results are comparable and, in case of obtaining higher useful energy, isolate the increase in the efficiency in the combustion process from the addition of more energy in the fuel. Following this methodology with a fuel such as H_2 with a high energy content implies that the amount of CNG introduced in the mixture actually decreases more than 25% compared to the pure CNG case, thus implying a much significant decrease in the fuel carbon content. On the other hand,

there is a significant increase in the indicated efficiency motivated by the addition of H_2, which decreases the fuel consumption for a given driving cycle.

The emissions for the case of 100% H_2 are not zero since there is some CO_2 content produced from burning the lubricant that is required in the combustion engine. Therefore, although these emissions may seem negligible, it would not be correct to address the H_2 ICE as a carbon-free tank-to-wheel emission technology.

This graph, together with Fig. 3.11 and Fig. 3.13 indicates that there would be a trade-off in the well-to-wheel emissions due to how the HCNG mixture affects both the tank-to-wheel and the well-to-tank cycles.

3.4.4. Well-to-wheel emissions

The results in terms of the well-to-tank and well-to-wheel emissions for different HCNG mixtures and vehicles are presented in Fig. 3.15. Both phases are presented in the water electrolysis dominant scenario (graphs A and C) and for the SMR-dominant scenario (graphs B and D).

The emissions associated with the production of the HCNG mixtures show a unique trend for both scenarios from 2020 to 2040. In this timeframe, the well-to-tank emissions are lower for high CNG content mixtures since the share of H_2 produced from biogas or renewable energy is not enough and the additional energy consumption required to produce H_2 outweighs the progress towards a more sustainable H_2 production mix. Nonetheless, in 2050 the fuel production emissions in the electrolysis-dominant scenario are similar for all the HCNG mixtures while the trends in the SMR-dominant scenario indicate that the H_2 production could imply even lower emissions than the CNG production. This can only be analyzed in terms of trends since the uncertainty in the SMR-dominant scenario in 2050 is so high that identifying the HCNG mixture in terms of well-to-tank emissions would be incorrect.

It is observed that the overall uncertainty in the well-to-tank phase of an HCNG mixture increases with time irrespective of the scenario. However, the increase in this uncertainty is significantly different in the two scenarios (electrolysis-dominant and SMR-dominant). In the electrolysis-dominant scenario, the uncertainty in the HCNG mixture decreases in 2050 with an increase in the H_2 content of the mixture. This is because H_2 relies mainly on the electrolysis technology, and the uncertainty produced by the biogas share in the NG mix is minimized. On the other hand, in the SMR-dominant scenario, increasing the H_2 content of the HCNG mixture increases the

uncertainty since the H_2 production relies significantly on the SMR process from NG. Therefore, it can be deduced that in terms of reducing emissions in the well-to-tank process, the SMR-dominant scenario is superior, provided that there is enough conventional NG and biogas to support this scenario. In contrast, the electrolysis-dominant scenario also has the potential of offering negative emissions with much lower uncertainties, provided that there is enough renewable energy to support the H_2 production. It should be noted that this study does not aim to evaluate the feasibility of these scenarios as it depends on natural resources availability, investments to advance towards the Hydrogen Economy, and politics.

The well-to-wheel GHG emissions (graphs C and D of Fig. 3.15) are obtained as the combination of the results presented in Fig. 3.15 (graphs A and B) with those in Fig. 3.14. Here, it is possible to identify how in 2020 there is not a significant difference between the HCNG mixtures in terms of well-to-wheel emissions except for the pure-CNG case, where the emissions are 11.9-20.6% higher in average, since the low well-to-tank emissions are compensated by the high GHG tank-to-wheel emissions. In this case, it seems that for the short term even a moderate amount of H_2 added to the CNG (25%, for instance) could provide great benefits in terms of well-to-wheel emissions, but adding more H_2 does not significantly benefit the sustainability of HCNG vehicles.

In 2030, the impact of adding a higher fraction of H_2 to the HCNG mixture has a noticeable impact on the well-to-wheel GHG emissions. In this sense, the emissions of the pure-H_2 technology are 49.2% lower than a pure-CNG vehicle in the electrolysis-dominant scenario and 31.8% in the SMR-dominant scenario. This difference is lower in the latter case since the biogas fraction is still small and thus producing H_2 from SMR does not decrease significantly the environmental impact. Still, the difference in emissions between the HCNG mixtures and the uncertainties are moderate.

In the following decade (2040), the electrolysis-dominant scenario still offers lower emissions than the SMR-dominant one, but no HCNG mixture or even the pure-H_2 solution offers zero well-to-wheel emissions within the possible scenarios, as can be seen from the error bars. In both scenarios, the difference between any HCNG mixture and the pure-H_2 vehicle is significant, thus indicating that a complete transition towards H_2-fueled vehicles could bring noticeable environmental benefits. In this case, the transition from a pure-CNG technology towards the pure-H_2 vehicles could reduce the well-to-wheel emissions by 83.9% in the electrolysis-dominant scenario and by 74.2% in the SMR-dominant scenario.

It is not until 2050 that the trend between these two scenarios is reversed, namely due to the significant increase in the biogas share in the NG mix following the SDS scenario in 2050 (43% as in Fig. 3.3A). This is most likely produced since the 2050 timeframe is perceived as a long-term goal, so the targets in terms of sustainability are ambitious and may be unrealistic. Nonetheless, the reader should note that analyzing the feasibility of such targets is not within the scope of this study and is left for future work.

Following the scenarios proposed by the EU, zero well-to-wheel emissions are only reachable after 2040 and close to 2050, but this will ultimately depend on how the production pathways evolve and, in the case of HCNG vehicles, on the availability of both biogas and H_2 to transition to the pure-H_2 solution. In this case, following the possible scenarios considered in this study, no pure-CNG vehicle could reach zero well-to-wheel GHG emissions by 2050. Nevertheless, as explained previously, the further it is predicted in time, the higher the uncertainty. The error considered in this study when assessing the possible scenarios in terms of electricity, NG and H_2 mixes brings to light how these emissions may change since at some points the uncertainty is several times higher than the average values. Nevertheless, the lowest values are representative of the potential of these strategies and scenarios if combined correctly. In this sense, it is important to note how until 2040, the data showed how it was more environmentally beneficial to put efforts into increasing the renewable energy share in the electricity mix to produce green H_2 and transition to pure-H_2 vehicles rather than increasing the amount of biogas in the NG mix. Nonetheless, in 2050, the lower emissions presented by the SMR-dominant scenario indicate how in the long term increasing the biogas share in the NG mix is critical to achieving negative emissions in the well-to-wheel phase and potentially zero emissions in the cradle-to-grave cycle.

It is important to note at this point that the negative emissions in Fig. 3.15 may be misleading. One may think that this is environmentally beneficial with these results, but this is only under the assumption of producing enough energy and biogas, which may not be the case in the long term for large HCNG vehicle fleets. Furthermore, the energy efficiency of using biogas to produce H_2 and then consuming it to power a vehicle may not be the ideal solution to decarbonize the economy, but it indeed is to decarbonize the transportation sector.

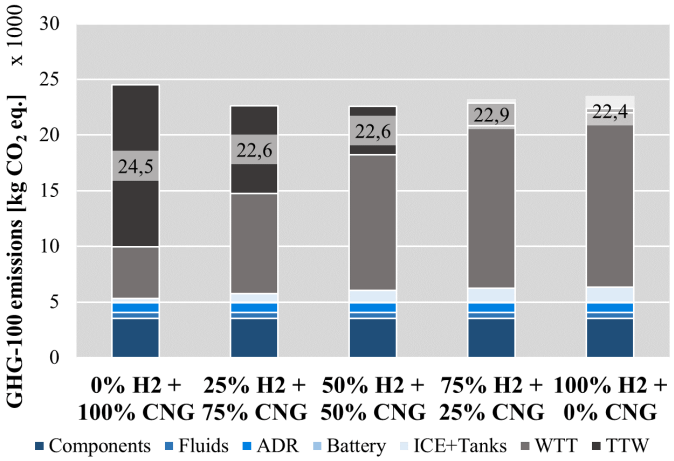

Figure 3.16: Cradle-to-grave GHG emissions breakdown of HCNG vehicles in 2020

Finally, in order to obtain meaningful conclusions about the environmental impact of HCNG vehicles, it is imperative to include the vehicle manufacturing process (cradle-to-gate), thus offering a comprehensive cradle-to-grave process as in section 3.4.5.

3.4.5. Environmental impact and optimal HCNG mixtures

This section comprises the environmental analysis in the cradle-to-grave cycle, thus including both the well-to-wheel emissions (section 3.4.4) and the cradle-to-gate or vehicle manufacturing emissions (section 3.4.1).

3.4.5.1. Current scenario

The cradle-to-grave emissions of HCNG light-duty vehicles in 2020 are presented in Fig. 3.16. The results in this figure are averaged and do not include the error bars for simplicity and since they are included in Fig. 3.17.

The results in this figure show the trade-off between the decrease in well-to-wheel GHG emissions presented in Fig. 3.15 and the increase in cradle-to-gate emissions due to the bigger H_2 tanks (Fig. 3.10A and Fig. 3.10B) required when increasing the H_2 content of the fuel. For these vehicles, the well-to-wheel phase dominates the overall cradle-to-grave emissions since they are responsible for most of the environmental impact and follow a similar trend, i.e., they decrease the higher the H_2 fuel content. Nonetheless,

a local minimum is found around an HCNG mix of 25-50% of CNG and 50-75% of H_2 due to the non-linearities of the fuel consumption and tailpipe emissions produced from the experimental results (Fig. 3.9) coupled with the comparatively low emissions of manufacturing a CNG tank against those of manufacturing a H_2 tank. Nonetheless, the cradle-to-grave emissions are nearly constant and lower than the pure-CNG case if H_2 is added to the fuel mixture due to the increase in the combustion efficiency and the decrease in the carbon content of the fuel. Therefore, with the H_2 mix of the electrolysis-dominant scenario in 2020 it is recommended to operate with HCNG mixtures with low-H_2 content since the H_2 availability is low and there are no significant environmental benefits from increasing the H_2 fraction.

In the current scenario, the vehicle manufacturing phase produces 21.7% of the total GHG emissions in the pure-CNG vehicle while this fraction increases to 28.3% for the pure-H_2 technology. This change is mainly due to the decrease in the well-to-wheel emissions and the increase in the vehicle manufacturing environmental impact when increasing the H_2 fuel fraction. As can be seen, the cradle-to-gate phase constitutes a significant fraction of the overall life cycle and, although it may not be the major impact, it needs to be indeed considered to achieve the zero-emission vehicle. This concept is only achievable if the vehicle manufacturing emissions are compensated with negative emissions in the well-to-wheel phase.

3.4.5.2. Future scenarios

The evolution of the cradle-to-grave emissions in Fig. 3.16 is projected to 2030, 2040 and 2050 in both the electrolysis-dominant (Fig. 3.17A) and the SMR-dominant (Fig. 3.17B) scenarios. The information contained within these results describes the potential of each scenario for different HCNG mixtures, thus allowing the identification of the optimal mixture according to the scenario and timeframe, thus providing valuable information to support the evolution of HCNG vehicles that minimizes their environmental impact.

In the electrolysis-dominant (Fig. 3.17A) and the SMR-dominant (Fig. 3.17B) scenarios, the short-term results (2020) indicate how adding any fraction of H_2, among those considered in this study, implies a noticeable change with respect to the cradle-to-grave emissions produced with the pure-CNG vehicle but they remain similar despite increasing the H_2. Therefore, the 2020 timeframe could be defined as the starting point for the transition towards pure-H_2 vehicles by adding a small amount of H_2 with a positive

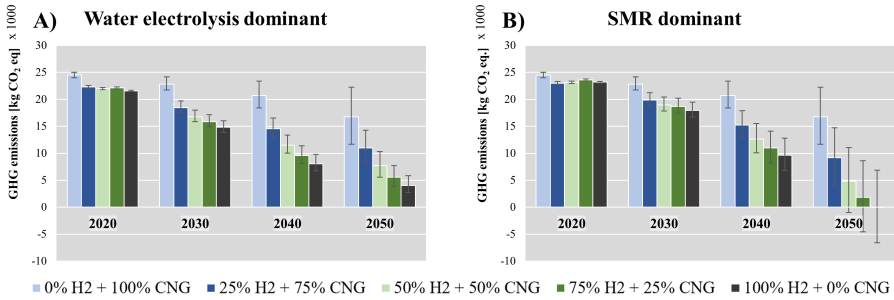

Figure 3.17: Evolution of the cradle-to-grave GHG emissions in the electrolysis-dominant (A) and SMR-dominant (B) scenarios from 2020 to 2050

impact on the environment impact. This is additionally in line with the low H_2 production in the early stages of the transition. For this set of reasons, the recommended H_2 fraction in the mixture is 25% for 2020.

The 2030 timeframe is similar for both scenarios but the differences between HCNG mixtures are more noticeable in the electrolysis-dominant scenario since the biogas fraction in the NG mix is still small. In this case, the transition towards the pure-H_2 vehicles implies a decrease in GHG cradle-to-grave emissions of 35% for the electrolysis-dominant scenario and of 21.4% in the SMR-dominant scenario. Nonetheless, in any case, the difference in cradle-to-grave emissions falls below 6% when increasing the H_2 fraction from 50% to 75% when the electrolysis production pathway dominates and below 2% when the SMR process does, which can be considered small. Therefore, this timeframe could be suitable for progressively increasing the H_2 share to 50% in HCNG mixtures.

The 2040-2050 timeframes indicate that the transition towards the 75% H_2 mixture or pure-H_2 could bring significant benefits in terms of environmental impact. In the electrolysis-dominant scenario, the uncertainty increases the further away it is looked in time but it decreases the higher the H_2 content in the mixture since the dominance of green H_2 implies that the uncertainty is mainly due to the possible scenarios in the electricity mix, rather than in the NG mix. In this sense, despite not reaching negative emissions the decrease in emissions has a lower uncertainty. For this reason, the electrolysis-dominant scenario ensures lower emissions the higher the H_2 content in the HCNG mixture but it is not suitable for reaching the zero-emission vehicle concept since for that a higher amount of negative emissions coming from the use of biogas is required.

In contrast, the SMR-dominant scenario shows the potential of reaching and even surpassing the zero-emission concept due to the high share of biogas in the NG mix. In this sense, only the HCNG mixture with more than 50% of H_2 could approach this concept, but this will depend mainly on the investment and politics that foster the capture and usage of biogas. In the 2040-2050 decade, it is recommended to transition towards the pure-H_2 technology to minimize the environmental impact of these vehicles since, despite the increasing uncertainty, the trend indicates that this technology should offer lower emissions.

In conclusion, the strategy to minimize the environmental impact of HCNG vehicles without putting too much stress on the H_2 indicated that the transition towards a H_2 content of 25% should be carried out in the 2020-2030 decade. From 2030, the H_2 mixture should increase to 50% and in 2040-2050 the transition should aim towards pure-H_2 vehicles. The zero-emission concept is only feasible if enough biogas is introduced in the NG mix combined with the use of H_2. Therefore, in the early stages of the transition towards the H_2, the electrolysis-dominant is encouraged since it offers lower cradle-to-grave GHG emission through the use of green H_2 but in the long term, once there is enough renewable energy to produce H_2 the focus must change towards increasing the biogas share in the NG mix, thus approaching the SMR-dominant scenario in 2050. Following this hybrid strategy would not only allow minimizing the environmental impact of HCNG vehicles in terms of global warming but to reach the zero-emission concept in the long term-

3.5. Conclusion

This study examined the impact of transitioning to a fully developed H_2 economy on GHG emissions and considered multiple hydrogen blends on CNG in different scenarios. The most significant novelty in this study are the identification of the optimal blend of HCNG that minimizes emissions in the 2020-2050 period and the determination of the timeframe and HCNG blend that enables zero cradle-to-grave emissions for these vehicles. The findings suggest that hydrogen blending has the potential to reduce emissions and provide an alternative fuel source for cleaner and more efficient transportation systems. Increasing hydrogen content in blends improves engine performance but requires higher air dilution ratios to maintain efficiency and minimize thermal losses. As the H_2 content in blends increases, exhaust gas emissions reduce due to higher air-fuel equivalence ratios and

lower combustion temperatures. Using hydrogen instead of CNG lowered carbon emissions, but some carbon dioxide is still generated from lubricant oxidation.

Based on the results of this study, it is demonstrated that HCNG vehicles possess a significant potential to decarbonize the transportation sector in both water electrolysis and SMR-dominant scenarios. In the water electrolysis scenario, the cradle-to-grave emissions have been observed to decrease significantly from [24.5, 21.6] to [16.8, 4.1] tonnes of CO_2 eq. by the year 2050, with pure-H_2 vehicles experiencing the lowest value and CNG vehicles experiencing the highest. In the SMR scenario, there is a notable increase in the uncertainty of cradle-to-grave emissions, but it offers the possibility of reducing emissions to -0.1 tonnes of CO_2 eq., depending on the biogas share in the NG mix and the electricity mix.

The optimal HCNG blend evolution implies incorporating 25% H_2 content in 2020, 50% in 2030, and 75-100% between 2040 and 2050 to reduce greenhouse gas emissions in the transportation sector. While these suggested H_2 shares may not yield the lowest emissions in 2030 and 2040, they are chosen pragmatically due to potential feasibility constraints in H_2 availability. Achieving zero cradle-to-grave emissions in 2050 necessitates an SMR-dominant scenario with fuel mixtures exceeding 50% H_2 content, requiring increased use of biogas to promote negative emissions and offset environmental impact throughout the vehicle life cycle. The SMR-dominant scenario has the potential to either yield significant negative emissions or decrease environmental impact by 72% compared to pure-CNG vehicles in the least-optimistic scenario.

CHAPTER 4

Impact of medium-pressure direct injection in a spark-ignition engine fueled by hydrogen

[3] S. Molina, R. Novella, J. Gomez-Soriano, and M. Olcina-Girona. "Impact of medium-pressure direct injection in a spark-ignition engine fueled by hydrogen". Fuel 360, 2024, p. 130618.

4.1. Introduction

Reducing greenhouse gas (GHG) emissions is crucial to mitigating the global warming effect. The European Union (EU) aims to achieve zero net greenhouse gas emissions by 2050 through the planned Green Deal program. By 2030, the interim target is to reduce GHG emissions by 55% compared to 1990 levels. However, as of 2020, only a 20% decrease had been accomplished, highlighting the need for significantly greater efforts to achieve the goal.

Transportation represents a substantial source of GHG emissions, accounting for approximately 32% of the carbon dioxide (CO_2) emissions in Europe [30]. Furthermore, the escalation persists despite the implementation of new environmental regulations and the advancement of more efficient vehicle technologies. Hence, a potential solution to the problem lies in diversifying future fuels [110, 120], emphasizing the development of CO_2 neutral powertrains that also minimize emissions of other pollutant exhaust components [121, 122].

Hydrogen (H_2) fuel possesses properties that align with the needs of the automotive transportation sector. It exhibits approximately six times the combustion speed of gasoline, a wide flammability range, and serves as a carbon-free fuel. These characteristics indicate that hydrogen is a suitable fuel for achieving optimal engine performance while minimizing GHG and pollutant emissions. Moreover, hydrogen production can be coupled with renewable energy sources (RES) [123, 124], facilitating its integration into the grid as an energy vector. Power-to-gas (P2G) systems, which convert surplus renewable energy into hydrogen gas through electrolysis, become a viable option only when they serve as the sole means of achieving a high share of RES. The current natural gas grid has the potential to accommodate hydrogen as an energy vector in the transition toward a fully renewable energy system [22].

The use of H_2 as fuel for transportation through internal combustion engines (ICEs) has been the subject of research for decades. It has been employed as an additive to enhance the combustion characteristics of other fuels, such as gasoline [125, 126] or compressed natural gas (CNG) [8]. This approach has proven effective in reducing pollutant emissions, increasing fuel efficiency, and improving engine performance. Furthermore, studies have explored the possibility of onboard hydrogen generation within a vehicle through the reforming of a portion of the primary fuel [127]. This method enables on-demand hydrogen production, eliminating the need for dedicated hydrogen storage tanks with a limited range [128].

When H_2 is used as the sole fuel, operating under high dilution conditions proves beneficial in reducing knock susceptibility [39], nitrogen oxides (NO_x) emissions [45], and improving engine performance and efficiency [46–48]. However, several issues are associated with the utilization of hydrogen in internal combustion engines. These issues include the presence of high-pressure rise caused by combustion instabilities [129, 130], the occurrence of pre-ignition or knocking within the combustion chamber [130, 131], and the sequential progression of pre-ignition and backfire into the intake manifold [40, 50], particularly under high load conditions. The prevention of these abnormal combustion events is a crucial factor in ensuring the long-term durability of powerplants [132]. Recent studies have evaluated the impact of dilution in a medium-duty engine for transport applications [133]. Shi et al. [37] have recently studied the effect of water injection in a rotary engine, demonstrating a reduction in knock propensity and NO_x mitigation as the amount of injected water increases.

The delivery of hydrogen to an engine can be performed through various injection systems, with the most commonly employed ones being port fuel injection (PFI) and direct injection (DI). PFI involves injecting fuel into the inlet manifold, whereas DI involves injecting fuel directly into the combustion chamber. Port fuel injection hydrogen systems have limitations regarding volumetric efficiency and a higher probability of abnormal combustion events [134]. Conversely, direct injection hydrogen systems can overcome volumetric drawbacks but may necessitate specialized and expensive engine components [135].

Recent studies have showcased the potential of hydrogen direct injection (H2-DI) in attaining remarkable performance and efficiency [136]. Through precise control of the intake valve closing and exhaust valve opening timing, researchers achieved an impressive brake thermal efficiency (BTE) of 42.2% [79]. Furthermore, the characterization of knock intensity in H2-DI was also investigated [137].

The direct injection process induces higher in-cylinder turbulence and stratification compared to the premixed charge PFI counterpart, leading to accelerated fuel combustion [135]. It was observed that the variation in knock intensity is non-linear with the retardation of the start of injection (SoI), which can be attributed to the distribution of the cylinder mixture. Several researchers [138, 139] investigated mixture formation in an optically accessible hydrogen-fueled engine. By employing Planar Laser-Induced Fluorescence (PLIF), they discovered that injector tip geometry, injector location, injection timing, nozzle design, and injector geometry are critical parameters affecting the in-cylinder mixing process in direct-injection HICE. Eichlseder et al. [140] discovered that at low equivalence ratios, the indicated thermal efficiency (ITE) increases with a delay in the start of injection (SoI). This increase is attributed to a reduction in compression work resulting from variations in mixture gas properties and charge mass associated with a delayed SoI. However, Kim et al. [141] present conflicting results to those of Eichlseder et al. [140]. They found that for both low and high loads, thermal efficiency decreases consistently as the SoI is delayed. In a multi-cylinder automotive engine, Kim et al. [142] observed a 30% increase in power density when transitioning from PFI to DI while maintaining the same brake thermal efficiency with delayed ignition timings. Similarly, Maio et al. [143] observed equivalent trends in a single-cylinder heavy-duty engine.

These contradictory findings could potentially be attributed to variations in mixture formation. This perspective is supported by the findings of Shudo et al. [144], who demonstrated that by implementing charge stratification

in a manner that promotes a lean local mixture fraction near the wall region compared to the overall mixture, significant reductions in cooling losses can be achieved alongside improved thermal efficiency. These findings have arisen in the context of SI engines using gasoline direct injection (GDI) systems loosely adapted for extensive use with hydrogen as fuel and complying with the necessary safety measures for vehicle use. In this type of injector, fuel is introduced into the combustion chamber through single or multiple cylindrical or conical nozzles, exhibiting the conventional injection patterns observed in gasoline-based engines.

However, from a technological development perspective, there is a new trend towards using gas-based injectors due to their advantages in terms of safety and control [145]. Unlike conventional DI injectors, whether single- or multi-hole with inwardly opening designs and cylindrical nozzles, which are susceptible to opening under cylinder pressure if the injection pressure is lower, gas-based injectors inject hydrogen through an outwardly opening poppet valve. This results in entirely different spray patterns and mixture rates [146]. These latter parameters are directly related to the injection channel design and are completely distinct from those observed in conventional GDI nozzles [147].

None of the works conducted to date have employed a combination of a modern engine platform and an outwardly opening poppet valve gas direct injector. While numerous studies exist that assess the impact of direct injection on modern, small-displacement, turbocharged engines with new combustion chamber designs, all of them use GDI-adapted injectors with single or multiple cylindrical nozzles to supply hydrogen into the combustion chamber. Therefore, further research is needed to explore how this kind of hydrogen injection system impacts combustion, emissions, and engine performance under different dilutions and operating conditions.

This study aims to contribute to the existing knowledge regarding the effects of mixture formation by utilizing different injection strategies. It seeks to assist in advancing current technology for implementing hydrogen as a fuel in light road transportation applications. The authors conducted an extensive experimental campaign using a single-cylinder spark-ignition research engine for light-duty applications to analyze the performance, combustion process, and emissions when the engine is equipped with two outwardly opening poppet valve hydrogen injectors (PFI and DI) under various levels of air dilution. Additionally, the impact of mixture stratification is evaluated by manipulating the injection timing of the DI system, transitioning from lean homogeneous charge to lean stratified charge combustion mode.

4.2. Material and methods

This section describes the experimental tools and methods used in the investigation to give a clear and concise understanding of the experiment procedures and the processing methodology.

4.2.1. Experimental tools

The experiments were conducted on a single-cylinder SI engine with a displacement of 454.2 cm^3. The experimental facilities were previously utilized in the investigation performed by Molina et al. [**Molina2022**, 8]. The main engine specifications are listed in Table 4.1 for reference. The engine featured an 86-mm stroke with a compression ratio (CR) of 10.7:1 and a 4-valve pent-roof cylinder head. A conventional spark-plug ignition system was used for all the experimental tests. The fuel was supplied by two different outwardly opening poppet valve gas injection systems: a PFI system with a maximum injection pressure of 5 bar and a medium-pressure DI injection system with a maximum injection pressure of 30 bar. The DI system ensured that the injection duration was sufficiently short to inject the required fuel quantity when the injection was moved towards the top dead center (TDC). The injection duration was used as a parameter to control the amount of fuel injected.

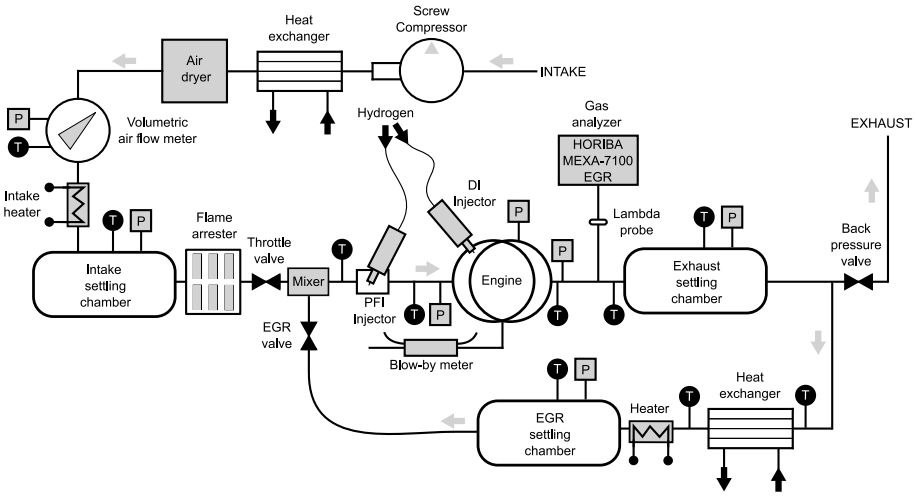

Figure 4.1: Experimental engine layout

Table 4.1: Main engine specifications

Number of cylinders	1
Number of strokes	4
Displaced volume	454.2 cm^3
Stroke	86.0 mm
Injection systems	PFI-DI
Ignition system	Spark plug
Cylinder diameter	82.0 mm
Compression ratio	10.7
Connecting rod length	144.0 mm
Valves per cylinder	2 intake, 2 exhaust
Engine management system	AVL PREMS GDI
Combustion system	4-valve pent-roof GDI
Intake Valve Opening (IVO)*	-380 CAD
Intake Valve Closing (IVC)*	-135 CAD
Exhaust Valve Opening (EVO)*	-600 CAD
Exhaust Valve Closing (EVC)*	-338 CAD

*with respect to the firing TDC (0 CAD)

Figure 4.1 depicts a sketch of the test cell utilized in this experimental research. The original layout of the test bench was modified to accommodate hydrogen operation. To ensure safety, a flame arrester was installed in the intake manifold upstream of the EGR mixer, and a dedicated hydrogen supplier system was implemented to furnish the injectors.

The experimental facility enables comprehensive control of each relevant parameter during engine operation. High-diluted air conditions were achieved using an external compressor, while an exhaust back-pressure control was achieved through a knife-gate valve located on the exhaust line. Automated valves were employed to manage the hydrogen injection pressure when transitioning between PFI and DI modes.

The test bench is fully equipped with state-of-the-art measurement devices. A piezoelectric sensor was used to measure in-cylinder pressure, and two different piezoresistive sensors were utilized to measure intake and exhaust pressures. The Bronkhorst F-113AC-1M0-AAD-55-V flowmeter was employed to register the hydrogen flow rate. All signals were recorded at a sampling frequency of 0.2 CAD. For the analysis of NO_x emissions and other relevant exhaust gases, a HORIBA MEXA-7600EGR equipment was utilized. The accuracy of the main instrumentation is presented in Tables 4.2 and 4.3. The measurement equipment employed in this study is state-of-the-art technology in the field of ICE research, and the measurement protocol is sufficiently robust and reliable to trust the obtained results.

Table 4.2: Instrumentation accuracy.

Signal (High frequency)	Sensor	Specification	Accuracy
In-cylinder pressure	Piezoelectric sensor	0 to 250 bar ± 0.3% linearity	± 0.8%
Intake pressure	Piezoresistive sensor	0 to 10 ± 0.001 bar	± 0.8%
Exhaust pressure	Piezoresistive sensor	0 to 10 ± 0.001 bar	± 0.8%
Variable (Low frequency)	**Sensor**	**Specification**	**Accuracy**
Engine Speed	Optical angular encoder	1 to 6000 ± 1 rpm	± 0.1%
Engine Torque	Strain-gauges torque-meter	-200 to 200 ± 1 N m	± 0.4%
Intake pressure	Piezoresistive transducer	0 to 10 bar ± 1%	± 0.8%
Exhaust pressure	Piezoresistive transducer	0 to 10 bar ± 0.3%	± 0.8%
Intake temperature	Thermocouple type K	0 to 1000 ± 0.5 °C	± 1.0%
Exhaust temperature	Thermocouple type K	0 to 1000 ± 0.5 °C	± 1.0%
Fluid temperature	Pt100 thermoresistance	-200 to 850 ± 0.3°C	± 0.6%
Air mass flow	Air flow meter	0.6-100 m^3/h ± 1%	± 1.0%
Hydrogen mass flow	Thermal mass flow meter	200-1600 l/min (based on N_2) ± 0.5 %	± 0.1%

Table 4.3: Accuracy levels of HORIBA MEXA 7100 DEGR for measurements of gaseous species.

Pollutant	Analyzer	Range	Accuracy
HC	FID	min. 0 to 10 ppm C max. 0 to 50 kppm C	± 3%
NO_x	CLD	min. 0 to 10 ppm max. 0 to 10 kppm C	± 3%
CO	NDIR	min. 0 to 3 kppm C max. 0 to 12 vol%	± 3%
CO_2	NDIR	min. 0 to 5 kppm C max. 0 to 20 vol%	± 3%
O_2	PMA	min. 0 to 5 vol% max. 0 to 25 vol%	± 3%

The IMEP, cycle-to-cycle variability (CCV) expressed by the IMEP coefficient of variation (COV_{IMEP}), emissions, and indicated efficiency levels were determined using a specialized in-house combustion diagnosis tool [94, 95], which was specifically adapted for hydrogen fuel usage. The software incorporated an estimation of combustion efficiency by analyzing the oxygen measurements in the exhaust. This estimation accounted for the excess oxygen corresponding to the air dilution ratio and other contaminants that rely on oxygen for their formation, such as NO_x.

4.2.2. Experimental method

The aforementioned facility served as the primary tool for the investigation. The experimental campaign involved measuring various conditions at two relevant operating points, characterized by 4 bar and 7 bar of IMEP while running at 1500 rpm (referred to as 1500@4 and 1500@7). A summary of all operating point conditions is presented in Table 4.4.

Table 4.4: Testing conditions and operating points.

Operating Point	λ [-]	**Injection system**	**SoI** [CAD aTDC]
1500@4	2.2:0.2:3.2	PFI/DI	-340/-130
	2.6	DI	[-340:10:-40]
1500@7	2.2:0.2:3.2	PFI/DI	-340/-130
	2.6	DI	[-130:10:-85]

The IMEP targets were established by operating the engine with a reference air-to-fuel ratio and the PFI configuration. Once the desired load level was achieved, the fuel quantity was recorded and used in subsequent tests conducted for a given operating point. In this regard, the injected fuel mass was adjusted to maintain the same energy available for combustion at that specific load level. It should be noted that under these conditions, the IMEP level may vary if the thermal efficiency changes due to modifications in other parameters, such as the dilution ratio or combustion phasing. Therefore, the target values of engine load used to designate the operating points should be considered qualitative references that simply indicate whether the engine load is low or medium.

The external air compressor was employed to regulate the amount of air and achieve the desired dilution ratios. The backpressure was maintained at 0.1 bar higher than the intake pressure to mimic realistic conditions at the turbine entry. The energy deposition supplied by the spark plug remained constant throughout all tests. The intake temperature, measured at the surge tank, was set at 308.2 K, while the oil and coolant temperatures were maintained at a constant 363.2 K. The measurement process followed a rigorous protocol, including three repetitions for each considered operating condition. Measurements were only accepted when the variation of key variables was within the uncertainty of the sensor or they did not exhibit a deviation greater than 2% compared to the other repetitions. The controlled variables were: engine speed, engine torque, intake/exhaust pressures, air mass flow, hydrogen mass flow, indicated mean effective pressure (IMEP),

COV_{IMEP}, combustion phasing (CA50) and NO_x levels. All high-frequency signals were sampled with a resolution of 0.2 CAD. The results presented in the following sections represent the average value obtained from these three repetitions, with each repetition consisting of 250 engine cycles.

Two studies were proposed: a comparison of the injection systems under identical conditions of fuel-air mixture and load, and an examination of how the injection timing influences the engine emissions and performance. The first study was conducted within a range of λ (2.2 to 3.2) values where emissions and engine performance are analyzed. The second study involved sweeping the injection timing, ranging from the start of the intake stroke when the intake valve is open to as close as possible to the firing TDC during the compression stroke. This range covered both valve-open and valve-closed injection with the DI injector, limited by misfiring.

4.3. Results and discussion

This section presents the results obtained from the application of the methodology described. The analysis is divided into two subsections, corresponding to the two studies outlined in the previous section.

4.3.1. Comparative analysis of PFI and DI hydrogen systems

The objective of this study is to compare the PFI and DI injection systems under homogeneous charge-lean combustion conditions. To achieve this goal, results from both systems are presented at various air dilution ratios. To ensure the utmost air-fuel mixture homogeneity, the injection timing was set to -130 CAD aTDC, immediately following the IVC. This enabled the analysis of the impact on volumetric efficiency by eliminating hydrogen from the intake ports.

The impact of the injection system on intake pressure and the volumetric performance of the engine is illustrated in Fig. 4.2. In this figure, both PFI and DI systems were used for different combinations of engine load and air-to-fuel ratios. For both operating points analyzed, the spark timing was optimized to minimize specific fuel consumption (ISFC).

The results demonstrate a consistent decrease in intake pressure when utilizing the DI system, with a difference of approximately 0.2 bar compared to the PFI system along the whole range of dilution ratio. This reduction in intake pressure is directly linked to the enhanced volumetric efficiency observed. Such an effect, which stands as one of the primary advantages of DI systems, was also identified by Maio et al. [143].

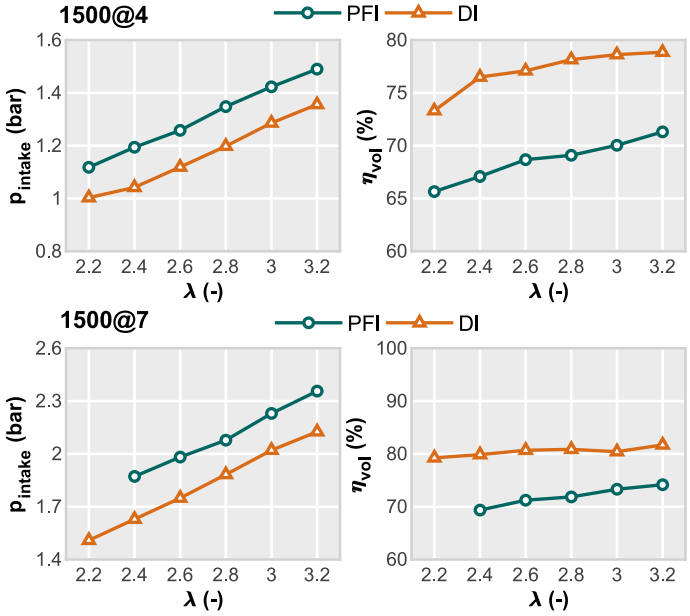

Figure 4.2: Impact of the injection system on intake pressure and volumetric efficiency for different air-to-fuel ratios.

This advantage allows the DI system to overcome the limitations associated with the PFI system, which stem from the low density of hydrogen. By improving the engine power output, the DI system also enables the attainment of higher dilution ratios under identical boosting conditions, increments of around 16%-17% of dilution are found by injecting hydrogen with the DI system.

To observe the impact of the injector system on engine performance, Fig. 4.3 depicts the key engine outputs. As evident from the figure, the DI system yields higher performance levels for both operating conditions. At the operating point of 1500@4, consistent improvements of 4% in IMEP (with PFI system results used as a reference) are observed across all air dilution values. The minimum ISFC is achieved at $\lambda = 3.2$ for both systems, with values of 75.2 g/kWh for PFI and 72.9 g/kWh for DI. In this operating condition, higher dilution conditions for DI have the potential to yield further efficiency gains. At $\lambda = 3.2$, an efficiency of 41.2% is achieved, and the trend suggests that the efficiency may continue to increase, while for PFI, no efficiency values above 40% are reached. Similar gross indicated efficiency

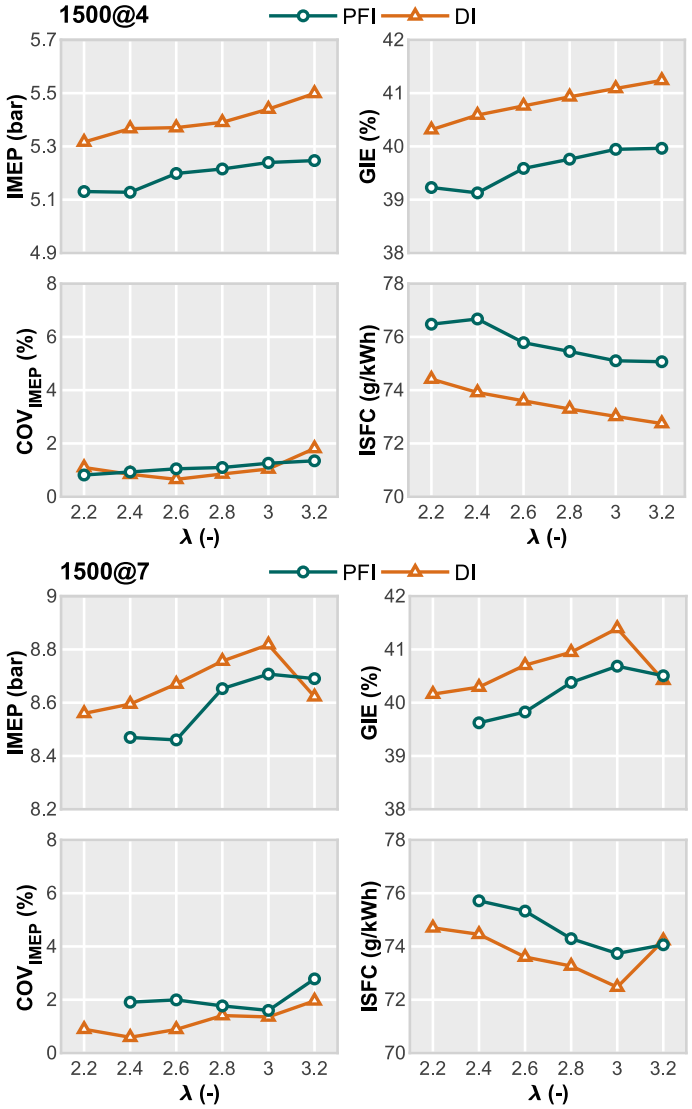

Figure 4.3: Impact of the injection system on the performance level for different air-to-fuel ratios.

(GIE) values are attained at $\lambda = 3.0$ and 3.2, indicating a performance peak with respect to air dilution. COV_{IMEP} remains below 2% for all λ cases in both PFI and DI systems, indicating consistent combustion stability.

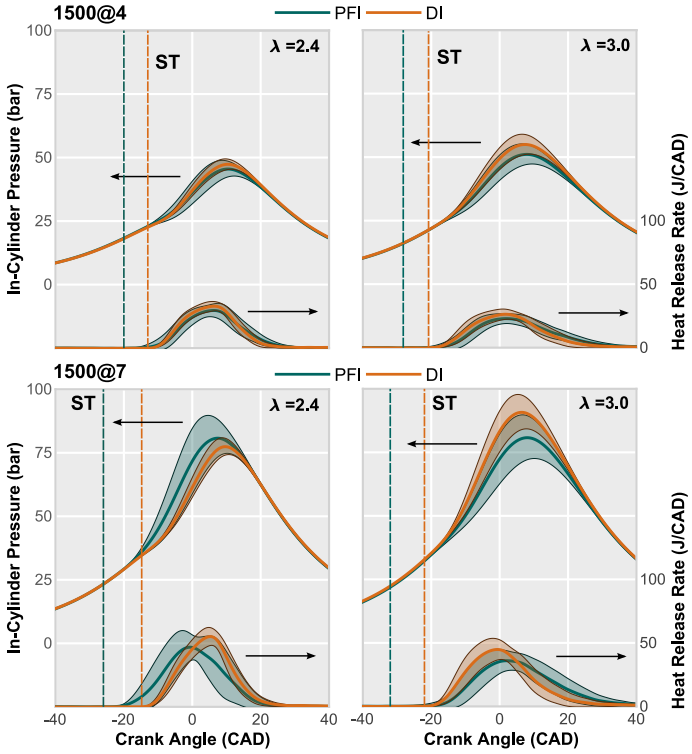

Figure 4.4: In-cylinder pressure and HRR profiles for different λ values (2.4 and 3.0) and operating points (1500@4 and 1500@7).

Moreover, the use of a direct injection system enables operation at lower minimum λ values even under higher engine loads. This feature helps to mitigate the increased tendency for abnormal combustion events and enables an increase in maximum engine torque [130]. For instance, at the operating point of 1500@7, knocking conditions were found with PFI injection when λ is reduced up to 2.2, while the DI system was able to operate without knocking in these particular dilution conditions. The specified operating condition for the PFI system could not be measured as the knock intensity was alarmingly high, even at $\lambda = 2.3$.

At this operating condition, the DI system demonstrated the highest performance, although not equally distributed across the λ range as observed at 1500@4. The maximum IMEP was achieved at $\lambda = 3.0$ for both injection strategies, reaching 8.9 bar for DI and 8.7 bar for PFI. This difference translates to a 1% GIE gain. The maximum performance is achieved at $\lambda = 3.0$, after which the performance declines for the DI system. In contrast, when

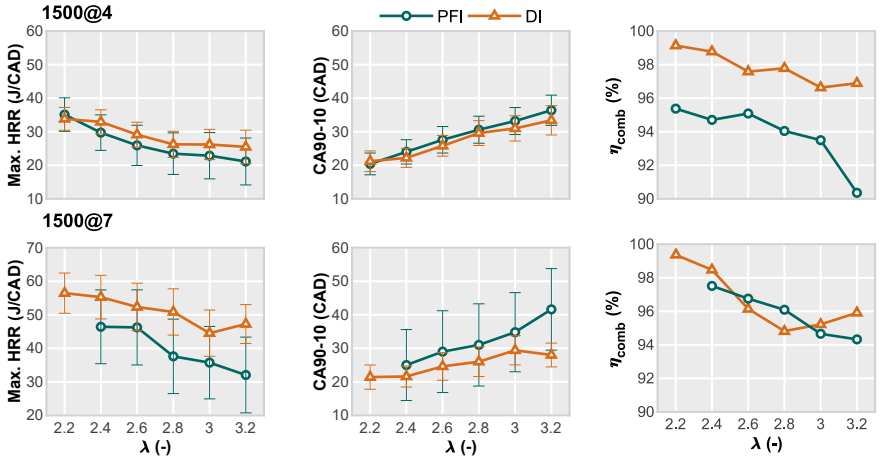

Figure 4.5: Impact of the injection system on the combustion performance for different air-to-fuel ratios.

utilizing the PFI system, the peak IMEP values are attained within the λ range of 2.8 to 3.2. These values stabilize at approximately 8.7 bar of IMEP, signifying a notable 2.4% increase in comparison to λ levels of 2.4 and 2.2. The maximum peak in GIE for 1500@7 is around 0.2%-0.5% higher for both injection systems compared to 1500@4, with DI achieving 41.5% and PFI reaching approximately 40.5%. For the PFI system, COV_{IMEP} results are observed to be above the DI system results, reaching a 1% difference at some λ values, although both remain below the instability limit.

The DI system demonstrates performance advantages over the PFI system at 1500@7, although these benefits are lower compared to 1500@4. These variations in performance are discussed from a combustion perspective, considering the in-cylinder pressure and heat release rate (HRR) profiles displayed in Fig. 4.4. The in-cylinder pressure was averaged per cycle over 250 engine cycles, and the point-to-point standard deviation was included (shadow zones) to illustrate cyclic variation. These data were obtained by using both PFI and DI systems under different air dilution conditions (λ = 2.4 and 3.0) and load conditions. The average cycle is shown, along with the point-to-point standard deviation (SD), which takes into account the CCV. The dashed line indicates the crank angle of the spark discharge.

As can be observed, the in-cylinder pressure profiles from the DI and PFI systems overlap during the compression stroke due to the identical air-fuel mixture conditions enforced in both scenarios. However, the gap between the spark timing and the start of combustion (SOC) is consistently larger in

PFI compared to DI. It is worth noting that in DI, the HRR profile increases immediately after the spark timing, whereas in PFI, it takes some time (5 to 10 CAD). Additionally, at low engine load, the HRR profiles resemble each other in terms of peak and duration, while at high load, they exhibit noticeable differences. The combustion duration is significantly shorter in DI, accompanied by a higher HRR peak above 10 J/CAD.

In terms of CCV, both systems demonstrate comparable values at low-load operating points; however, they exhibit substantial differences at higher loads. Specifically, DI exhibits a lower cycle-to-cycle variation, particularly at a lower air-to-fuel ratio ($\lambda = 2.4$). Furthermore, an incremental trend is observed in the standard deviation of the HRR profiles, starting with low values and increasing as the crank angle advances. In contrast to the results of the DI system, the PFI system exhibits an approximately constant and higher standard deviation. This fact suggests that the SOC can be better controlled by the DI system. Note that the point-to-point SD is almost zero at the beginning of combustion when using DI, whereas it starts with larger values in PFI. Additionally, it is worth highlighting that the second hump observed in some HRR traces, specifically those with higher CCV, is not a consequence of abnormal combustion events due to end-gas autoignition. This effect is caused by the averaging procedure, which tends to generate the mentioned second hump in the HRR when there is significant cycle-to-cycle dispersion.

To analyze the combustion process of all the conditions considered in this section, relevant combustion parameters are included in Fig. 4.5. The error bars included in this figure account for the CCV of the presented parameter. As evident from the data, DI consistently exhibits a 2 CAD shorter combustion duration at all λ values, and an approximately 25% higher peak in HRR, indicating that local temperatures may be higher compared to PFI. The peak values of HRR show a tendency to decrease as the air dilution ratio increases. Additionally, the larger gap in GIE observed between PFI and DI at lower loads (1500@4) can be partially attributed to the improved combustion efficiency displayed in the corresponding figure. While there is an approximate difference of 1.5 percentage points between the two injection systems at low loads (1500@4), no substantial differences are observed at higher loads (1500@7).

Regarding the CCV of these parameters, the error bars show consistent results to those presented in Fig. 4.4. At low load conditions, differences between PFI and DI are almost negligible over the entire dilution range. However, the CCV of both the maximum HRR peak and CA90-10 seems

independent of the dilution rate in the DI system, whereas it tends to increase in the PFI system. In contrast, differences are notably higher in high-load conditions. The maximum HRR peak variation remains almost constant around ±6 J/CAD in all dilution conditions in DI, whereas it increases from ±9 to ±12 J/CAD as dilution increases in PFI. Similarly, the CA90-10 variation is around ±5 CAD in DI and from ±10 to ±14 CAD in PFI.

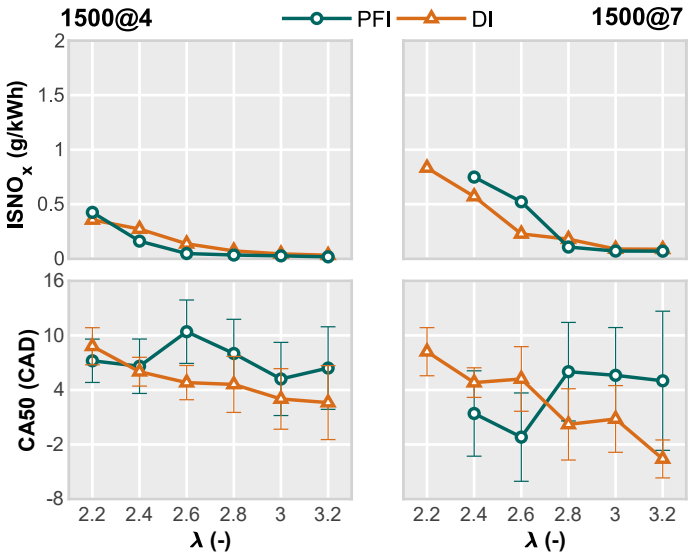

Figure 4.6: Impact of the injection system on NO_x emissions and MBT combustion phasing for different air-to-fuel ratios.

Focusing on pollutant emissions, the NO_x emissions are presented in Fig. 4.6. It can be observed that at 1500@7, almost double the specific emission levels are attained compared to 1500@4 at the same λ value. As the load increases, so do the temperatures and pressures in the combustion chamber, leading to the activation of thermal NO_x formation.

Although similar trends are observed between both injection systems, especially at low load conditions, the increase in NO_x starts at $\lambda = 2.8$ with PFI whereas this inflection point decreases up to $\lambda = 2.6$ with DI. It seems that the particular design of the injector leads to a unique mixture stratification that may influence the λ value at which the NO_x levels start to rise, even if the overall air-to-fuel ratio is the same as the PFI case. Therefore, although injecting just after IVC may seem suitable to achieve a homogeneous mixture in the combustion chamber, it does not appear to be sufficient in cases with high dilution (above λ 2.4) where spark timing

must be significantly advanced to achieve optimal combustion phasing. This can be inferred from the CA50 obtained in each of the dilution conditions and injection systems represented in Fig. 4.6. Focusing on the dilution range where NO_x levels are very close to 0 ($\lambda = 2.6$ for DI and $\lambda = 2.8$ for PFI), it can be seen that the CA50 hardly changes in PFI, while it advances from 6 CAD after TDC to 4 CAD before TDC. This suggests that the mixture distribution in the combustion chamber at the spark timing favors combustion with lower local temperatures, leading to a reduction in NO_x comparable to that of $\lambda = 2.8$ in PFI. However, this is something that should be verified through advanced numerical simulations where it is possible to observe the equivalence ratio distribution in the chamber.

In any case, it seems that under homogeneous mixing conditions, the DI system should not provide any advantage in terms of emissions. It is necessary to rely on air dilution to lower combustion temperatures and achieve low levels of NO_x emissions.

4.3.2. Impact of injection timing on H2-DI

The second study focuses on analyzing the impact of injection timing (SoI) using the DI system on engine performance, combustion, and emissions. Initially, the study examines the low-load point (1500@4), where a sweep of start of injection was performed, considering instants during both intake stroke and compression stroke. In this regard, the analysis encompasses a transition from a homogeneous mixture, with the SoI ranging from -340 to -180, to a stratified mixture, with the SoI ranging from -140 to -65.

Figure 4.7 illustrates the effect of the SoI on intake pressure and volumetric efficiency. Two different regimes are demarcated by the IVC position. In regime I, the fuel is injected while the intake valve is still open, requiring higher pressure to push the air into the cylinder due to the resistance caused by the low density of hydrogen. Conversely, in regime II, where the start of injection occurs with the intake valves closed, the intake pressure decreases, and the volumetric efficiency increases. In both regimes, the intake pressure remains independent of the SoI, exhibiting a purely binary behavior. It is evident that injecting after the valves closing event has some advantages from the point of view of engine scavenging. However, it may pose disadvantages in terms of mixture formation due to the limited time span between the SoI and the start of combustion.

The most relevant engine performance parameters are plotted in Fig. 4.8 as the SoI is varied while keeping the air-to-fuel ratio ($\lambda = 2.6$) constant. Once again, two distinct trends are observed based on the intake valve closing

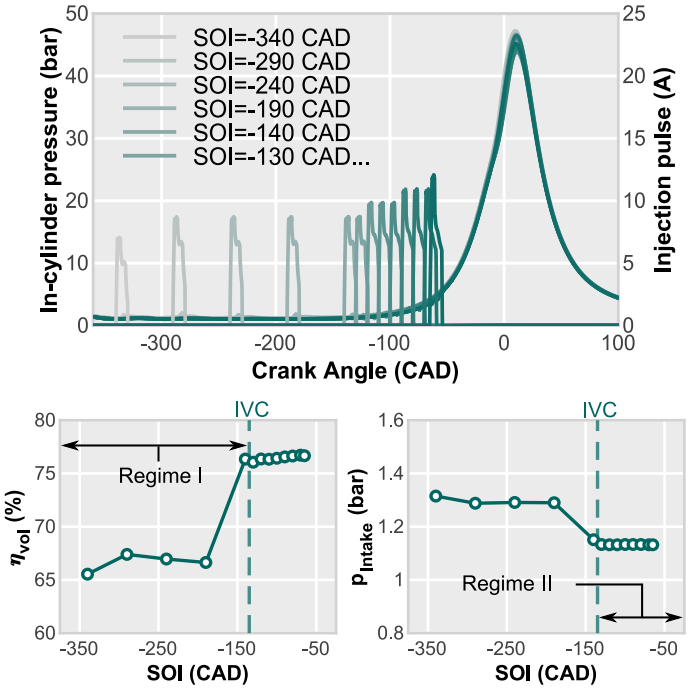

Figure 4.7: The impact of injection timing on intake pressure and volumetric efficiency using the DI system under constant λ (2.6) and low-load conditions. In-cylinder pressure profiles have been also included together with the injection pulses for reference.

event. In regime I, the engine performance remains almost constant with SoI retardation. The thermal efficiency is around 40%, and the CCV is below or close to 1%, indicating remarkable operational stability.

In relation to regime II, delaying the SoI leads to a significant increase in performance. The GIE increases from 40% to nearly 43%, while the CCV remains below 1%-2% (SoI = -70 CAD aTDC). Consequently, the IMEP increases, and the ISFC decreases to 70 g/kWh, indicating a 0.1% improvement in ISFC per degree of delayed SoI. However, a peak of instability is observed when injection starts at -65 CAD aTDC. At this point, the CCV increases up to 4% and the GIE slightly decreases, indicating that the peak performance has been reached. However, what is truly intriguing is what the graph does not reveal. The subsequent SoI (-60 CAD aTDC) could not be measured due to the high CCV, which jeopardized operational stability as a result of excessive misfiring cycles. This implies that crucial factors

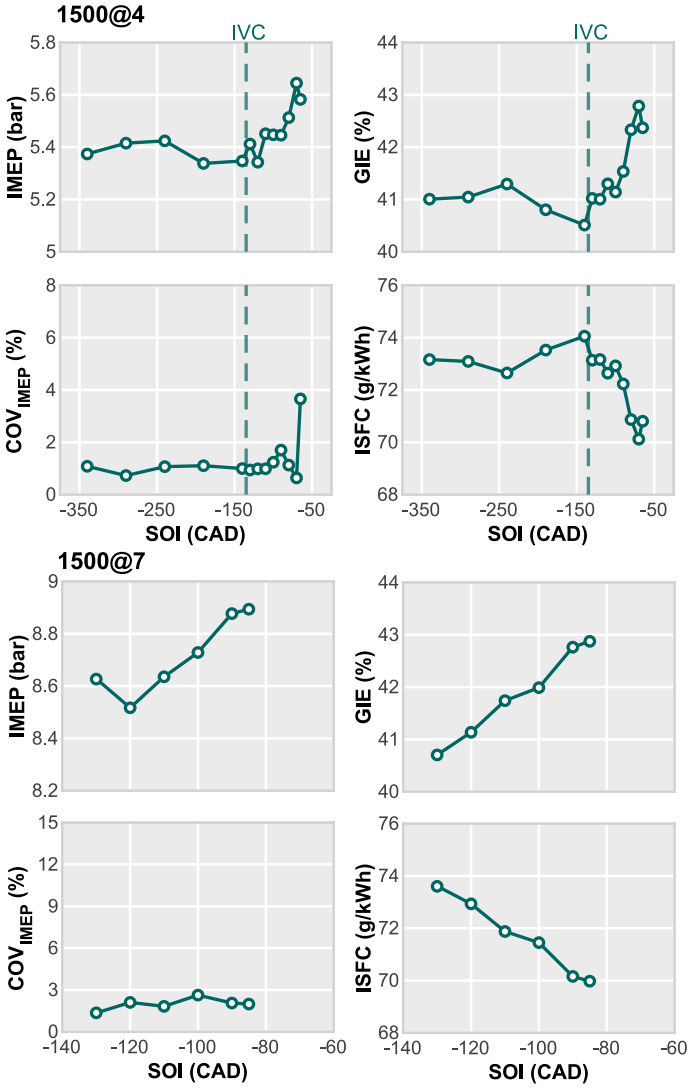

Figure 4.8: The impact of injection timing on engine performance parameters using the DI system under constant λ (2.6).

such as mixing preparation, flow velocity field, and turbulence levels within the combustion chamber are being impacted by late injection, exerting a negative influence on combustion stability.

To conduct a comprehensive analysis of this specific behavior, Fig. 4.9 depicts the maximum in-cylinder peak pressure for all recorded cycles. The plot illustrates the relationship between the peak pressure and its angular

position for the two most delayed SoI cases (-70 and -65 CAD aTDC). This visualization allows us to observe how combustion deteriorates as the SoI is delayed closer to top dead center.

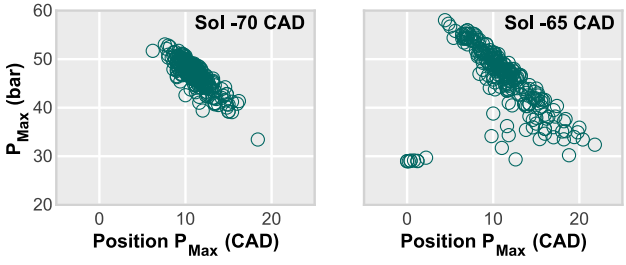

Figure 4.9: Cycle-to-cycle variation for extreme SoI conditions (-70 and -65 CAD aTDC). The plot illustrates the maximum peak pressure inside the cylinder against its angular position for the low load case (1500@4) at λ=2.6.

The plot reveals that combustion deterioration occurs with a relatively minor variation of SoI. The measured cycles transition from exhibiting low cycle-to-cycle variation (SoI = -70 CAD aTDC) to compromising engine stability in a span of fewer than 10 CAD of injection delay. The repetitiveness of the pressure peaks is evident at SoI = -70 CAD, where a strong correlation between these peaks and their angular position is observed. This indicates consistent combustion velocity for each cycle. However, for the delayed SoI case, this relationship is less clear, suggesting issues with initial flame development in multiple engine cycles. Some of these cycles even exhibit complete misfiring, with maximum pressure peaks approaching values attained during motored conditions at TDC (approximately 30 bar).

The examination of the high load point (1500@7) results in Fig. 4.8, also revealing similar trends as the low load case (1500@4). In this instance, the sweep of the SoI was performed between -130 and -85 CAD aTDC, considering only the observed regime II when injection occurs during the compression stroke. Once again, a significant gain in thermal efficiency is observed, with GIE increasing from nearly 41% to 43%. The ISFC can be decreased to 70 g/kWh while maintaining the COV_{IMEP} around 2%. The only difference is in the maximum allowable delay for the start of injection before combustion stability is lost. While the low load point allowed an injection timing of -65 CAD aTDC, this higher load point cannot sustain stable operation with further delays beyond -85 CAD aTDC.

To investigate the underlying cause of this specific behavior, Fig. 4.10 provides an overview of the combustion periods gathered by the spark timing (ST), CA10, CA50, and CA90. This representation, derived from the cycle-averaged heat release rate profiles, facilitates the analysis of how combustion is influenced by the injection event. Examining the data for the 1500@4 point, the results demonstrate that delaying the injection up to -70 CAD aTDC leads to an acceleration of combustion during the initial stages (ST-CA10 and CA10-CA50), indicating improved mixing and turbulence conditions in the vicinity of the spark plug. However, with further injection delays, combustion deteriorates across all stages. It is noteworthy that all the depicted stages lengthen with the SoI at -65 CAD aTDC. This behavior, however, is not precisely replicated at higher loads. Transitioning from a stable SoI (-130 CAD aTDC) to the most delayed SoI (-85 CAD aTDC) reveals that the burning rate remains largely unchanged during the early stages of combustion, while the third stage (CA50-CA90) elongates, indicating that combustion instability has shifted towards the latter part of the combustion process.

This phenomenon can be attributed to multiple factors, including inadequate turbulence in the combustion chamber, which hampers the effective mixing of fuel and air as well as the propagation of the turbulent flame. Additionally, inappropriate matching between the injector and chamber design could also contribute to this issue. Regrettably, in order to gain a comprehensive understanding of the influence of injection timing on combustion stability and efficiency, as well as to develop strategies for optimizing injection timing under diverse operating conditions, further research is required. This research should involve advanced optical techniques and/or numerical models to delve deeper into the subject matter and are out of the scope of this investigation.

To assess the influence of these combustion variations on pollutant levels, the results of NO_x emissions are presented in Fig. 4.11 for both load levels operating at $\lambda = 2.6$. It can be observed that NO_x emissions remain consistently low throughout most of the SoI sweep, primarily due to the inhibitory effect of high dilution rates on NO_x formation through the thermal mechanism. However, as the injection is further delayed beyond -110 CAD a TDC during low load conditions, a noticeable increase in NO_x emissions becomes evident. This trend suggests the onset of stratified charge, where a locally richer mixture forms, leading to higher flame temperatures and subsequently increased NO_x production. At the 1500@7 load point, NO_x

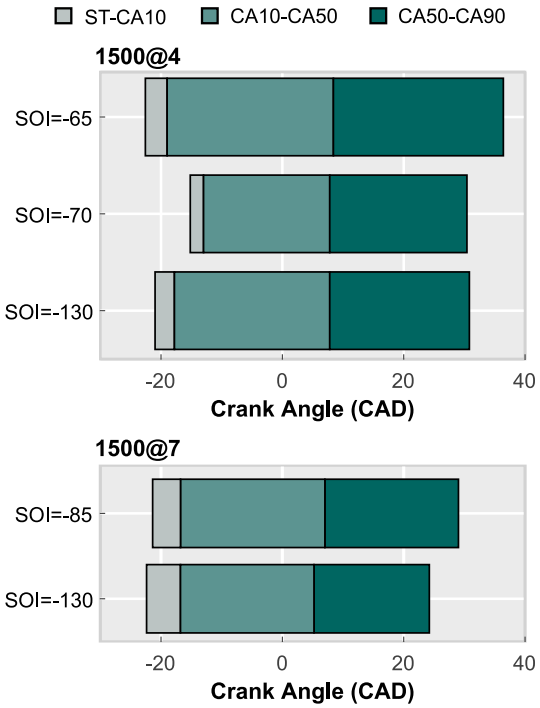

Figure 4.10: Combustion periods for different SoI and load conditions operating at $\lambda = 2.6$

levels are slightly elevated but still below 0.5 g/kWh before experiencing a sharp increase due to mixture inhomogeneity. In this particular case, the turning point occurs at -90 CAD aTDC.

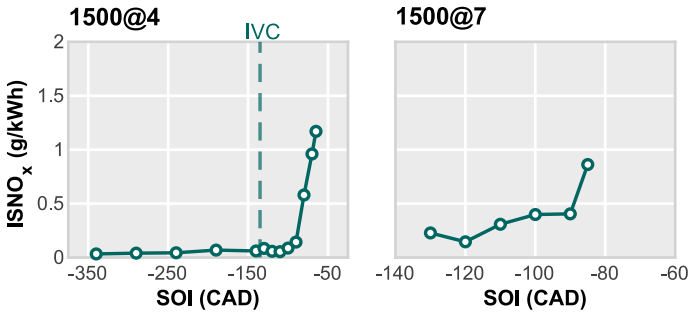

Figure 4.11: NO_x emission levels for different SoI and load conditions operating at $\lambda = 2.6$.

This trend contradicts the performance gains observed in Fig. 4.8. Therefore, understanding the source of this efficiency improvement can aid in resolving this issue. Examining the pressure-volume diagrams presented in Fig. 4.12 for the low load point provides insight into how the compression work is affected as the injection is shifted towards TDC. It can be observed that as the injection is delayed, the compression work is reduced. Computing this parameter at -20 CAD aTDC (ensuring that combustion is not initiated in all considered points), there is a 7.6% reduction at low load and a 3.9% reduction at high load before compromising combustion stability. This translates to the observed 3.1-3.2% improvement in ISFC (Fig. 4.8) for both load conditions considered. The area of this diagram, corresponding to the indicated work, increases with injection delay. This effect is amplified by the low density of hydrogen, which makes it more prominent compared to other gaseous fuels such as natural gas.

These findings carry significant implications for the design and optimization of DI hydrogen combustion engines, emphasizing the crucial role of precise injection timing control in achieving both high performance and low emissions. Moreover, this study underscores the necessity for further research to examine the effects of delayed injection on emissions and combustion stability.

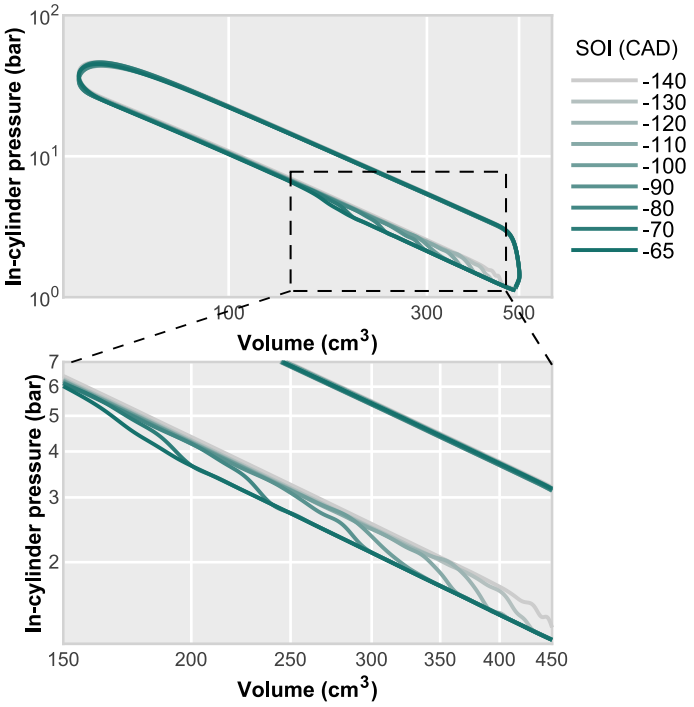

Figure 4.12: P-V diagrams for the SoI sweep at $\lambda=2.6$ cases. The pumping losses were not included to evaluate only the work produced in the firing cycle.

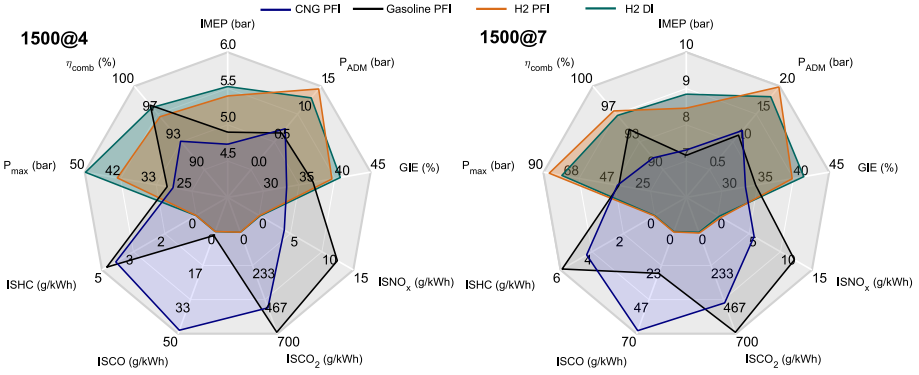

Figure 4.13: Comparison between the engine most significant parameters when operating with hydrogen and conventional fuels like gasoline and CNG.

4.3.3. Comparison with other fuels and injection technologies

This concluding section summarizes the performance and emissions levels achieved when utilizing hydrogen as fuel in a spark-ignition engine, emphasizing significant findings relevant to the advancement of hydrogen-powered engines. Additionally, a comparison is drawn between hydrogen and conventional fuels, such as gasoline and compressed natural gas which are commercially available at present. This comparison is feasible as equivalent operating conditions to those employed in this study were measured for gasoline and CNG under PFI conditions. The engine measurements utilizing both gasoline and CNG were carried out on the same engine and under identical operating conditions. These datasets have already been published in previous works [8] and serve as baseline tests for comparison with conventional fuels. To achieve this, the authors maintained consistent operating conditions, including engine speed and load, while adjusting the fuel injected mass to ensure the total energy available for combustion remained constant.

The comparison of the results shown in Fig. 4.13 highlights that hydrogen engines have the potential to outperform gasoline and CNG engines. This can be attributed to their higher efficiency and lower GHG and pollutant emissions. NO_x can be effectively controlled by implementing high dilution levels, which in turn enable the attainment of high thermal efficiency while preserving combustion stability. Moreover, this approach helps maintain very low levels of hydrocarbon (HC) and carbon monoxide (CO) emissions (although not reaching zero due to potential interactions with the oil).

As depicted in Fig. 4.13, there is a paradigm shift where emissions are effectively controlled, resulting in improved efficiency and reduced fuel consumption. However, this shift presents various technological challenges. These include the need for turbocharging systems that can handle high intake pressures in PFI systems, injectors capable of operating with low-density fluids and moderate backpressure chamber pressures, as well as addressing issues related to distribution and storage, among others.

In contrast, gasoline and CNG enjoy wide availability and can offer short-term cost-effectiveness. However, the environmental advantages of hydrogen and CNG should not be overlooked, as their utilization can contribute to the reduction of greenhouse gas emissions in the transportation sector. Therefore, a practical solution for achieving a balance between performance and sustainability during the transition towards a more environmentally friendly future could involve a combination of fuels, such as hydrogen blends or hybrid systems.

4.4. Conclusions

The study explores the potential of using a modern spark ignition engine with an outwardly opening poppet valve hydrogen injector. To achieve this, two different injection technologies–PFI and DI–are implemented in a single-cylinder SI engine. The comparison of emission levels, performance, and combustion characteristics has been conducted under various dilution, load, and injection timing conditions. Overall, this study provides valuable insights into the use of such injectors for internal combustion engines in light-duty applications and highlights key areas for future research.

The results demonstrate that the direct injection system outperforms the port fuel injection system along the entire range of air dilutions considered in this study. Gains of approximately 0.6 to 1.1% in gross indicated efficiency are observed at the two load conditions considered. Additionally, the direct injection system exhibits the advantage of requiring a lower intake pressure when the injection timing is set after the intake valves closing event, thereby alleviating the stress on the boosting system.

In terms of NO_x emissions, both injection systems achieve similar levels and trends, although some differences can be found at high load. The injector-specific design seems to create a distinct mixture stratification, potentially impacting the λ at which NO_x levels rise, despite an identical overall air-to-fuel ratio compared to the PFI case.

A precise injection timing control is crucial to achieving both high performance and low emissions in DI hydrogen combustion engines. Delaying the start of injection results in a 7.6% reduction in compression work at low load and a 3.9% reduction at high load before compromising combustion stability. This results in a 3.1-3.2% improvement in ISFC in both load conditions considered. However, this action also results in a reduced mixing time, which leads to charge stratification. This effect contributes to increased NO_x emissions, as hydrogen is burned under richer conditions compared to the overall dilution condition.

The conclusions of this research should be considered as an initial starting point for future investigations since some of the conclusions presented here are completely based on experimental observations, which can make it challenging to provide a comprehensive explanation of the observed trends. Results evinced that understanding the local thermodynamic conditions within the combustion chamber is crucial for achieving stable flame development. Similarly, it is essential to manage the local equivalence ratios effectively in order to control the production of NO_x.

Therefore, further research should combine experimentation with simulations to understand and overcome these limitations. In this context, a deeper understanding of local phenomena can lead to substantial reductions in cooling losses and improvements in thermal efficiency. This involves promoting a lean local mixture fraction near the wall region while simultaneously maintaining a uniformly distributed and sufficiently high air-to-fuel ratio to prevent NO_x production.

CHAPTER 5

New combustion modeling approach for methane-hydrogen fueled engines using machine learning and engine virtualization

[4] S. Molina, R. Novella, J. Gomez-Soriano, and M. Olcina-Girona. "New combustion modelling approach for methane-hydrogen fueled engines using machine learning and engine virtualization". Energies 14 (20), 2021, p. 6732.

5.1. Introduction

The increased public awareness about climate change led countries to establish greenhouse gas (GHG) emission reduction targets. In this context, hydrogen (H_2) is a possible energy vector to decarbonize the economy and society. The absence of carbon dioxide (CO_2) emissions on hydrogen combustion and its high heating value make its use attractive for a future fuel substitute. Moreover, hydrogen could help countries to reach energy independence, to avoid a vulnerable position in diplomatic relationships due to the unequal distribution of fossil fuel reservoirs around the Earth.

Furthermore, the fast development of renewable energies, such as wind power or solar energy, is helping to redistribute the energy sources. These methods offer an irregular energy generation since they depend on external factors which change sharply throughout the day (i.e. the wind intensity or the number of daylight hours). Therefore, the control of energy production

remains the main disadvantage of these generation methods, highlighting the need for an energy carrier to manage the irregular distribution of energy production.

According to the Hydrogen Council, the cost of hydrogen production will be reduced by approximately 60% in 2030 if they are compared with the predicted levels of 2020 [148]. This prediction considers the most relevant aspects of hydrogen production: reduction in Capital Expenditures (CapEx) requirements, cheaper renewable energy, and increase in system optimization.

For all these reasons, hydrogen is a fundamental piece to achieve Conference of the Parties (COP21) Paris agreement objectives [17]. The European Union (EU), framing itself in the pact to keep the increase in the global temperature below 2 degrees Celsius concerning pre-industrial levels, has developed a roadmap in the economy's decarbonization. In particular, some sectors, such as gas grid decarbonization for industrial high-grade heat purposes and transport, must be completely adapted. Transport emissions, which are 32% of total CO_2 emissions in the EU, have to be reduced by 72% [80] though renewable energy systems, green hydrogen, energy supply systems, hydrogen pipelines or power-to-hydrogen [149].

The implementation of hydrogen on internal combustion engines (ICE) could help to reduce GHG emissions in two ways: during the production process (well-to-tank) and the vehicle operation (tank-to-wheel). Lean combustion is one of the most interesting strategies for decreasing tank-to-wheel emissions. Fuel consumption can be improved by increasing the specific heat ratio as the percentage of the fuel is reduced in the intake mixture [150]. Maintaining combustion stability in a lean environment requires high-energy ignition systems [151]. Long-duration sparks, multiple spark plugs in one cylinder, or pre-chamber ignition systems [121, 152, 153] are recently on the scope.

However, there are some disadvantages of applying hydrogen to ICEs. Its low density reduces the operating range of the vehicle due to the size of the tanks for fuel storage. In addition, abnormal combustion problems due to the high flammability properties of H_2 demand other strategies to control the combustion stability (i.e. combining H_2 with other less reactive fuels).

Hydrogen mixed with Compressed Natural Gas (CNG), which is mostly based on methane fuel, is one of the most promising fuel blends, pointing to reach a fully developed decarbonized hydrogen economy. Although methane combustion produces CO_2, its low carbon content makes it very attractive as a partial solution to the problem of GHG emission [152]. Moreover, the

production of CNG is also interesting due to its low carbon cost. Animal waste, landfills, waste of the food industry, aquatic biomass, or agricultural waste are some examples of feedstock for the CNG generation from renewable sources (also known as biogas). The two larger biogas producers in the world are Brazil and the USA. However, the lack of investment policies to enhance production procedures hinders the substantial growth of this technology. Despite this, Brazilian biogas production may increase from 5.3 million m^3/day in 2030 to 19.7 million by 2050 [154].

In addition, several works investigated the safety concerns about the hydrogen-enriched premixed flames. Law et al. [155] studied the effects of partial hydrocarbon substitution on hydrogen–air flames. Motivated by security considerations, the authors identified propane, methane and ethylene as suitable hydrocarbon substitutes, based on storage and combustion performance considerations. The explosion behaviour of methane/hydrogen/air mixtures was experimentally characterized by Li et al. [156] and Salzano et al. [157], in an attempt of enhancing the security of its use. To this end, the flame behavior of premixed hydrogen-enriched fuel blends was also studied [157, 158] considering a turbulent flow field.

Engine experiments using hydrogen are expensive due to the needs of specific experimental equipment, safety considerations, time, and qualified personnel. To reduce the number of experiments, virtual engine modelling is a useful tool. These modelling approaches, mostly based on coupling 0D and 1D simulations, help to perform exploratory studies to choose the best medium/long-term strategy while defining the path towards the objectives set for 2050. These are especially helpful in the development of new technologies where the high number of variables leads to a huge amount of experiments and related costs.

In the past, several investigations tried to predict the combustion process inside the combustion chamber of ICEs, including the turbulence-combustion interaction [159, 160]. In this framework, 1D simulations based on two-zone quasi-dimensional models [161–163] are the most extended ones. The flame development inside the cylinder during the combustion process is described by different theoretical approaches. For instance, some models use Wiebe functions to model the mass burned fraction [164–167]. Despite being extremely fast, the accuracy of these models is not good enough when changing the fuel or air-fuel mixture conditions. The fractal combustion models are based on the hypothesis that turbulence increases the burning rate as the flame surface is also increased. They are extensively used in several research works [168, 169] since they allow to improve the accuracy

in a wide range of operating conditions. However, problems in estimating the laminar properties of the flame when switching the fuel or when mixtures of several fuels are used, limit the application of these models in exploratory studies.

Currently, data-driven modelling, specifically based on Artificial Neural Networks (ANN), is being implemented in many fields of science and technology [170–172], opening up a new dimension to data analysis and prediction algorithms. Using machine learning, the ANN will get the laminar flame speed from the thermo-chemical conditions existing inside the combustion chamber on run time, eliminating one of the main limitations of the fractal combustion models.

The main objective of this investigation is to implement a modelling approach that allows estimating the burning rate of the air-fuel blend inside the combustion chamber using a combination of an existing combustion model, ANN, and virtual engine modelling. The target is to find a new way to enhance the accuracy of combustion modelling in a wide range of operating conditions, air-fuel dilutions, and fuels while maintaining the computational time.

5.2. Experimental setup

5.2.1. Engine and test cell configuration

The experimental data were obtained from a single-cylinder research version of a 4 cylinder light-duty vehicle, whose specifications and relevant geometrical features are presented in Table 5.1. The engine was assembled in a test cell in which a high number of instruments measure and control every relevant variable. For instance, a dedicated compressor controls pressure conditions at the intake, the low-pressure EGR system controls the mixture reactivity in the cylinder recirculating part of the combustion products, and independent oil and water cooling circuits manage the temperature of the fluids. The fuel is injected in the manifold, 270 mm away from the cylinder to ensure a suitable mixing between air and fuel, using a port fuel injection system and measured by a BRONKHORST F-113AC-M50-AAD-44-V flowmeter. The experimental setup is widely described in previous research works [121, 152, 153].

All relevant combustion parameters, such as the indicated gross mean effective pressure (IMEP), start of combustion (CA10), combustion duration (CA10-90), combustion phasing (CA50), maximum cylinder pressure,

Engine	4-Stroke SI
Number of cylinders [-]	1
Displacement [cm3]	404
Bore - Stroke [mm]	80.0 -80.5
Compression ratio [-]	13.4:1
Valvetrain [-]	DOHC
Number of valves [-]	2 intake and 2 exhaust
Fuel injection system [-]	PFI (Pmax = 6 bar)

Table 5.1: Main engine specifications

heat release rate (HRR), combustion stability, and in-cylinder gas temperature were calculated from the cylinder pressure signal by an in-house 0D combustion diagnostics software [173, 174].

5.2.2. Properties of fuels

Table 5.2 summarizes the main properties of the fuels used in this investigation. As explained, hydrogen could be applied to the transport sector to reduce the percentage of CO_2 emissions. The low auto-ignition properties point out that spark-ignition engines fueled with hydrogen should be more feasible than compression-ignition ones. The hydrogen wide flammability range allows combustion in ultra-lean conditions, increasing thermal efficiency by reducing heat transfer losses. Also, to avoid abnormal combustion phenomena such as backfiring, it is highly recommended to operate in a lean environment. The low ignition energy and high burning speed of hydrogen reduce misfire.

Methane appears as a good candidate to complement hydrogen as fuel. Mixing hydrogen with other fuels, such as gasoline, alcohol, diesel or methane enhances the ignition and burning control. Methane also shares with hydrogen a high auto-ignition temperature reducing the possibility of reaching knocking conditions. The low number of carbon atoms per methane molecule and the possibility to produce biogas also contribute to reducing GHG emissions.

Property	Unit	Methane CH_4	Hydrogen H_2
Molecular Weight	[u]	16.04	2.02
A/Fst	[-]	17.2	34.3
Lower Heating Value	[MJ/kg]	50	120
Density	[kg/m3]	0.657	0.0823
Carbon Atoms per Molecule	[-]	1	0
Hydrogen Atoms per Molecule	[-]	4	2
RON	[-]	>120	>130
Auto-ignition temperature	[K]	600	645

Table 5.2: Hydrogen and methane fuel properties

5.3. Methodology

In pursuit of the objective of this investigation, several simulations will be performed considering different fuel blends and air dilution levels in one operating point. This operating point corresponds to a high engine speed (4000 rpm) and mid-to-high engine load (14 bar of IMEP). For the reference point, CNG fuel is used in stoichiometric conditions while using a Spark Timing (ST) that guarantees the Maximum Brake Torque (MBT) conditions.

Using this point as a baseline for the study, the fuel sharing and dilution conditions were modified as in the simulation plan presented in Fig. 5.1. In all these simulations, the amount of energy injected was kept constant by adjusting the total amount of fuel and fixing the desired mixture conditions (air-to-fuel ratio). The ST was shifted to reach MBT conditions by optimizing the combustion phasing.

In order to account for the different thermo-chemical conditions that modify the combustion process of each simulation, a database of 10,000 situations was generated using a 1D laminar flamelet code with the input ranges detailed in Table 5.3. All these values were selected to gather all possible situations achieved in the simulations.

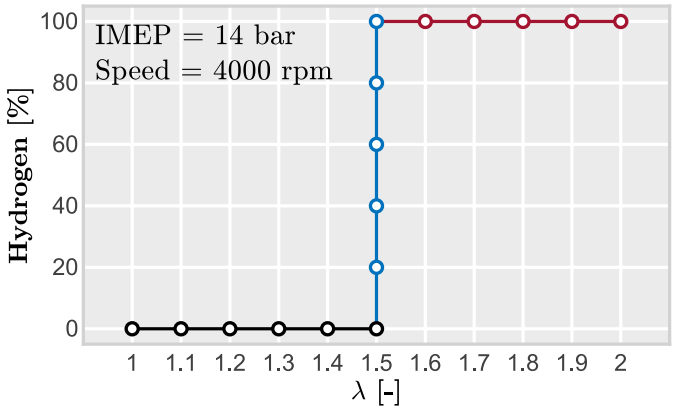

Figure 5.1: Simulations plan. The black line corresponds with the CNG simulation plan, sweeping the air dilution until $\lambda = 1.5$. The blue line sweeps the amount of hydrogen in the fuel from 0% to 100%. The red line considers pure hydrogen combustion varying λ from 1.5 to 2.

Once this database was created, several architectures of ANN were tested to get the best modelling approach for this particular application. The inputs for the ANN are the in-cylinder pressure and temperature, the air-to-fuel ratio, the amount of EGR, and the percentage of H_2 in the fuel blend.

The turbulent properties of the in-cylinder flow required for mimicking the turbulent flame characteristics were obtained from Computational Fluid Dynamics (CFD) simulations. Several calculations of the complete engine cycle were performed considering different engine speeds (1350, 2500 and 4500 rpm) and fuel compositions (25%, 50%, 75% and 100% of H_2). The CFD model setup was obtained from previous works [125, 175] that consider the same engine hardware.

Finally, and before proceeding with the analysis of the results, the model was validated in two stages. First, the new combustion modelling approach coupled with the virtual engine was validated in a steady operating condition: the reference condition (4000@14) using a stoichiometric CNG/air mixture. Then, the basis of the combustion model, that is the laminar flame speed, is validated at several lean conditions considering pure CNG, pure hydrogen, and a set of mixtures of them.

Sweeping Variable	Unit	Range
Temperature	[K]	800 - 300
Pressure	[bar]	30 - 10
λ	[-]	2 - 1
EGR	[%]	40 - 0
H_2 mass	[%]	100 - 0

Table 5.3: Range of variables for the flame speed simulation table to feed the ANN model.

5.4. Numerical setup

5.4.1. Virtual model of the engine

A numerical tool based on a 1D Wave Action Model was used. The engine simulations were performed by Gamma Technologies GT-SUITE v2020 software whereas the ANN training was performed using the different machine learning tools available in the same software. The geometrical information of the single-cylinder engine was implemented to create a model as closely as the experimental setup, recreating the different parts; intake, exhaust, exhaust gas recirculation (EGR), and fuel injection systems. The original model of the test bench layout was developed in previous work [153] and adapted to implement the new combustion model. This model was also used in previous research works [121, 152].

5.4.2. Combustion modelling

The combustion process is simulated by the phenomenological combustion model developed by Wahiduzzaman et al. [176] and later refined by Mirzaeian et al. [177]. The basis of this modelling approach can be summarized by the evolution of the entrained mass rate of the unburned gas and the rate of burnup described in Eq. 5.4.1 and Eq. 5.4.2.

The rate of the unburned gas depends on the unburned gas density (ρ_u), the flame front area (A_f) computed by a geometric sub-model detailed in [176] and the sum of the laminar and turbulent flame speeds (s_L and s_T).

$$\frac{\mathrm{d}M_e}{\mathrm{d}t} = \rho_u A_f \left(s_L + s_T\right) \tag{5.4.1}$$

The rate of burnup ($\frac{dM_b}{dt}$) is related to the unburned mass behind the flame front ($M_e + M_b$) as in Eq. 5.4.2.

$$\frac{dM_b}{dt} = \frac{M_e + M_b}{\tau} \tag{5.4.2}$$

The τ parameter, expressed in Eq. 5.4.3, represents the time needed by the laminar flame to cover the Taylor microscale (λ) of turbulence. This parameter can be obtained by Eqs. 5.4.4 and 5.4.5 if considering isotropic turbulence. C_λ is a calibration parameter.

$$\tau = \frac{\lambda}{s_L} \tag{5.4.3}$$

$$\lambda = \frac{C_\lambda \, L_t}{\sqrt{\mathrm{Re}_T}} \tag{5.4.4}$$

$$\mathrm{Re}_T = \frac{\rho_u \, u' \, L_t}{\mu} \tag{5.4.5}$$

The laminar flame speed is traditionally obtained from empirical correlations adjusted for a specific fuel blend. For instance, Huang et al. [178] established a relationship for mixtures of methane and hydrogen whereas Ömer et al. [179] got a correlation for light hydrocarbons. Di Sarli et al. [180] obtained a good prediction by means of a Le Chatelier's Rule-like formula, this correlation together with the laminar flame speed expression obtained by Ma et al.[181] were implemented with success in the quasi-dimensional combustion model proposed by Perini et al. [182]. However, the accuracy of this method over a wide range of dilution and/or thermodynamic conditions is rather limited. Therefore, in recent years there has been growing interest in developing new methods to obtain the laminar burning velocity while maintaining the calculation speed and improving the accuracy over a wide range of conditions to increase the flexibility of the model.

The transition from laminar to turbulent flame is accounted by the Eq. 5.4.6. In this equation three turbulent characteristics are included: the flame radius (R_f), the fluctuation of the velocity field (u'), and turbulent length scale (L_t). In addition, the flame kernel growth multiplier (C_k) scales the flame structure from a smooth surface (characteristic of the laminar conditions) to a fully developed turbulent wrinkled surface. Finally, the turbulent flame speed multiplier (C_s) is a scaling parameter for calibration.

$$s_T = C_s\, u' \left(1 - \frac{1}{1 + \frac{C_k R_f^2}{L_t^2}} \right) \tag{5.4.6}$$

5.4.2.1. Modelling laminar flame speed

In the present work, an ANN to estimate the laminar flame speed for the combustion modelling is used. The basis of ANNs relies on the data used for its training. These data can be obtained from experiments, as did Huang et al. [178] for mixtures of hydrogen and methane, or from simulations. In this case, the database was generated by a 1D laminar flamelet code that calculates the flame speed of the combustion reaction using a freely propagating flame in a simulated channel with a fixed cross-sectional area. To extend the range of application, simulations included multiple situations on hydrogen and methane mixtures in numerous conditions of pressure, temperature, air, and exhaust gases dilution.

For these simulations, a chemical kinetic mechanism is required, several of them are available in the literature. According to Ji et al. [183] in a recent investigation, the GRI-Mech mechanism [184] has the best performance when simulating the combustion process of methane and hydrogen mixtures for different air dilution (λ) conditions. This mechanism contains 325 chemical reactions with 53 species and the possibility of using it in a wide range of conditions, especially in the case of light hydrocarbon fuels (CH_4, C_2H_6, CO and H_2).

This mechanism was validated in relevant conditions for this investigation: pure methane combustion, pure hydrogen combustion, and different blends of both fuels. This wide validation was done to increase the reliance on the results obtained.

Figure 5.2 shows a comparison of the laminar flame speed obtained by the flamelet code and measured by Dong et al. [185] for different air-to-fuel ratios of methane. As it can be seen, results are reasonably close to experiments in the whole dilution range.

Experimental results of pure hydrogen combustion obtained by Ravi and Petersen [186] for different dilution cases are presented in Fig. 5.3. Again good results are obtained for the whole range of dilution.

Finally, results for the validation of different mixtures of methane and hydrogen are included in Fig. 5.4. Trends are well captured by the model in the whole range of H_2 substitution percentage.

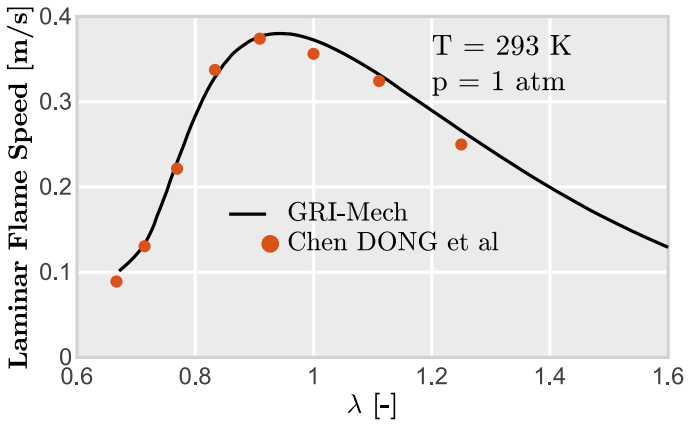

Figure 5.2: Validation of CNG laminar flame speed for different air-to-fuel ratios.

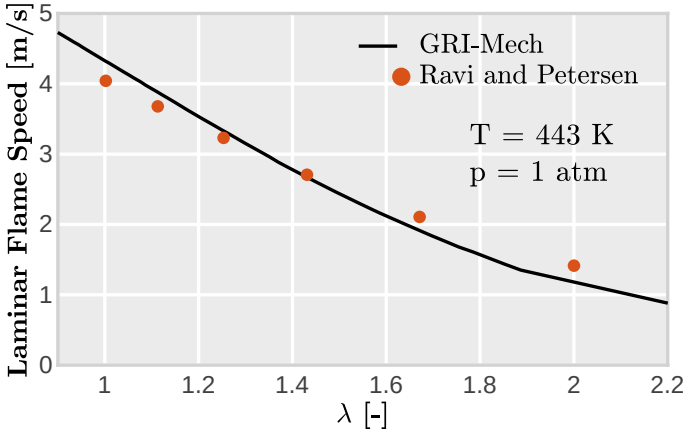

Figure 5.3: Validation of H_2 laminar flame speed for different air-to-fuel ratios.

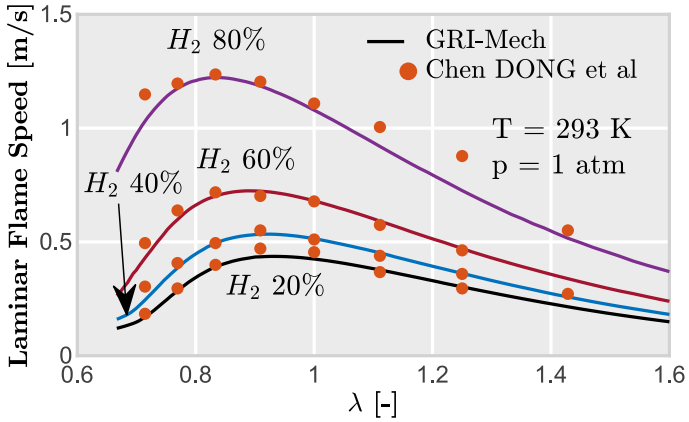

Figure 5.4: Validation of methane-H_2 laminar flame speed for different air-to-fuel ratios. The hydrogen percentage is expressed in the volume percentage of the total fuel volume.

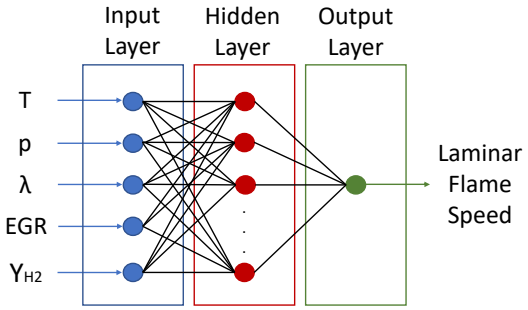

Figure 5.5: Artificial Neural Network architecture used for the laminar flame speed modelling.

A database was generated considering the input ranges summarized in Table 5.3. These ranges were specifically defined to gather all the possible conditions simulated by the virtual engine model. A 26-neuron 3-Layer Feedforward ANN was chosen after an optimization and selection procedure. This ANN architecture is represented in Fig. 5.5 where the three layers of output nodes are fed directly via a series of weights applied to the inputs.

This ANN calculates the outputs (y) using the equation Eq. 5.4.7.

$$y = f(w \cdot g(z \cdot h(v \cdot u + a) + b) + c) \tag{5.4.7}$$

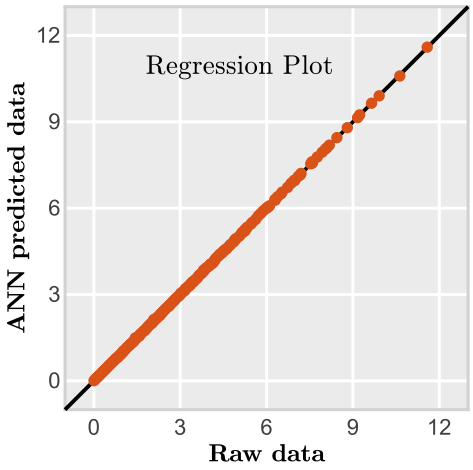

Figure 5.6: Training results for the ANN used for the laminar flame speed modeling.

where u is the input data. (v and a), (z and b) and (w and c) are the weights and biases of input, hidden and output layers respectively. Functions $g(x)$ and $h(x)$ are the activation functions for the input and hidden layers, being both expressed by Eq. 5.4.8.

$$g(x) = h(x) = -1 + \frac{2}{1 + e^{-2x}} \tag{5.4.8}$$

Lastly, $f(x)$ is the activation function for the output layer which corresponds with the identity function presented in Eq. 5.4.9.

$$f(x) = x \tag{5.4.9}$$

25% of the data is randomly selected to validate the neural network after the training process. These data points were not used in the training process. The training process is based on the Levenberg-Marquardt algorithm. The performance of the ANN is presented in Fig. 5.6. The RMS training error is 5.63e-03 and the RMS testing error is 6.04e-03, both values can be considered acceptable for this investigation.

5.4.2.2. Modelling turbulent flame speed

The turbulence properties needed for calculating the turbulent flame properties were estimated from a Computational Fluid Dynamics model. Although the turbulent length scale and the velocity fluctuation can be obtained by simpler models (such as the energy cascade method [187]), CFD offers improved accuracy and further information about the turbulence field.

The CFD model used for this purpose has been widely used in other investigations [125, 175]. Using this configuration, several simulations were performed to obtain the evolution of L_t and u' along the engine cycle for different engine speeds. Results of these simulations are presented in Fig. 5.7, where the turbulent length scale and the velocity fluctuation are shown for three different engine speeds. Data from this figure was used to approximate the temporal evolution of both parameters as a function of the engine speed in the virtual engine model. The profiles were normalized and later customized to obtain the turbulent values for the combustion modelling. It was found, after calculating multiple simulations with different CNG/hydrogen mixtures, that fuel composition does not affect the turbulent length scale nor the velocity fluctuation, being equally valid these parameters for CNG as for hydrogen.

5.4.3. Validation of the virtual engine model

The virtual engine model was validated using the operating condition defined in Section5.3. This operation condition consists of an engine speed of 4000 rpm and 14 bar of IMEP operating with pure methane fuel in stoichiometric conditions.

Figure 5.8 shows the comparison between the instantaneous signals obtained by the model and measured in the engine. In the case of simulations, two different cases are included to compare the performance of the proposed model against the more conventional combustion modelling approaches (i.e. empirical models based on flame speed correlations). The top graph shows the good agreement observed when contrasting the in-cylinder pressure signal. Similarly, the accuracy of the model to predict the combustion process is depicted in the bottom graph through the instantaneous evolution of the heat release rate (HRR). Although there are more differences than in the pressure, the characteristic values, such as combustion onset (CA10), combustion duration (CA90-10), and maximum HRR peak are well captured. All these parameters, included in Table 5.4, show an acceptable scatter from the experiments. Similarly, some of the most relevant engine outputs

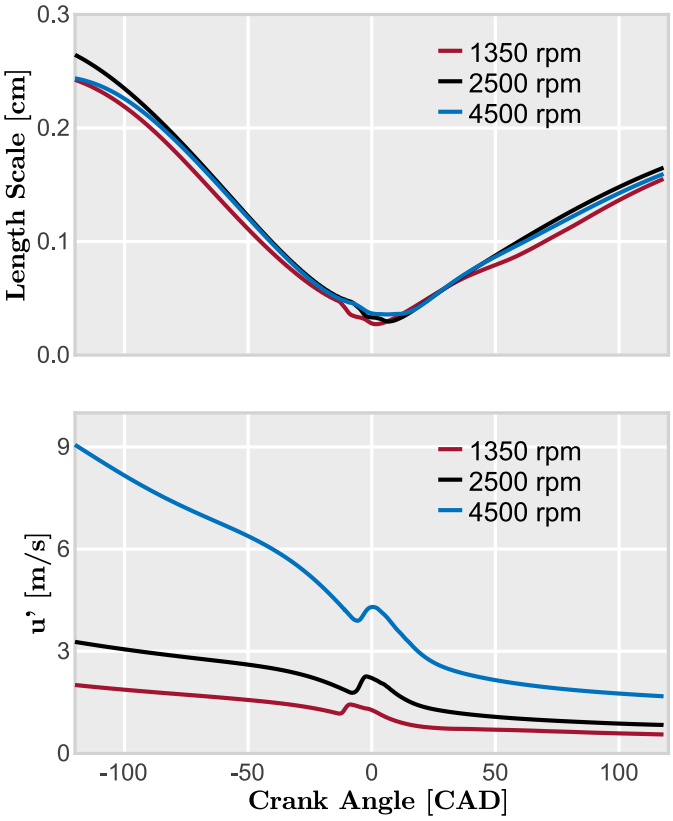

Figure 5.7: Temporal evolution of the turbulent length scale (L_t) and the velocity fluctuation (u') inside the combustion chamber for three engine speeds.

Parameter	Experiment	Simulation
CA10 [CAD]	-8.8	-10.8
CA50 [CAD]	4.8	1.7
CA90-10 [CAD]	35.4	30.2
HRR_{max} [J/CAD]	43.5	40.1
IMEP [bar]	13.58	12.71
ISFC [g/kWh]	171.9	167.0
Ind. eff. gross [%]	42.78	43.06

Table 5.4: Validation of the virtual engine model coupled with the combustion model. Combustion-related parameters are included together with other engine outputs.

(indicated) are also included for verifying the model response to engine-related parameters. The difference in the CA50 estimation comes from the limitations of the model. As will explain later, the model cannot predict the cycle-to-cycle variation which is critical in this operating condition. That means that the dispersion observed in the HRR profiles and then, in the CA50 estimation, is significant. The difference observed in CA50 between the simulation and the experiments can be explained by a combination of modelling limitations and experimental uncertainties due to CCV.

Fig. 5.8, a shows a comparison between the ANN and the empirical model. The ANN model presents a better accuracy. The empirical model shows in-cylinder pressure and heat release rate profiles that are further from the experimental results. Not only accuracy, also flexibility make, the ANN model, a more attractive approach.

5.5. Results and discussion

After explaining the numerical methodology, this section discusses the results obtained from the virtual model simulations. The analysis is focused on the combustion process itself and the engine performance when the dilution ratio and the fuel composition are modified.

5.5.1. Combustion of methane

Results from pure CH_4 combustion are summarized in this section. The combustion process is analyzed in Fig. 5.9, where the HRR profiles are plotted for different air dilution rates. These curves evince how the combustion

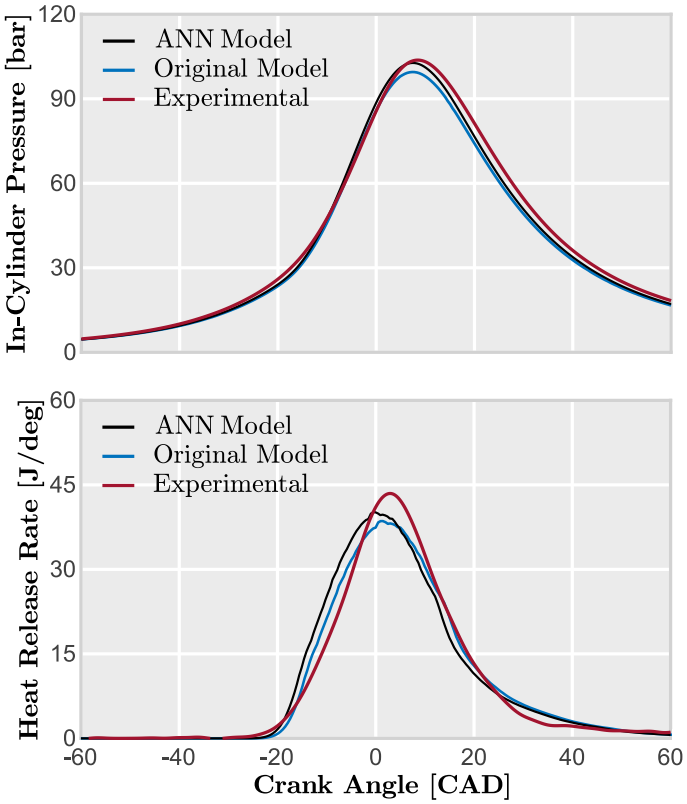

Figure 5.8: Validation of the virtual engine model coupled with the combustion model. In-cylinder pressure and HRR signals are compared with the results measured in the test bench.

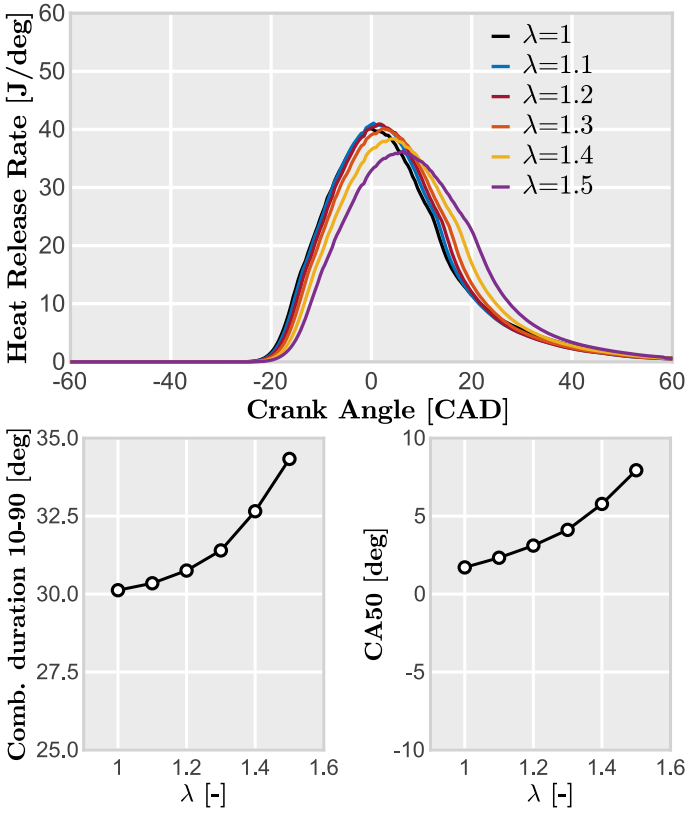

Figure 5.9: Trends of the main characteristics of the combustion process. Heat release rate profiles (top), combustion duration (bottom-left), and combustion phasing (bottom-right) for different air-to-fuel ratios considering methane fuel.

process degrades as the dilution rate increases. While the curves scarcely differ between cases gathered by $\lambda = 1.0$ and $\lambda = 1.3$, they significantly change for values above $\lambda = 1.3$: the leaner condition, the wider HRR profile. In addition, the peak of the energy released is reduced approximately 12% from $\lambda = 1.1$ to $\lambda = 1.5$. The drop of the burning velocity due to the leaner conditions increases the combustion duration as it is shown in Fig. 5.9. The combustion phasing is delayed towards the expansion stroke, moving from a CA50 of 1.5 CAD aTDC to 7.5 CAD aTDC.

In-cylinder pressure profiles simulated by the virtual model are shown in Fig. 5.10. As observed for the HRR trends, the maximum peak of the in-cylinder pressure is similar from $\lambda = 1.0$ to $\lambda = 1.3$, reaching a maximum

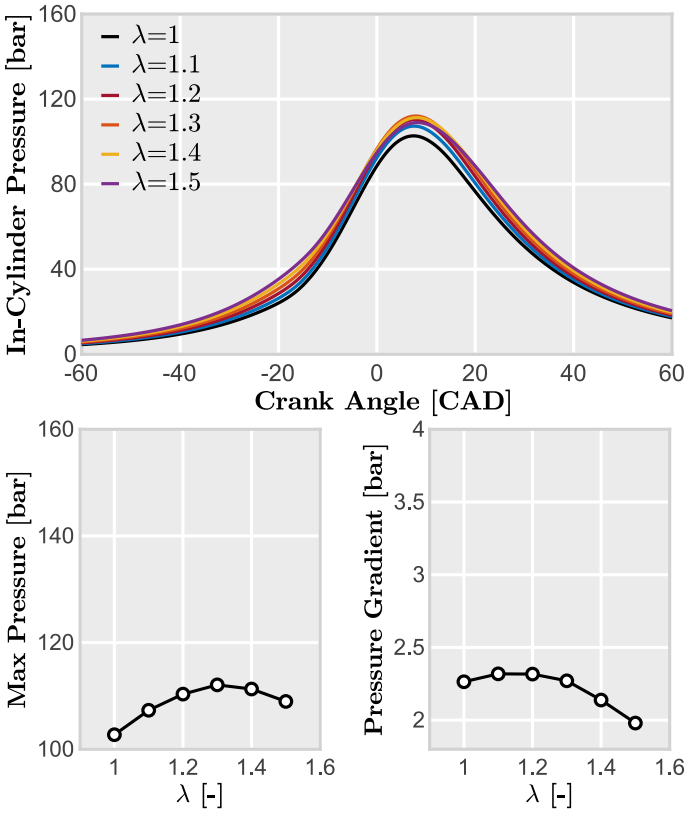

Figure 5.10: In-cylinder pressure evolution. Pressure profiles (top), maximum peak pressure (bottom-left), and maximum pressure change rate (bottom-right) for different air-to-fuel ratios considering methane fuel.

value at $\lambda = 1.3$. Moreover, the decreased flame speed due to leaner combustion conditions produces a distributed energy release that also affects the maximum pressure change rate. Since combustion noise is strongly related to this parameter [188, 189], it can be claimed that increasing air dilution could contribute to reducing noise, vibration, and harshness (NVH).

Inspecting the indicated efficiency trends plotted in Fig. 5.11, it can be seen the efficiency gains obtained as the dilution rate is increased. Here, no maximum is reached for indicated efficiency, despite the reduction in the growth rate observed after $\lambda = 1.4$. Considering the iso-energy assumption, the IMEP trend is equal to the indicated efficiency, reaching at $\lambda = 1.5$ a maximum value of approximately 13.4 bar.

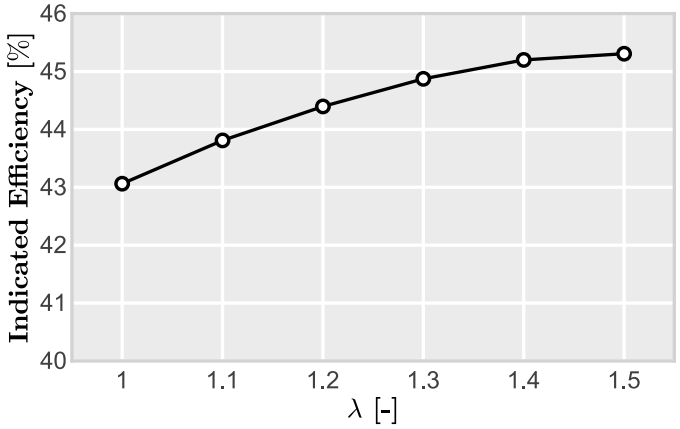

Figure 5.11: Indicated efficiency trends when the air dilution rate is increased from $\lambda = 1.0$ to $\lambda = 1.5$ using methane as fuel.

Although these trends make sense from a theoretical point of view, other research works based on engine experiments [121, 190] showed that the indicated efficiency slightly decrease before reaching the maximum dilution rate. In both investigations, the maximum dilution rate achieved before facing excessive misfiring is gathered between $\lambda = 1.4$ and $\lambda = 1.5$ depending on the operating condition. Considering a similar operating condition, the indicated efficiency reaches a maximum around $\lambda = 1.4$ and then decreases with higher dilution rates. This behavior can be explained by the increased cycle-to-cycle variability (CCV) experienced when the dilution rate reaches $\lambda = 1.5$. As the proposed combustion model does not take into account this cyclic variability, it is not possible to capture this trend.

5.5.2. Combustion of methane-hydrogen blends

In this section, the simulated results obtained when changing the fuel blend composition from pure methane to pure hydrogen are presented. For this study, the fuel composition is varied by 20% of hydrogen and the air dilution rate is fixed at $\lambda = 1.5$. As shown in Fig. 5.12, the heat release rate profile does not change proportionally with the addition of hydrogen. The maximum peak value increases with the amount of H_2 in the fuel blend, reaching a maximum value when the fuel blend sharing is between 40% and 60% of hydrogen. The combustion duration is reduced as hydrogen percentage

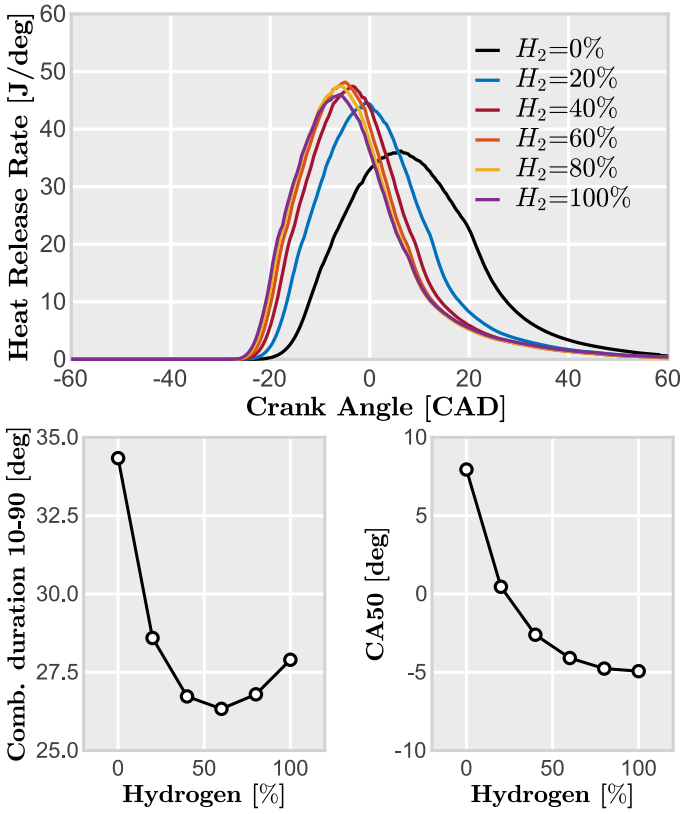

Figure 5.12: Trends of the main characteristics of the combustion process. Heat release rate profiles (top), combustion duration (bottom-left), and combustion phasing (bottom-right) for different fuel compositions.

increases and the optimum CA50 is advanced towards the compression stroke. This trend of decreasing combustion duration as the hydrogen percentage increase is also reported in previous research works [181, 191].

Focusing on in-cylinder pressure profiles, Fig. 5.13 shows the same parameters studied in the previous section for methane combustion. Pressure profiles indicate that the maximum peak pressure increases with the amount of H_2 present in the fuel. The maximum is achieved around 80% and then, it is maintained for further increments of H_2. Moreover, pressure profiles practically overlap from 40% to 100% of H_2. Similarly, the pressure rise rate also increases with the amount of H_2, suggesting an increase of the combustion noise when switching from 0% of H_2 to 60%.

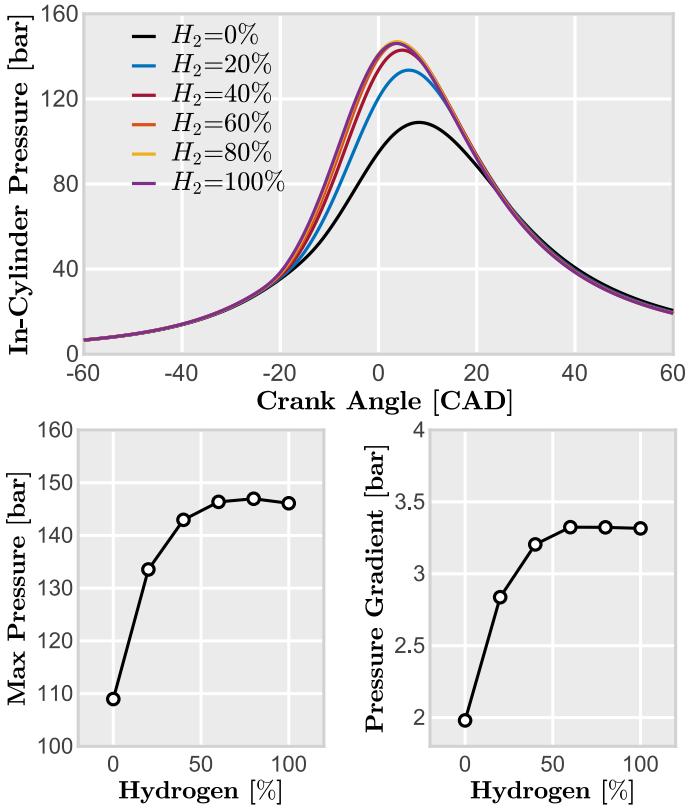

Figure 5.13: In-cylinder pressure evolution. Pressure profiles (top), maximum peak pressure (bottom-left), and maximum pressure change rate (bottom-right) for different fuel compositions.

Figure 5.14 shows the evolution of the indicated efficiency as the H_2 amount increases in the fuel. This parameter is progressively reduced from 45.4% to 42.1%, showing a relevant efficiency loss related to the hydrogen addition. Referring to previous research studies, it is possible to qualitatively validate the trends obtained using the current modelling approach. In the work of Nagalingam et al. [192], different methane-hydrogen mixtures were used to compare the most relevant engine outputs, such as IMEP or indicated efficiency. The experimental results were obtained under the iso-energy assumption also considered in the current study. In this investigation, the reference methane fuel was supplemented with H_2, showing a reduction of the engine power and the indicated efficiency.

This research work [192] also evinced that the optimum spark timing has to be delayed as more and more methane is replaced by H_2. The high knock resistance of methane is reduced with the addition of hydrogen, favouring the end-gas auto-ignition while compromising the engine integrity due to severe knocking combustion. This phenomenon limits the spark advance in the search of MBT conditions as also shown by Lim et al. [193].

Contrary to these results, the proposed modelling approach shows the opposite effect when increasing the percentage of H_2 in the fuel: the optimum spark timing is advanced as the burning rate is increased due to H_2 addition. Thus, this trend cannot be captured without a knocking combustion model that predicts the end-gas auto-ignition of the mixture.

In absence of a knock limitation, the spark timing can be freely advanced to optimize the indicated efficiency, predicting higher efficiency values than expected. Therefore, the proposed approach tends to advance the combustion process as the burning rate increases due to the H_2 addition. Consequently, the results in this section should be treated with care, although the physics related to flame propagation shows consistent results, an additional model needs to be implemented to account for the knock phenomenon.

5.5.3. Combustion of hydrogen

This section discusses the results of changing air dilution using hydrogen as fuel. As in Fig. 5.9, results of Fig. 5.15 show the effect of increasing the air dilution on combustion-related parameters. In this case, the air-to-fuel ratio is increased from 1.5 to 2. Similar to what we observed for the methane combustion, the HRR profile becomes wider and its peak is reduced as the air dilution increases. However, this trend is slightly different: the combustion duration is reduced until reaching a minimum around $\lambda = 1.7$ which coincides with the maximum peak on the HRR profiles. Then, the

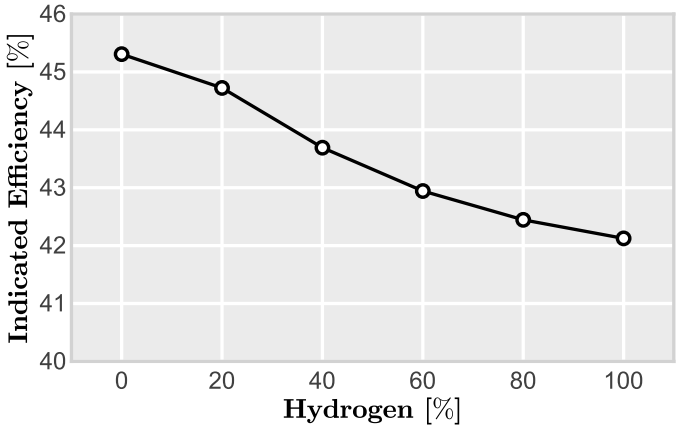

Figure 5.14: Indicated efficiency trends when the amount of hydrogen is increased in the fuel blend at $\lambda = 1.5$.

combustion process is extended again when increasing the dilution ratio. At $\lambda = 2$ condition, the combustion duration reach similar values as $\lambda = 1.5$ conditions. The combustion phasing is progressively delayed due to this effect.

The in-cylinder pressure increases with the air dilution until $\lambda = 1.8$ is reached, as Fig. 5.16 shows. Pressure profiles almost collapse in all cases between $\lambda = 1.7$ and $\lambda = 2$. The differences observed during the compression and expansion strokes are a direct consequence of the physical properties of the air-fuel mixture. Regarding the maximum pressure rate of change, results show a maximum around $\lambda = 1.7$ following the inverse trend as the combustion duration.

Values of indicated efficiency are shown in Fig. 5.17. Increasing the air dilution, indicated efficiency increase, recovering similar levels to those obtained when operating with methane. Therefore, this confirms the potential of lean hydrogen combustion to reduce the CO_2 footprint of internal combustion engines.

5.5.4. Effects on fuel consumption

In this final section, a comparison between all simulated cases is performed to identify the benefits of using hydrogen as partial or complete fuel in gas-powered engines. In addition, this section could be considered as a small flavor of the potential applications of this modelling approach, being extended to more complex and interesting studies in the future.

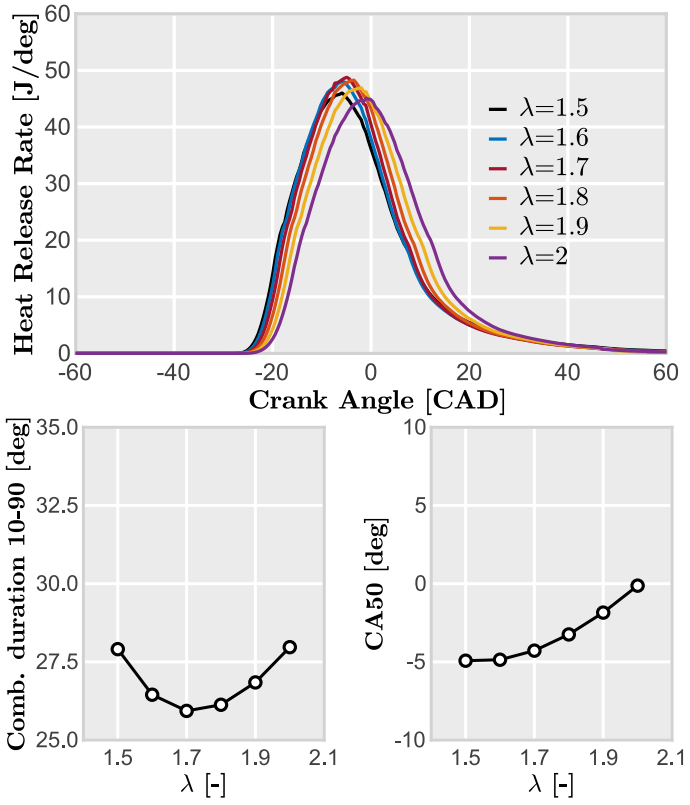

Figure 5.15: Trends of the main characteristics of the combustion process. Heat release rate profiles (top), combustion duration (bottom-left), and combustion phasing (bottom-right) for different air-to-fuel ratios considering hydrogen fuel.

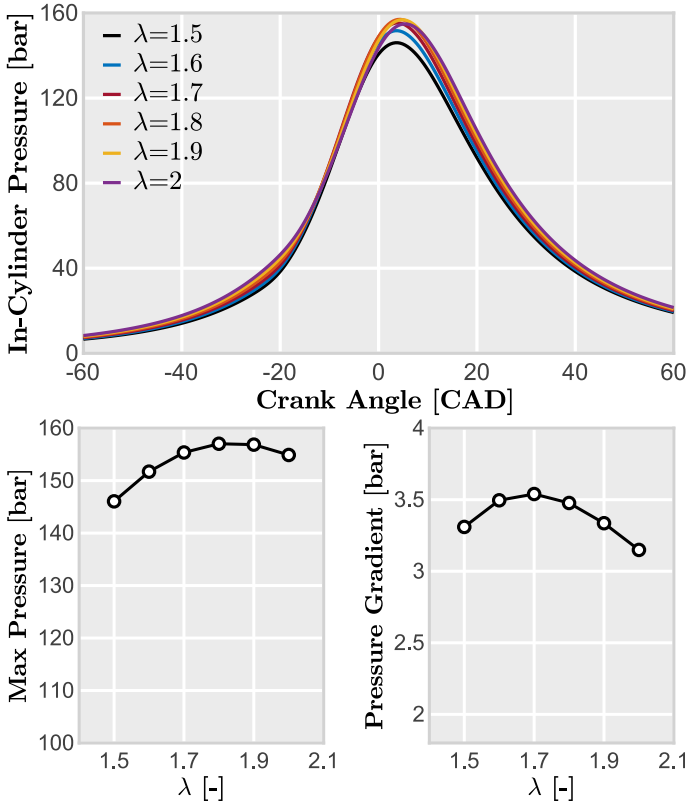

Figure 5.16: In-cylinder pressure evolution. Pressure profiles (top), maximum peak pressure (bottom-left), and maximum pressure change rate (bottom-right) for different air-to-fuel ratios considering hydrogen fuel.

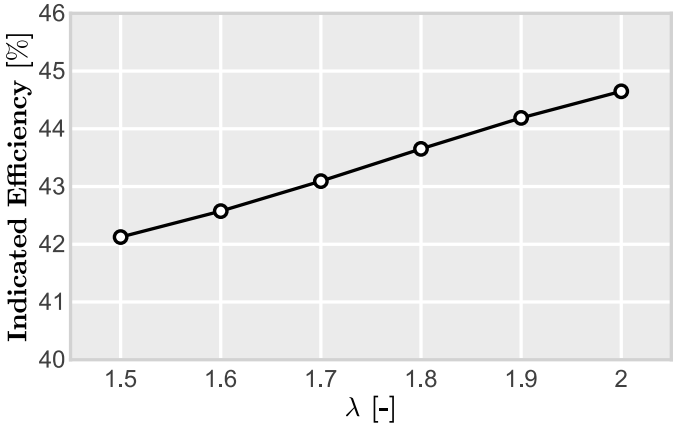

Figure 5.17: Indicated efficiency trends when the air dilution rate is increased from $\lambda = 1.5$ to $\lambda = 2.0$ using hydrogen as fuel.

Results of the Indicated Specific Fuel Consumption (ISFC) are presented in Fig. 5.18. The positive impact of including hydrogen in the fuel is evident in this figure. The ISFC decreases from almost 170 g/kWh to 70 g/kWh if the methane is completely replaced by H_2. The effect of the dilution is not so marked in both fuels.

These results can be qualitatively validated with the experiments performed by Singh et al. [194]. They operated an SI engine with methane and methane-hydrogen blends (18% H_2), observing an important gain in terms of specific fuel consumption (SFC).

5.6. Conclusions

A new modelling approach for methane-hydrogen combustion in SI engines has been proposed in this paper. This model has been implemented and coupled with a virtual model of a light-duty engine version for automotive applications. The combustion model estimates the flame propagation from the laminar flame speed predicted by an ANN. The ANN was trained by a set of data that considers a wide range of operating conditions including both air and exhaust gases dilution.

The model has been widely validated, from the most fundamental aspects (laminar flame speed) to the most complex ones (real engine experiments), including different dilution and blend sharing conditions.

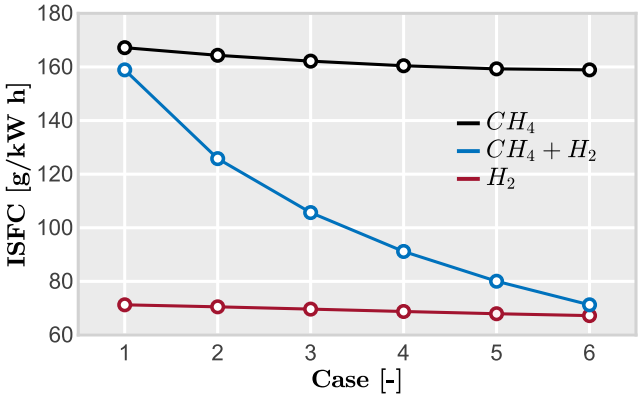

Figure 5.18: Specific fuel economy of all simulated conditions. The black line corresponds with the CNG simulation plan, sweeping the air dilution from $\lambda = 1$ to $\lambda = 1.5$. The blue line sweeps the amount of hydrogen in the fuel from 0% to 100%. The red line considers pure hydrogen combustion varying λ from 1.5 to 2.

Results demonstrate how machine learning and data-driven modelling techniques, can be implemented in several science fields reducing time calculation while allowing more complex and interesting studies which contribute to finding new solutions for the most relevant problems of society.

Modelling results indicate that hydrogen addition helps to increase the burning rate, overcoming the negative effects of lean mixture environments on combustion. However, there are some thermodynamic losses due to the physical properties of the fuel blend when adding hydrogen. Nevertheless, the potential advantages of using H_2 as fuel for internal combustion engines have been evidenced.

Despite the benefits of this modelling approach, several limitations have been identified that need to be corrected in the future to improve the model accuracy. The cycle-to-cycle variation should be estimated to correctly predict the losses due to excessive misfiring at high dilution rates. Moreover, the auto-ignition of the mixture must be considered in a dedicated submodel to predict the efficiency losses due to severe knocking combustion. To this end, several submodels available in the literature will be evaluated and validated in relevant engine conditions with hydrogen-enriched CNG fuel blends. Finally, a quantitative validation is required in a wider range of operating conditions, including other engine speeds and loads, and dilution conditions using exhaust gases.

CHAPTER 6

Discussion of results

This section presents a comprehensive discussion of the results obtained from the various articles that constitute this thesis. The goal is to integrate the individual findings of each article to provide a coherent overview of the research topic.

6.1. General Contextualization

Each article included in this thesis addresses specific aspects of the overarching research theme. Below is a brief description of the objectives and main findings of each article, which will serve as the foundation for the detailed discussion that follows.

6.1.1. Brief Summary

Below is a concise summary of the key results obtained in each article:

- **Article 1:** This paper proposed a new approach to reducing greenhouse gas emissions by analyzing the effects of various fuel compositions and dilution conditions on emissions and efficiency. The study conducted an extensive experimental campaign on a single-cylinder spark-ignition engine using HCNG blends. The findings highlight that even small additions of hydrogen (1-3% by mass) stabilize combustion, improve thermal efficiency by about 1.5%, and reduce CO_2 and CH_4 emissions. Larger hydrogen quantities (25-75% by mass) significantly reduce greenhouse gas and pollutant emissions, although thermal efficiency may decrease with higher hydrogen content due to

increased heat transfer to the chamber walls. The study establishes a flexible roadmap for reducing the transportation sector's carbon footprint during the transition to a hydrogen-based economy.

- **Article 2:** This study explored the impact of transitioning to a hydrogen economy on greenhouse gas emissions, focusing on different HCNG blends in various scenarios from 2020 to 2050. It identified the optimal HCNG blend that minimizes emissions and the timeframe in which zero cradle-to-grave emissions can be achieved. The study found that increasing hydrogen content in blends enhances engine performance and reduces exhaust gas emissions, though higher air dilution ratios are necessary to maintain efficiency. The results demonstrate that HCNG vehicles can significantly decarbonize the transportation sector, particularly in a scenario dominated by steam CNG reforming, where cradle-to-grave emissions could be reduced to negative levels with a higher biogas share in the natural gas mix.

- **Article 3:** This study examined the potential of using a modern spark-ignition engine equipped with an outwardly opening poppet valve hydrogen injector. It compared port fuel injection and direct injection technologies in a single-cylinder engine under various conditions. The results show that the DI system outperforms the PFI system in terms of gross indicated efficiency and requires lower intake pressure, reducing stress on the boosting system. However, precise injection timing is crucial to balance performance and emissions, as delayed injection improves efficiency but can lead to increased NO_x emissions due to charge stratification. The study emphasizes the need for further research combining experimentation with simulations to better understand and control local phenomena within the combustion chamber.

- **Article 4:** This paper proposed a new modeling approach for CNG-hydrogen combustion in spark-ignition engines, integrating it with a virtual model of a light-duty engine for automotive applications. The combustion model was validated against both fundamental aspects and real engine experiments under varying dilution and blend conditions. The findings indicate that adding hydrogen increases the burning rate, mitigating the negative effects of lean mixture environments, though thermodynamic losses occur due to the physical properties of the fuel blend. The study highlights the potential of machine learning

and data-driven modeling in developing new solutions for societal challenges but also identifies several limitations that need addressing in future research.

6.1.2. Integration of Results

The results obtained from the articles in this thesis reveal several key patterns, similarities, and discrepancies.

First, the findings from **Article 1** and **Article 2** are complementary. Both studies emphasize the importance of hydrogen as a key component in reducing greenhouse gas emissions within the transportation sector. While **Article 1** focuses on the experimental effects of adding hydrogen to fuel blends and its impact on engine performance and emissions, **Article 2** extends this analysis by exploring the long-term implications of a hydrogen economy, taking into account the environmental impact across every phase of its lifecycle—from production to waste. Together, these articles suggest that hydrogen can play a pivotal role in achieving a sustainable transition to low-carbon transportation.

Article 3 introduces a new technological perspective by investigating the use of a specific hydrogen injection system. The study's findings underscore the significance of injection timing and technology in optimizing engine performance and emissions. The results from this article align with the broader conclusions of **Articles 1** and **2**, but also introduce new challenges related to the control of local combustion phenomena, which were not addressed in the other studies.

Finally, **Article 4** presents a different approach by introducing a new modeling method for CNG-hydrogen combustion. This approach, distinct from the experimental focus of **Articles 1–3**, offers a theoretical framework that is validated against real engine conditions. The discrepancies between the experiments and simulations in **Article 4** highlight the complexities involved in accurately modeling combustion processes.

6.2. Analysis and interpretation of results

The results of **Article 1** provide valuable insights into combustion engineering and the energy transition. Partially substituting compressed natural gas with hydrogen in spark-ignition engines offers key advantages in terms of performance and environmental sustainability. Specifically, increasing the hydrogen content in the fuel blend significantly reduces CO_2 and CH_4 emissions, a crucial finding considering CNG's greenhouse effect, which is 25

times greater than that of CO_2. This research advances the understanding of hydrogen-CNG blends by demonstrating that hydrogen enhances engine thermal efficiency by promoting faster and more complete combustion.

Moreover, the study shows that engine thermal efficiency improves with the proportion of hydrogen, reaching an optimal balance at approximately 25% hydrogen by mass, which maximizes combustion stability and minimizes pollutant emissions. The high flame speed of hydrogen allows for a broader dilution range, improving efficiency, particularly in scenarios where stable combustion is maintained through high dilution rates combined with hydrogen enrichment. These results suggest that HCNG blends could serve as a viable alternative to fossil fuels for transportation, offering an intermediate solution toward a hydrogen economy by significantly reducing emissions in the short and medium term while maintaining optimal operational efficiency.

The findings of **Article 2** have significant implications for sustainable transportation and the transition to low-emission systems. The study demonstrates that using HCNG blends with increasing hydrogen levels is essential for reducing greenhouse gas emissions and improving energy efficiency. In particular, progressively increasing the hydrogen content in blends—from 25% in the 2020-2030 decade, to 50% in 2030-2040, and up to 100% in 2040-2050—emerges as an optimal strategy for balancing emission reduction with hydrogen production sustainability.

This approach contributes to the development of a hydrogen economy by showing that gradually increasing hydrogen in HCNG blends is a feasible strategy to minimize the environmental impact of passenger internal combustion vehicles. Additionally, the study highlights that the carbon content in natural gas significantly influences CO_2 emissions, underscoring the importance of reducing reliance on fossil fuels and transitioning toward renewable energy and biogas sources for hydrogen production. Emission analysis as a function of hydrogen proportion showed significant reductions in pollutants such as CO and NO_x due to lower combustion temperatures and increased combustion efficiency.

Article 3 has important implications for combustion engineering and the use of alternative fuels. Comparing DI and PFI systems suggests that DI improves volumetric efficiency and reduces specific fuel consumption (ISFC) by approximately 3.1–3.2% under various load conditions. These findings advance the knowledge of hydrogen combustion by demonstrating that direct injection enables higher dilution ratios and efficiency compared to port injection, which may facilitate hydrogen adoption in light transportation applications.

The DI hydrogen injection tests reveal that injection timing directly impacts the air-fuel mixture and, consequently, combustion efficiency. Delayed injection, for example, can enhance the hydrogen-air mixture, resulting in more complete and efficient combustion and reduced ISFC under both low and high load conditions. However, this approach may also increase NO_x emissions, as richer mixtures can elevate combustion temperatures, favoring NO_x formation. Thus, finding a balance between injection optimization and emission control is essential, presenting a significant challenge in hydrogen engine design.

Comparing results with conventional fuel engines, such as gasoline and CNG, shows that hydrogen engines may outperform conventional counterparts in terms of efficiency and emissions reduction, suggesting hydrogen as a viable and sustainable alternative in the transport sector, aligned with global policies to reduce fossil fuel dependence.

Article 4 provides significant contributions to combustion modeling in spark-ignition engines using CNG-hydrogen blends. The implementation of an artificial neural network (ANN)-based model to predict combustion speed in various CNG-hydrogen mixtures suggests that machine learning models surpass traditional methods by improving accuracy and computational speed in complex simulations. The proposed model accurately predicts laminar flame speed in the combustion chamber, facilitating simulations under variable operating conditions, fuel mixtures, and air dilution rates, with enhanced computational speed compared to previous methods, such as fractal combustion models.

These findings advance knowledge in modeling alternative fuel internal combustion engines by combining machine learning with virtual models that expand the range of simulatable operating conditions without compromising prediction accuracy. This paves the way for combustion models that are not only more accurate but also faster, making them applicable to exploratory studies of new combustion strategies with lower costs and associated experimental times. Additionally, ANN-based modeling offers a scalable approach for future simulations involving fuels with unconventional combustion properties, such as hydrogen.

6.3. Comparison with previous studies

In comparing this study's findings with previous research on hydrogen and CNG combustion mixtures, significant points of convergence and divergence emerge.

On the one hand, our results align with previous studies regarding the benefits of hydrogen-CNG mixtures in improving thermal efficiency and reducing greenhouse gas emissions. For instance, Mehra et al. [85] demonstrated that hydrogen reduces unburned hydrocarbons and CO_2, optimizes combustion stability, and extends the operating range under high dilution conditions. Similarly, Du et al. [83] confirmed that HCNG mixtures effectively lower NO_x emissions through diluted combustion, supporting the feasibility of these blends for meeting stringent environmental standards.

However, divergences arise on certain aspects. Kosmadakis's research [84] suggests that increasing the hydrogen proportion can lead to greater cyclic variability, particularly in high-load engines. This effect is attributed to hydrogen's rapid combustion properties, which may induce instability under specific operational scenarios. In contrast, Ji et al. [79, 183] observed that hydrogen enrichment might increase NO_x emissions under certain temperature and pressure conditions—a phenomenon mitigated in the present study through air dilution strategies.

Comparing these findings with additional studies further highlights a mix of agreement and challenges. Nagalingam et al. [192], for example, showed that hydrogen as an additive in natural gas engines accelerates the combustion process, consistent with our observation that higher hydrogen content improves combustion rates. Ma et al. [181, 191] also reported that hydrogen reduces cycle-to-cycle variations in lean-burn conditions, aligning with this study's results on combustion stability.

When examining hydrogen direct injection systems, this study's findings on improved volumetric efficiency and reduced intake pressure are consistent with Maio et al. [143], who observed increased efficiency and lower emissions with DI technology in hydrogen combustion. However, some studies diverge by suggesting that port fuel injection PFI may equal or outperform DI under low-load conditions. These studies argue that PFI offers a more homogeneous mixture in specific scenarios, potentially leading to more efficient combustion. Variations in engine design, operating conditions, and injection configurations likely explain these discrepancies.

Additionally, differences in results may stem from the lack of standardization in testing methods and experimental conditions. For instance, while this research was conducted on a single-cylinder engine with a specific injector design, other studies employed different configurations and injection systems, potentially affecting their outcomes. Kim et al. [129], for example,

reported a 30% increase in power density when transitioning from PFI to DI, underscoring the critical role that engine design and injection strategy play in determining performance outcomes.

In summary, while there is broad agreement in the literature on the advantages of DI for hydrogen combustion—such as improved efficiency, reduced emissions, and enhanced volumetric performance—there are also notable divergences. These differences underscore the complexity of hydrogen-CNG combustion and the need for further research to address variations across engine designs, operating conditions, and injection configurations. Effective implementation of DI in hydrogen engines will require careful adaptation to specific applications to fully realize its potential in advancing sustainable transportation technologies.

6.4. Strengths and limitations

It is important to acknowledge the limitations of this research, which include the following:

- **Methodological limitations:**
  - The experiments were conducted under controlled laboratory conditions, which may not fully replicate realistic driving scenarios.
  - The modeling approach presented in **Article 4** relies on a simplified combustion model, which may not fully capture the complexities of CNG-hydrogen combustion under diverse operating conditions.
- **Contextual limitations:**
  - The availability and cost of hydrogen as a fuel were not comprehensively addressed, potentially affecting the practical implementation of the proposed solutions.
- **Theoretical limitations:**
  - There may be biases in the assumptions underlying the combustion models, which could influence the accuracy of the findings.
  - Predicting long-term environmental impacts remains inherently challenging due to the complexity of the factors involved.

These limitations may have affected specific aspects of the results, such as the generalizability of the findings to different engine types. They may also impact the precision of emission reduction projections.

Despite these limitations, this research offers several notable strengths:

- **Comprehensive experimental design: Article 1** employs robust experimental methods to analyze the effects of hydrogen blending on engine performance and emissions, providing valuable data for further analysis.
- **Innovative injection technologies: Article 3** explores advanced injection strategies, delivering critical insights into the optimization of injection timing and technology for hydrogen combustion.
- **Integration of experimental and modeling approaches:** The combination of empirical data and theoretical insights in **Article 4** offers a holistic understanding of the combustion process, enhancing the reliability of the results.

The research also makes significant contributions to the field:

- **Greenhouse gas reduction roadmap: Articles 1** and **2** propose a flexible and practical roadmap for reducing greenhouse gas emissions in the transportation sector.
- **Technological advancements in injection systems:** The experimental validation of hydrogen injection technologies in **Article 3** offers practical solutions for improving engine performance and reducing emissions, paving the way for future innovations in combustion engineering.
- **Application of low-order models: Article 4** highlights the potential of machine learning-based models to improve combustion predictions, offering a forward-looking approach to future engine design.

In summary, while acknowledging its limitations, this research advances the understanding of hydrogen-CNG combustion and provides a foundation for future studies aimed at developing cleaner, more efficient transportation technologies.

CHAPTER 7

Conclusions and future works

The concluding remarks of this doctoral thesis are summarized in this final chapter, providing an overview of the main findings presented throughout the document and highlighting the original contributions of this research to the scientific community. Additionally, topics of interest are suggested for potential future work, aimed at expanding the knowledge acquired, enhancing the rigor of the methodologies developed, and addressing their application to industry requirements.

7.1. Conclusions

This thesis has investigated the potential of hydrogen as a fuel when combined with compressed natural gas for use in internal combustion engines, emphasizing its role in reducing carbon emissions in the transportation sector as part of a broader decarbonization strategy. The results obtained through the methods applied have provided deeper insights into key aspects of the combustion process, enabling improvements in engine performance, emissions reduction, and minimized environmental impact. The main contributions and conclusions are summarized as follows:

7.1.1. Experimental analysis of HCNG blends

The experimental evaluation of HCNG blends in light-duty engines provided a clear understanding of how hydrogen can enhance combustion properties and reduce greenhouse gas emissions.

- The results demonstrated that hydrogen-enriched fuel blends, specifically HCNG, have significant potential to reduce CO_2 emissions while accelerating combustion. Small hydrogen additions (1–3%) were

found to stabilize combustion at moderate dilution ratios, improving efficiency by approximately 1.5% and reducing CO_2 and CH_4 emissions. Increasing hydrogen content to higher levels (25–75%) resulted in even lower emissions; however, heat transfer to the chamber walls became a limiting factor for thermal efficiency. An optimal HCNG blend, with a hydrogen content of 25%, was identified as providing the best trade-off between thermal efficiency and emissions under lean operation conditions ($\lambda \approx 2$). Beyond this point, the benefits in emissions reduction are offset by thermodynamic losses associated with increased heat transfer due to higher hydrogen content.

- As the hydrogen content in fuel increases, losses in thermal efficiency are offset by the reduction in carbon elements, making CO_2 emissions primarily dependent on the hydrogen level once it exceeds 5% by mass. In pure hydrogen combustion, where GHG emissions are not a concern if hydrogen is produced from renewable sources, the key challenge is to develop an engine that maintains reasonable thermal efficiency while minimizing NO_x emissions. However, small amounts of CO and CO_2 can still be produced due to the oxidation of lubricating oil.

- Despite improvements in GHG emissions, NO_x remained a challenge, particularly at high loads. However, scenarios with high hydrogen content allowed higher dilution, reducing NO_x emissions to below 1 g/kWh. Effective NO_x control will require advanced combustion strategies or after-treatment technologies.

7.1.2. Life cycle assessment of HCNG-powered vehicles

The life cycle assessment (LCA) of HCNG-powered vehicles demonstrated the environmental benefits of combining hydrogen with CNG, identifying the optimal blend to minimize cradle-to-grave emissions under scenarios spanning 2020 to 2050.

- The analysis underscored the critical role of green hydrogen availability and the necessity for an optimized roadmap to facilitate the transition to a hydrogen-based economy.

- The findings also highlighted the significance of biogas in achieving zero-emission targets, particularly in scenarios integrating hydrogen and natural gas. This thesis proposed a roadmap for the gradual

adoption of hydrogen in transportation, outlining an evolution of fuel blends with increasing hydrogen content (from 25% in 2020 to 75–100% by 2050). This transition is deemed essential for achieving zero cradle-to-grave emissions, especially in regions where hydrogen is produced from renewable sources.

- HCNG vehicles, particularly under water electrolysis and SMR scenarios, demonstrate substantial potential for decarbonizing transportation. By 2050, the water electrolysis scenario achieves significant emissions reductions, with pure hydrogen vehicles reaching the lowest emission levels. The SMR scenario, when combined with biogas and an optimized electricity mix, can reduce emissions to near-zero or even negative levels. To effectively minimize emissions, the optimal hydrogen content in HCNG blends should progress from 25% in 2020 to 75–100% by 2050. Achieving zero emissions by 2050 will require an SMR-dominant approach, incorporating over 50% hydrogen along with increased biogas utilization.

7.1.3. Hydrogen as a sole fuel source in ICE

The investigation of various hydrogen injection strategies revealed that direct injection systems offer significant advantages in terms of performance and emissions control, particularly when manipulating injection timing to optimize mixture stratification. This insight paves the way for more efficient use of hydrogen in spark-ignition engines.

- A comparison between direct injection and port fuel injection of hydrogen showed that DI systems outperform PFI in terms of thermal efficiency. The DI system exhibited a gain of 0.6–1.1% in indicated gross efficiency and reduced the required intake pressure, thereby alleviating the load on the boosting system. However, precise control of injection timing was essential to balance efficiency and NO_x emissions.

- Precise control of injection timing is crucial for balancing performance and emissions in DI hydrogen engines. Delaying the injection start reduces compression work by 7.6% at low load and 3.9% at high load, improving indicated specific fuel consumption by 3.1–3.2% at both load conditions. However, this delay shortens the mixing time, leading to charge stratification and resulting in higher NO_x emissions due to hydrogen burning in richer conditions compared to the overall air-fuel mixture.

7.1.4. Development of the HCNG combustion model

The development of a flexible combustion model for HCNG fuel blends enabled accurate prediction of engine performance across a range of operating conditions and fuel compositions. This model enhances the understanding of how hydrogen can be integrated into internal combustion engines while maintaining computational efficiency.

- The modeling approach demonstrated that adding hydrogen increases flame propagation speed, mitigating the negative effects of lean mixtures on combustion stability. However, physical limitations, such as misfiring and knocking at high dilution rates, remain challenges that future models must address.
- The implementation of a low-order combustion model based on artificial neural networks for predicting laminar flame speed proved effective in simulating flame propagation and combustion behavior under various conditions using HCNG fuel blends in a spark-ignition engine.
- Nonetheless, several limitations were identified. For instance, the model does not account for auto-ignition events or cycle-to-cycle variations, leading to inaccuracies in scenarios involving high dilution or knocking. Future developments should integrate sub-models to simulate these phenomena and enhance prediction accuracy under extreme conditions.

7.2. Future Work

While this research has made significant contributions to the understanding and optimization of HCNG-fueled internal combustion engines, several areas warrant further exploration and development. Future work should aim to expand the scope of this research in the following directions:

- **Advanced combustion strategies**: Additional studies are needed to develop advanced combustion techniques that effectively control NO_x emissions, particularly at higher hydrogen blend ratios. Strategies such as exhaust gas recirculation and water injection should be explored to achieve an optimal balance between efficiency and emissions.

- **Improved injection strategies**: While direct injection has demonstrated advantages over port fuel injection in terms of efficiency and emissions, further optimization of DI systems is essential. Future research should focus on multi-pulse injection strategies, variable injection pressures, and innovative injector designs to enhance mixture formation and combustion control.

- **Hydrogen blends with other renewable fuels**: Beyond compressed natural gas, future studies should investigate the potential of blending hydrogen with other renewable fuels. This could support a more diverse fuel portfolio, particularly in regions where biogas production is feasible, fostering a sustainable and adaptable energy mix.

- **Real-world testing and optimization**: Future research should involve real-world testing of hydrogen engines under diverse operating conditions, focusing on factors such as cold-start performance, transient operations, and long-term durability. Optimizing engine calibration to accommodate various driving conditions and load demands will be critical for practical implementation.

- **Expanded life cycle analysis**: Although this study conducted an initial life cycle assessment of HCNG-powered vehicles, future LCAs should account for regional variations in hydrogen production, distribution logistics, and infrastructure development. This will provide a more nuanced understanding of the environmental impact of hydrogen in different geographical and economic contexts.

- **Fuel economy and cost analysis**: Further studies should evaluate the economic viability of hydrogen as a mainstream fuel, assessing production costs, infrastructure requirements, and its long-term competitiveness compared to other low-carbon alternatives such as electric and hybrid vehicle technologies.

- **Low-order combustion models**: Future combustion models should incorporate submodels to account for cycle-to-cycle variations and auto-ignition phenomena. Hybrid approaches combining machine learning techniques with physical modeling could also be explored to improve predictive accuracy and computational efficiency.

Bibliography

[1] S. Molina, R. Novella, J. Gomez-Soriano, and M. Olcina-Girona. "Study on hydrogen substitution in a compressed natural gas spark-ignition passenger car engine". Energy Conversion and Management 291, 2023, p. 117259 (cited in pp. 52, 57, 67).

[2] S. Molina, J. Gomez-Soriano, M. Lopez-Juarez, and M. Olcina. "Evaluation of the environmental impact of HCNG light-duty vehicles in the 2020–2050 transition towards the hydrogen economy". Energy Conversion and Management 301, 2024, p. 117968.

[3] S. Molina, R. Novella, J. Gomez-Soriano, and M. Olcina-Girona. "Impact of medium-pressure direct injection in a spark-ignition engine fueled by hydrogen". Fuel 360, 2024, p. 130618.

[4] S. Molina, R. Novella, J. Gomez-Soriano, and M. Olcina-Girona. "New combustion modelling approach for methane-hydrogen fueled engines using machine learning and engine virtualization". Energies 14 (20), 2021, p. 6732.

[5] S. Molina, R. Novella, J. Gomez-Soriano, and M. Olcina-Girona. "Experimental evaluation of methane-hydrogen mixtures for enabling stable lean combustion in spark-ignition engines for automotive applications". SAE Technical Paper, 2022 (cited in pp. 24, 34, 35).

[6] J. Gomez-Soriano, P. Sapkota, S. Wijeyakulasuriya, M. D'Elia, et al. "Numerical modeling of hydrogen combustion using preferential species diffusion, detailed chemistry and adaptive mesh refinement in internal combustion engines". SAE Technical Paper, 2023.

[7] S. Molina, R. Novella, J. Gomez-Soriano, and M. Olcina-Girona. "Experimental Activities on a Hydrogen-Fueled Spark-Ignition Engine for Light-Duty Applications". Applied Sciences 13 (21), 2023, p. 12055.

[8] S. Molina, S. Ruiz, J. Gomez-Soriano, and M. Olcina-Girona. "Impact of hydrogen substitution for stable lean operation on spark ignition engines fueled by compressed natural gas". Results in Engineering 17, 2023, p. 100799 (cited in pp. 24, 52, 57, 67, 88, 91, 110).

[9] M. G. G. Mendoza, A. Garcia, S. Molina, M. Olcina-Girona, et al. "Toy Model: A Naive ML Approach to Hydrogen Combustion Anomalies". SAE Technical Paper, 2024.

[10] V. De Bellis, M. Piras, F. Bozza, E. Malfi, et al. "Development and validation of a phenomenological model for hydrogen fueled PFI internal combustion engines considering Thermo-Diffusive effects on flame speed propagation". Energy Conversion and Management 308, 2024, p. 118395.

[11] H. Ritchie, P. Rosado, and M. Roser. "Greenhouse gas emissions". Our World in Data, 2020. https://ourworldindata.org/greenhouse-gas-emissions (cited in p. 1).

[12] M. W. Jones, G. P. Peters, T. Gasser, R. M. Andrew, et al. National contributions to climate change due to historical emissions of carbon dioxide, methane and nitrous oxide. Version 2024.2. Zenodo, 2024 (cited in p. 2).

[13] IPCC. Summary for Policymakers: Climate Change 2022 Impacts, Adaptation and Vulnerability Working Group II contribution to the Sixth Assessment Report of the Intergovernamental Panel on Climate Change. August. 2022, p. 37 (cited in pp. 1, 51).

[14] M. Anshassi and T. G. Townsend. "The hidden economic and environmental costs of eliminating kerb-side recycling", 2023 (cited in pp. 1, 51).

[15] L. R. Vargas Zeppetello, A. E. Raftery, and D. S. Battisti. "Probabilistic projections of increased heat stress driven by climate change". Communications Earth and Environment 3 (1), 2022, pp. 1–7 (cited in pp. 1, 51).

[16] IPCC. "Climate Change 2021: The Physical Science Basis. Contribution of Working Group I to the Sixth Assessment Report of the Intergovernmental Panel on Climate Change [Masson-Delmotte, V., P. Zhai, A. Pirani, S. L. Connors, C. Pean, S. Berger, N. Caud, Y. Chen". Cambridge University Press (In Press), 2021, p. 3949 (cited in pp. 2, 19).

[17] N. Höhne, T. Kuramochi, C. Warnecke, F. Röser, et al. "The Paris Agreement: resolving the inconsistency between global goals and national contributions". Climate Policy 17 (1), 2017, pp. 16–32 (cited in pp. 2, 19, 114).

[18] International Energy Agency. Global Hydrogen Demand by Sector in the Net Zero Scenario, 2020-2030. Licence: CC BY 4.0. International Energy Agency. 2021. URL: https://www.iea.org/data-and-statistics/charts/global-hydrogen-demand-by-sector-in-the-net-zero-scenario-2020-2030 (cited in p. 6).

[19] U.S. Department of Energy. Hydrogen Production Processes. https://www.energy.gov/eere/fuelcells/hydrogen-production-processes. Accessed: 2024-08-28 (cited in p. 6).

[20] R. Förster, M. Kaiser, and S. Wenninger. "Future vehicle energy supply - sustainable design and operation of hybrid hydrogen and electric microgrids". Applied Energy 334 (November 2022), 2023 (cited in p. 7).

[21] Y. Dong, W. Zheng, X. Cao, X. Sun, and Z. He. "Co-planning of hydrogen-based microgrids and fuel-cell bus operation centers under low-carbon and resilience considerations". Applied Energy 336 (December 2022), 2023, p. 120849 (cited in p. 7).

[22] P. Danieli, A. Lazzaretto, J. Al-Zaili, A. Sayma, M. Masi, and G. Carraro. "The potential of the natural gas grid to accommodate hydrogen as an energy vector in transition towards a fully renewable energy system". Applied Energy 313 (March), 2022, p. 118843 (cited in pp. 7, 88).

[23] H. Ishaq, I. Dincer, and C. Crawford. "A review on hydrogen production and utilization: Challenges and opportunities". International Journal of Hydrogen Energy 47 (62), 2022. SI: Progress in Hydrogen Production, Storage and Distribution (Ahmadi), pp. 26238–26264 (cited in p. 7).

[24] P. R. Díaz-Herrera, G. Ascanio, A. Romero-Martínez, A. M. Alcaraz-Calderón, and A. González-Díaz. "Theoretical comparison between post-combustion carbon capture technology and the use of blue and green H2 in existing natural gas combined cycles as CO2 mitigation strategies: A study under the context of mexican clean energy regulation". International Journal of Hydrogen Energy 46 (2), 2021, pp. 2729–2754 (cited in p. 7).

[25] IEA. Global Hydrogen Review. License: CC BY 4.0. Paris, 2021 (cited in p. 7).

[26] IRENA. Global Hydrogen Trade to Meet the 1.5 °C Climate Goal: Part III—Green Hydrogen Cost and Potential. Int Renew Energy Agency. Abu Dhabi, 2022 (cited in p. 8).

[27] IEA. The Role of Low-Carbon Fuels in the Clean Energy Transitions of the Power Sector. License: CC BY 4.0. Paris, 2021 (cited in p. 8).

[28] C. A. Hunter, M. M. Penev, E. P. Reznicek, J. Eichman, N. Rustagi, and S. F. Baldwin. "Technoeconomic Analysis of Long-Duration Energy Storage and Flexible Power Generation Technologies to Support High-Variable Renewable Energy Grids". Joule 5 (8), 2021, pp. 2077–2101 (cited in p. 8).

[29] P. Denholm, W. Cole, A. W. Frazier, K. Podkaminer, and N. Blair. The Four Phases of Storage Deployment: A Framework for the Expanding Role of Storage in the U.S. Power System. Tech. rep. Golden, CO: National Renewable Energy Laboratory, 2021 (cited in p. 8).

[30] "Fuel Cells and Hydrogen Joint Undertaking (FCH). Hydrogen Roadmap Europe: A Sustainable Pathway for the European Energy Transition; Publications Office of the European Union: Luxembourg, 2019; p. 70." 2019 (cited in pp. 8, 87).

[31] G. Environment Agency. “Fact Sheet: EU 2050 strategic vision "A Clean Planet for All" Brief Summary of the European Commission proposal”. (December 2018), 2018 (cited in pp. 8, 19).

[32] J. M. Desantes, S. Molina, R. Novella, and M. Lopez-Juarez. “Comparative global warming impact and NOX emissions of conventional and hydrogen automotive propulsion systems”. Energy Conversion and Management 221 (X), 2020, p. 113137 (cited in pp. 8, 13, 15, 53, 54).

[33] R. Novella, J. D. la Morena, M. Lopez-Juarez, and I. Nidaguila. “Effect of differential control and sizing on multi-FCS architectures for heavy-duty fuel cell vehicles”. Energy Conversion and Management 293, 2023, p. 117498 (cited in p. 8).

[34] A. Sommermann, F. Hinrichsen, T. Malischewski, D. Hyna, et al. “MAN H45 hydrogen engine: A robust and highly efficient technology for CO2-neutral mobility”. In: Proceedings of the 18th Symposium on Sustainable Mobility, Transport and Power Generation. Graz, Austria, 2021 (cited in pp. 9, 12).

[35] G. Dober, G. Hoffmann, W. Piock, J. Shi, et al. “Hydrogen conversion of existing powertrains”. In: Proceedings of the 18th Symposium on Sustainable Mobility, Transport and Power Generation. Graz, Austria, 2021 (cited in p. 9).

[36] H. Yun, Z. Bu, Z. Yang, L. Wang, and B. Zhang. “Optimization of fuel injection timing and ignition timing of hydrogen fueled SI engine based on DOE-MPGA”. International Journal of Hydrogen Energy 48 (25), 2023, pp. 9462–9473 (cited in pp. 9, 21).

[37] C. Shi, S. Chai, H. Wang, C. Ji, Y. Ge, and L. Di. “An insight into direct water injection applied on the hydrogen-enriched rotary engine”. Fuel 339 (November 2022), 2023, p. 127352 (cited in pp. 9, 88).

[38] H. L. Yip, A. Srna, A. C. Y. Yuen, S. Kook, et al. “A Review of Hydrogen Direct Injection for Internal Combustion Engines: Towards Carbon-Free Combustion”. Applied Sciences 9 (22), 2019 (cited in p. 9).

[39] S. Verhelst and T. Wallner. “Hydrogen-fueled internal combustion engines”. Progress in Energy and Combustion Science 35 (6), 2009, pp. 490–527 (cited in pp. 9, 88).

[40] S. Verhelst. “Recent progress in the use of hydrogen as a fuel for internal combustion engines”. international journal of hydrogen energy 39 (2), 2014, pp. 1071–1085 (cited in pp. 9, 11, 88).

[41] B. Keppy. “The case for H2 engine in the future powertrain portfolio”. In: SAE, Sustainable Low-Impact Combustion Engine Symposium (SLICES). Detroit, US, 2022 (cited in p. 10).

[42] H. Xie, D. Makarov, S. Kashkarov, and V. Molkov. "Comparative analysis of CFD models to simulate temperature non-uniformity during hydrogen tank refuelling". International Journal of Hydrogen Energy 70, 2024, pp. 715–728 (cited in p. 10).

[43] K. W. G. P. and R. P.G. "An overview of underground hydrogen storage with prospects and challenges for the Australian context". Geoenergy Science and Engineering 231, 2023, p. 212354 (cited in p. 10).

[44] M. Khristamto Aditya Wardana and O. Lim. "Investigation of ammonia homogenization and NOx reduction quantity by remodeling urea injector shapes in heavy-duty diesel engines". Applied Energy 323 (June 2021), 2022, p. 119586 (cited in p. 11).

[45] L. zhi Bao, B. gang Sun, and Q. he Luo. "Experimental investigation of the achieving methods and the working characteristics of a near-zero NOx emission turbocharged direct-injection hydrogen engine". Fuel 319 (February), 2022, p. 123746 (cited in pp. 11, 88).

[46] L. zhi Bao, B. gang Sun, and Q. he Luo. "Optimal control strategy of the turbocharged direct-injection hydrogen engine to achieve near-zero emissions with large power and high brake thermal efficiency". Fuel 325 (April), 2022, p. 124913 (cited in pp. 11, 88).

[47] L. zhi Bao, B. gang Sun, Q. he Luo, J. cheng Li, et al. "Development of a turbocharged direct-injection hydrogen engine to achieve clean, efficient, and high-power performance". Fuel 324 (PB), 2022, p. 124713 (cited in pp. 11, 88).

[48] O. Barış, İ. Güler, and A. Yaşgül. "The effect of different charging concepts on hydrogen fuelled internal combustion engines". Fuel 343, 2023, p. 127983 (cited in pp. 11, 88).

[49] C. Park, S. Lee, C. Kim, and Y. Choi. "A comparative study of lean burn and exhaust gas recirculation in an HCNG-fueled heavy-duty engine". International Journal of Hydrogen Energy 42 (41), 2017, pp. 26094–26101 (cited in pp. 11, 22).

[50] J. Gao, X. Wang, P. Song, G. Tian, and C. Ma. "Review of the backfire occurrences and control strategies for port hydrogen injection internal combustion engines". Fuel 307, 2022, p. 121553 (cited in pp. 11, 88).

[51] Y. Shen, Y. Dong, X. Han, J. Wu, et al. "Prediction model for methanation reaction conditions based on a state transition simulated annealing algorithm optimized extreme learning machine". International Journal of Hydrogen Energy 48 (64), 2023. Catalytic Hydrogen Purification, pp. 24560–24573 (cited in p. 11).

[52] D. T. Koch, E. Eber, S. Kureti, and A. Sousa. "H2-deNOx Catalyst for H2 Combustion Engines". MTZ worldwide 81 (6), 2020, pp. 30–35 (cited in p. 11).

[53] B. Nork, A. Qriqra, and R. Kleuser. "DEUTZ Hydrogen-ICE—A simulation of the entire system". In: Proceedings of the 18th Symposium on Sustainable Mobility, Transport and Power Generation. Graz, Austria, 2021 (cited in p. 12).

[54] T. Ebert, D. Koch, D. Kerschl, M. Wehrli, M. Vonnoe, and T. Lahni. "Effectiveness of the H2-specific operating strategy in dynamic engine operation". In: Proceedings of the 18th Symposium on Sustainable Mobility, Transport and Power Generation. Graz, Austria, 2021 (cited in p. 12).

[55] D. Koch, A. Sousa, and D. Bertram. H2-engine operation with EGR achieving high power and high efficiency emission-free combustion. Tech. rep. 2019-01-2178. SAE Technical Paper, 2019 (cited in p. 13).

[56] J. Zareei, J. R. N. Alvarez, Y. L. Albuerne, M. R. Gámez, and Á. R. A. Linzan. "A Simulation Study of the Effect of HCNG Fuel and Injector Hole Number along with a Variation of Fuel Injection Pressure in a Gasoline Engine Converted from Port Injection to Direct Injection". Processes 10 (11), 2022 (cited in pp. 13, 52).

[57] A. Kakoee and A. Gharehghani. "Comparative study of hydrogen addition effects on the natural-gas/diesel and natural-gas/dimethyl-ether reactivity controlled compression ignition mode of operation". Energy Conversion and Management 196, 2019, pp. 92–104 (cited in pp. 13, 52).

[58] D. Karman. "Life-cycle analysis of GHG emissions for CNG and diesel buses in Beijing". 2006 IEEE EIC Climate Change Technology Conference, EICCCC 2006, 2006, pp. 0–5 (cited in pp. 13, 15, 53, 54).

[59] P. Tratzi, M. Torre, V. Paolini, L. Tomassetti, et al. "Liquefied biomethane for heavy-duty transport in Italy: A well-to-wheels approach". Transportation Research Part D: Transport and Environment 107 (April), 2022, p. 103288 (cited in pp. 13, 15, 53, 54).

[60] P. Atkins, G. Milton, A. Atkins, and R. Morgan. "A local ecosystem assessment of the potential for net negative heavy-duty truck greenhouse gas emissions through biomethane upcycling". Energies 14 (4), 2021 (cited in pp. 13, 15, 53, 54).

[61] M. Gustafsson and N. Svensson. "Cleaner heavy transports – Environmental and economic analysis of liquefied natural gas and biomethane". Journal of Cleaner Production 278, 2021, p. 123535 (cited in pp. 13, 15, 53, 54).

[62] M. Arfan, O. Eriksson, Z. Wang, and S. Soam. "Life cycle assessment and life cycle costing of hydrogen production from biowaste and biomass in Sweden". Energy Conversion and Management 291, 2023 (cited in pp. 13, 53).

[63] C. Kim, C. Park, Y. Kim, and Y. Choi. "Power characteristics with different types of turbochargers for lean boosted hydrogen direct injection engine in NOx-free operation". Heliyon 9 (3), 2023, e14186 (cited in pp. 13, 53).

[64] F. Zhang, E. Obeid, W. B. Nader, A. Zoughaib, and X. Luo. "Well-to-Wheel analysis of natural gas fuel for hybrid truck applications". Energy Conversion and Management 240, 2021 (cited in pp. 14, 53).

[65] M. Munagala, Y. Shastri, S. Nagarajan, and V. Ranade. "Production of Bio-CNG from sugarcane bagasse: Commercialization potential assessment in Indian context". Industrial Crops and Products 188, 2022 (cited in pp. 14, 53).

[66] R. Kotagodahetti, K. Hewage, F. Razi, and R. Sadiq. "Comparative life cycle environmental and cost assessments of renewable natural gas production pathways". Energy Conversion and Management 278, 2023 (cited in pp. 14, 53).

[67] M. M. Uddin, Z. Wen, and M. M. Wright. "Techno-economic and environmental impact assessment of using corn stover biochar for manure derived renewable natural gas production". Applied Energy 321, 2022 (cited in pp. 14, 53).

[68] P. Gupta, W. Zhuge, S. Luo, and F. Ma. "The well-to-wheel analysis of hydrogen enriched compressed natural gas for heavy-duty vehicles using life cycle approach to a fuel cycle". International Journal of Low-Carbon Technologies 14 (3), 2019, pp. 432–439 (cited in pp. 14, 15, 54, 55).

[69] P. Gupta, Y. Wu, X. He, W. Zhuge, and F. Ma. "Life cycle analysis of hcng light-duty vehicle demonstration project". Revista Materia 24 (2), 2019 (cited in pp. 14, 15, 54, 55).

[70] D. Candelaresi, A. Valente, D. Iribarren, J. Dufour, and G. Spazzafumo. "Comparative life cycle assessment of hydrogen-fuelled passenger cars". International Journal of Hydrogen Energy 46 (72), 2021, pp. 35961–35973 (cited in pp. 14, 15, 54, 55).

[71] D. Candelaresi, A. Valente, D. Iribarren, J. Dufour, and G. Spazzafumo. "Novel short-term national strategies to promote the use of renewable hydrogen in road transport: A life cycle assessment of passenger car fleets partially fuelled with hydrogen". Science of the Total Environment 859 (March 2022), 2023, p. 160325 (cited in pp. 14, 15, 54, 55).

[72] H. Ritchie and M. Roser. "CO and Greenhouse Gas Emissions". Our World in Data, 2020. https://ourworldindata.org/co2-and-other-greenhouse-gas-emissions (cited in p. 19).

[73] T. Burton, S. Powers, C. Burns, G. Conway, F. Leach, and K. Senecal. "A data-driven greenhouse gas emission rate analysis for vehicle comparisons". SAE International Journal of Electrified Vehicles 12 (1), 2023 (cited in p. 20).

[74] S. Kim and J. Kim. "Feasibility assessment of hydrogen-rich syngas spark-ignition engine for heavy-duty long-distance vehicle application". Energy Conversion and Management 252, 2022, p. 115048 (cited in p. 20).

[75] F. Li, Z. Wang, Y. Wang, and B. Wang. "High-Efficiency and Clean Combustion Natural Gas Engines for Vehicles". Automotive Innovation 2 (4), 2019, pp. 284–304 (cited in p. 20).

[76] U. Lee, J. Han, M. Urgun Demirtas, M. Wang, and L. Tao. "Lifecycle analysis of renewable natural gas and hydrocarbon fuels from wastewater treatment plants' sludge", 2016 (cited in p. 20).

[77] M. S. Jaro Jens David Gräf. "Market state and trends in renewable and low-carbon gases in Europe: A Gas for Climate report". European Biogas Association (December), 2021 (cited in p. 20).

[78] P. Muñoz, E. A. Franceschini, D. Levitan, C. R. Rodriguez, T. Humana, and G. Correa Perelmuter. "Comparative analysis of cost, emissions and fuel consumption of diesel, natural gas, electric and hydrogen urban buses". Energy Conversion and Management 257, 2022, p. 115412 (cited in p. 21).

[79] C. Ji, C. Hong, S. Wang, G. Xin, et al. "Evaluation of the variable valve timing strategy in a direct-injection hydrogen engine with the Miller cycle under lean conditions". Fuel 343 (October 2022), 2023, p. 127932 (cited in pp. 21, 89, 146).

[80] Fuel Cells and Hydrogen Joint Undertaking (FCH). Hydrogen Roadmap Europe. 2019, p. 70 (cited in pp. 21, 114).

[81] D. Serrano, O. Laget, D. Soleri, S. Richard, et al. "Effects of methane/hydrogen blends on engine operation: Experimental and numerical investigation of different combustion modes". SAE Technical Papers 3 (2), 2010, pp. 223–243 (cited in p. 21).

[82] H. Duan, X. Yin, H. Kou, J. Wang, K. Zeng, and F. Ma. "Regression prediction of hydrogen enriched compressed natural gas (HCNG) engine performance based on improved particle swarm optimization back propagation neural network method (IMPSO-BPNN)". Fuel 331 (P2), 2023, p. 125872 (cited in p. 21).

[83] Y. L. Du, Z. Y. Sun, Q. Huang, and Y. C. Sun. "Observation study on the flame morphology of outwardly propagating turbulent HCNG-30 premixed flames". International Journal of Hydrogen Energy 48 (19), 2023, pp. 7096–7114 (cited in pp. 21, 146).

[84] G. M. Kosmadakis, D. C. Rakopoulos, and C. D. Rakopoulos. "Assessing the cyclic-variability of spark-ignition engine running on methane-hydrogen blends with high hydrogen contents of up to 50". International Journal of Hydrogen Energy 46 (34), 2021, pp. 17955–17968 (cited in pp. 21, 146).

[85] R. K. Mehra, H. Duan, R. Juknelevičius, F. Ma, and J. Li. "Progress in hydrogen enriched compressed natural gas (HCNG) internal combustion engines - A comprehensive review". Renewable and Sustainable Energy Reviews 80 (June), 2017, pp. 1458–1498 (cited in pp. 21, 146).

[86] V. Pandey, I. A. Badruddin, and T. M. Khan. "Effect of H2 blends with compressed natural gas on emissions of SI engine having modified ignition timings". Fuel 321 (March), 2022, p. 123930 (cited in p. 21).

[87] S. Oh, C. Kim, Y. Lee, H. Park, et al. "Analysis of the exhaust hydrogen characteristics of high-compression ratio, ultra-lean, hydrogen spark-ignition engine using advanced regression algorithms". Applied Thermal Engineering 215, 2022, p. 119036 (cited in p. 22).

[88] P. Gupta, D. Tong, J. Wang, W. Zhuge, et al. "Well-to-wheels total energy and GHG emissions of HCNG heavy-duty vehicles in China: Case of EEV qualified EURO 5 emissions scenario". International Journal of Hydrogen Energy 45 (15), 2020, pp. 8002–8014 (cited in p. 22).

[89] S. Sagar and A. K. Agarwal. "Knocking behavior and emission characteristics of a port fuel injected hydrogen enriched compressed natural gas fueled spark ignition engine". Applied Thermal Engineering 141, 2018, pp. 42–50 (cited in p. 22).

[90] A. Rao, Y. Liu, and F. Ma. "Study of NOx emission for hydrogen enriched compressed natural along with exhaust gas recirculation in spark ignition engine by Zeldovich' mechanism, support vector machine and regression correlation". Fuel 318 (January), 2022, p. 123577 (cited in p. 22).

[91] A. Rao, H. Gao, and F. Ma. "Study of laminar burning speed and calibration coefficients of quasi-dimensional combustion model for hydrogen enriched compressed natural gas fueled internal combustion engine along with exhaust gas recirculation". Fuel 283 (x), 2021, p. 119284 (cited in p. 22).

[92] R. K. Prasad and A. K. Agarwal. "Experimental evaluation of laser ignited hydrogen enriched compressed natural gas fueled supercharged engine". Fuel 289 (October 2020), 2021, p. 119788 (cited in p. 22).

[93] A. A. Yontar and V. Wong. "Influence of laser ignition on characteristics of an engine for hydrogen enriched CNG and iso-octane usage". International Journal of Hydrogen Energy 46 (74), 2021, pp. 37071–37082 (cited in p. 22).

[94] F. Payri, P. Olmeda, J. Martin, and R. Carreño. "A New Tool to Perform Global Energy Balances in DI Diesel Engines". SAE International Journal of Engines 7 (1), 2014, pp. 43–59 (cited in pp. 25, 58, 93).

[95] J. Benajes, P. Olmeda, J. Martín, and R. Carreño. "A new methodology for uncertainties characterization in combustion diagnosis and thermodynamic modelling". Applied Thermal Engineering 71 (1), 2014, pp. 389–399 (cited in pp. 25, 60, 93).

[96] D. Pashchenko. "Thermochemical waste-heat recuperation as on-board hydrogen production technology". International Journal of Hydrogen Energy 46 (57), 2021, pp. 28961–28968 (cited in p. 29).

[97] V. Stefaan, S. Roger, and S. Verhelst. “Technical paper for students and young engineers -”. FISITA World Automotive Congress, Barcelona, 2004, pp. 1–9 (cited in p. 34).

[98] T. Shudo and S. Nabetani. “Analysis of degree of constant volume and cooling loss in a hydrogen fuelled SI engine”. SAE Technical Papers 2 (1), 2001 (cited in pp. 38, 68).

[99] J. Nieminen, N. D’Souza, and I. Dincer. “Comparative combustion characteristics of gasoline and hydrogen fuelled ICEs”. International Journal of Hydrogen Energy 35 (10), 2010, pp. 5114–5123 (cited in p. 38).

[100] J. Nieminen and I. Dincer. “Comparative exergy analyses of gasoline and hydrogen fuelled ICEs”. International Journal of Hydrogen Energy 35 (10), 2010, pp. 5124–5132 (cited in pp. 39, 68).

[101] J. Demuynck, M. De Paepe, I. Verhaert, and S. Verhelst. “Heat loss comparison between hydrogen, methane, gasoline and methanol in a spark-ignition internal combustion engine”. Energy Procedia 29, 2012, pp. 138–146 (cited in pp. 39, 68).

[102] F. Ma and Y. Wang. “Study on the extension of lean operation limit through hydrogen enrichment in a natural gas spark-ignition engine”. International Journal of Hydrogen Energy 33 (4), 2008, pp. 1416–1424 (cited in p. 39).

[103] H. Li, G. A. Karim, and A. Sohrabi. “Examination of the oil combustion in a SI hydrogen engine”. SAE Technical Paper, 2004 (cited in pp. 42, 44, 69).

[104] D. P. van Vuuren, K. I. van der Wijst, S. Marsman, M. van den Berg, A. F. Hof, and C. D. Jones. “The costs of achieving climate targets and the sources of uncertainty”. Nature Climate Change 10 (4), 2020, pp. 329–334 (cited in p. 51).

[105] J. Serrano, J. Martin, J. Gomez-Soriano, and R. Raggi. “Theoretical and experimental evaluation of the spark-ignition premixed oxy-fuel combustion concept for future CO2 captive powerplants”. Energy Conversion and Management 244, 2021, p. 114498 (cited in p. 52).

[106] G. Puig-Samper Naranjo, D. Bolonio, M. F. Ortega, and M. J. Garcia-Martinez. “Comparative life cycle assessment of conventional, electric and hybrid passenger vehicles in Spain”. Journal of Cleaner Production 291, 2021, p. 125883 (cited in p. 52).

[107] L. Oliveira, M. Messagie, S. Rangaraju, J. Sanfelix, M. Hernandez Rivas, and J. Van Mierlo. “Key issues of lithium-ion batteries – from resource depletion to environmental performance indicators”. Journal of Cleaner Production 108, 2015, pp. 354–362 (cited in p. 52).

[108] M. Nasser and H. Hassan. “Techno-enviro-economic analysis of hydrogen production via low and high temperature electrolyzers powered by PV/Wind turbines/Waste heat”. Energy Conversion and Management 278 (November 2022), 2023, p. 116693 (cited in p. 52).

[109] H. Nami, O. B. Rizvandi, C. Chatzichristodoulou, P. V. Hendriksen, and H. L. Frandsen. "Techno-economic analysis of current and emerging electrolysis technologies for green hydrogen production". Energy Conversion and Management 269 (July), 2022, p. 116162 (cited in p. 52).

[110] R. Novella, J. Pastor, J. Gomez-Soriano, and J. Sánchez-Bayona. "Numerical study on the use of ammonia/hydrogen fuel blends for automotive spark-ignition engines". Fuel 351, 2023, p. 128945 (cited in pp. 52, 87).

[111] R. J. Saunders and R. Moreno. "Natural gas as a transportation fuel". Natural Gas: Its Role and Potential in Economic Development 115 (February 2017), 2019, pp. 251–271 (cited in p. 56).

[112] Fuel Cells and Hydrogen 2 Joint Undertaking. "Hydrogen Roadmap Europe - A sustainable pathway for the European energy transition", 2019 (cited in pp. 61–63).

[113] International Energy Agency (IEA). "Outlook for biogas and biomethane, Prospects for organic growth - World Energy Outlook Special Report", 2020 (cited in pp. 61, 62).

[114] European Commission. Directorate-General for Energy. and European Commission. Climate Action DG. and European Commission. Directorate General for Mobility and Transport. "EU reference scenario 2016 - Energy, transport and GHG emissions: trends to 2050", 2016 (cited in p. 66).

[115] Z. Savva, K. C. Petallidou, C. M. Damaskinos, G. G. Olympiou, V. N. Stathopoulos, and A. M. Efstathiou. "H2-SCR of NOx on low-SSA CeO2-supported Pd: The effect of Pd particle size". Applied Catalysis A: General 615 (x), 2021 (cited in p. 68).

[116] M. Borchers, K. Keller, P. Lott, and O. Deutschmann. "Selective catalytic reduction of NOxwith H2for cleaning exhausts of hydrogen engines: Impact of H2O, O2, and NO/H2Ratio". Industrial and Engineering Chemistry Research 60 (18), 2021, pp. 6613–6626 (cited in p. 68).

[117] NGVA Europe. "Vehicle Catalogue", 2019 (cited in p. 70).

[118] Baigong Industrial. CNG Cylinder For Sale, Natural Gas CNG Cylinder. 2023 (cited in p. 71).

[119] Department of Energy. DOE Technical Targets for Onboard Hydrogen Storage for Light-Duty Vehicles. 2020 (cited in p. 71).

[120] B. Zhang, Y. Chen, Y. Jiang, W. Lu, and W. Liu. "Effect of compression ratio and Miller cycle on performance of methanol engine under medium and low loads". Fuel 351, 2023, p. 128985 (cited in p. 87).

[121] R. Novella, J. Gomez-Soriano, P. J. Martínez-Hernándiz, C. Libert, and F. Rampanarivo. "Improving the performance of the passive pre-chamber ignition concept for spark-ignition engines fueled with natural gas". Fuel 290, 2021, p. 119971 (cited in pp. 87, 114, 116, 120, 132).

[122] J. M. Garcia-Oliver, Y. Niki, R. Rajasegar, R. Novella, et al. “An experimental and one-dimensional modeling analysis of turbulent gas ejection in pre-chamber engines”. Fuel 299, 2021, p. 120861 (cited in p. 87).

[123] A. M. Al-Orabi, M. G. Osman, and B. E. Sedhom. “Analysis of the economic and technological viability of producing green hydrogen with renewable energy sources in a variety of climates to reduce CO2 emissions: A case study in Egypt”. Applied Energy 338 (March), 2023, p. 120958 (cited in p. 88).

[124] L. Zhang, C. Jia, F. Bai, W. Wang, et al. “A comprehensive review of the promising clean energy carrier: Hydrogen production, transportation, storage, and utilization (HPTSU) technologies”. Fuel 355 (April 2023), 2024, p. 129455 (cited in p. 88).

[125] J. Benajes, R. Novella, J. Gomez-Soriano, I. Barbery, and C. Libert. “Advantages of hydrogen addition in a passive pre-chamber ignited SI engine for passenger car applications”. International Journal of Energy Research 45 (9), 2021, pp. 13219–13237 (cited in pp. 88, 119, 126).

[126] L. Qian, J. Wan, Y. Qian, Y. Sun, and Y. Zhuang. “Experimental investigation of water injection and spark timing effects on combustion and emissions of a hybrid hydrogen-gasoline engine”. Fuel 322 (April), 2022, p. 124051 (cited in p. 88).

[127] W. Liu, Y. Qi, R. Zhang, Q. Zhang, and Z. Wang. “Hydrogen production from ammonia-rich combustion for fuel reforming under high temperature and high pressure conditions”. Fuel 327, 2022, p. 124830 (cited in p. 88).

[128] H. Zhang, G. Li, Y. Long, Z. Zhang, et al. “Numerical study on combustion and emission characteristics of a spark-ignition ammonia engine added with hydrogen-rich gas from exhaust-fuel reforming”. Fuel 332, 2023, p. 125939 (cited in p. 88).

[129] Y. Kim, J. T. Lee, and G. H. Choi. “An investigation on the causes of cycle variation in direct injection hydrogen fueled engines”. International Journal of Hydrogen Energy 30 (1), 2005, pp. 69–76 (cited in pp. 88, 146).

[130] C. White, R. Steeper, and A. Lutz. “The hydrogen-fueled internal combustion engine: a technical review”. International journal of hydrogen energy 31 (10), 2006, pp. 1292–1305 (cited in pp. 88, 98).

[131] C. H. Byun, J. T. Lee, and O. C. Kwon. “An experimental study on the self-ignition and knocking characteristics for hydrogen-fueled homogeneous compression charge ignition engines”. Fuel 351 (March), 2023, p. 128970 (cited in p. 88).

[132] S. Szwaja and J. D. Naber. “Dual nature of hydrogen combustion knock”. International Journal of Hydrogen Energy 38 (28), 2013, pp. 12489–12496 (cited in p. 88).

[133] R. Novella, A. García, J. Gomez-Soriano, and Á. Fogué-Robles. "Exploring dilution potential for full load operation of medium duty hydrogen engine for the transport sector". Applied Energy 349, 2023, p. 121635 (cited in p. 88).

[134] S. Verhelst, P. Maesschalck, N. Rombaut, and R. Sierens. "Increasing the power output of hydrogen internal combustion engines by means of supercharging and exhaust gas recirculation". International Journal of Hydrogen Energy 34 (10), 2009, pp. 4406–4412 (cited in p. 89).

[135] A. Thawko, S. A. Persy, A. Eyal, and L. Tartakovsky. "Effects of Fuel Injection Method on Energy Efficiency and Combustion Characteristics of SI Engine Fed with a Hydrogen-Rich Reformate". SAE Technical Papers (2020), 2020, pp. 1–12 (cited in p. 89).

[136] J. Gao, X. Wang, G. Tian, P. Song, C. Ma, and L. Huang. "Effect of hydrogen direct injection strategies and ignition timing on hydrogen diffusion, energy distributions and NOx emissions from an opposed rotary piston engine". Fuel 306 (May), 2021 (cited in p. 89).

[137] F. yu Lai, B. gang Sun, X. Wang, D. sheng Zhang, Q. he Luo, and L. zhi Bao. "Research on the inducing factors and characteristics of knock combustion in a DI hydrogen internal combustion engine in the process of improving performance and thermal efficiency". International Journal of Hydrogen Energy 48 (20), 2023, pp. 7488–7498 (cited in p. 89).

[138] S. Kaiser and C. M. White. "PIV and PLIF to evaluate mixture formation in a direct-injection hydrogen-fuelled engine". SAE International Journal of Engines 1 (1), 2009, pp. 657–668 (cited in p. 89).

[139] V. M. Salazar and S. A. Kaiser. "An optical study of mixture preparation in a hydrogen-fueled engine with direct injection using different nozzle designs". SAE International Journal of Engines 2 (2), 2010, pp. 119–131 (cited in p. 89).

[140] H. Eichlseder, T. Wallner, R. Freymann, and J. Ringler. The potential of hydrogen internal combustion engines in a future mobility scenario. Tech. rep. SAE Technical Paper, 2003 (cited in p. 89).

[141] Y. Kim, J. T. Lee, and J. A. Caton. "The development of a dual-Injection hydrogen-fueled engine with high power and high efficiency". J. Eng. Gas Turbines Power 128 (1), 2006, pp. 203–212 (cited in p. 89).

[142] Y. Kim, C. Park, J. Oh, S. Oh, Y. Choi, and J. Lee. "Effect of Excessive Air Ratio on Hydrogen-Fueled Spark Ignition Engine with High Compression Ratio Using Direct Injection System Toward Higher Brake Power and Thermal Efficiency". Available at SSRN 4012806, 2023 (cited in p. 89).

[143] G. Maio, A. Boberic, L. Giarracca, D. Aubagnac-Karkar, et al. "Experimental and numerical investigation of a direct injection spark ignition hydrogen engine for heavy-duty applications". International Journal of Hydrogen Energy 47 (67), 2022, pp. 29069–29084 (cited in pp. 89, 95, 146).

[144] T. Shudo, W. Cheng, T. Kuninaga, and T. Hasegawa. “Reduction of cooling loss in hydrogen combustion by direct injection stratified charge”. SAE transactions, 2003, pp. 2118–2123 (cited in p. 89).

[145] A. Y. Deshmukh, C. Giefer, D. Goeb, M. Khosravi, D. van Bebber, and H. Pitsch. “A quasi-one-dimensional model for an outwardly opening poppet-type direct gas injector for internal combustion engines”. International Journal of Engine Research 21 (8), 2020, pp. 1493–1519 (cited in p. 90).

[146] A. Deshmukh, G. Vishwanathan, M. Bode, H. Pitsch, M. Khosravi, and D. van Bebber. “Characterization of hollow cone gas jets in the context of direct gas injection in internal combustion engines”. SAE International Journal of Fuels and Lubricants 11 (4), 2018, pp. 353–378 (cited in p. 90).

[147] M. Lazzaro, F. Catapano, and P. Sementa. “Experimental characterization of methane direct injection from an outward-opening poppet-valve injector”. SAE Technical Paper, 2019 (cited in p. 90).

[148] McKinsey. “Hydrogen Insights”. (February), 2021 (cited in p. 114).

[149] D. G. Caglayan, H. U. Heinrichs, M. Robinius, and D. Stolten. “Robust design of a future 100% renewable european energy supply system with hydrogen infrastructure”. International Journal of Hydrogen Energy (xxxx), 2021 (cited in p. 114).

[150] G. J. Germane, C. G. Wood, and C. C. Hess. Lean combustion in spark-ignited internal combustion engines-a review. Tech. rep. SAE Technical Paper, 1983 (cited in p. 114).

[151] J. Dale, M. Checkel, and P. Smy. “Application of high energy ignition systems to engines”. Progress in Energy and Combustion Science 23 (5), 1997, pp. 379–398 (cited in p. 114).

[152] J. López, R. Novella, J. Gomez-Soriano, P. Martinez-Hernandiz, et al. “Advantages of the unscavenged pre-chamber ignition system in turbocharged natural gas engines for automotive applications”. Energy 218, 2021, p. 119466 (cited in pp. 114, 116, 120).

[153] J. Benajes, R. Novella, J. Gomez-Soriano, P. Martinez-Hernandiz, C. Libert, and M. Dabiri. “Evaluation of the passive pre-chamber ignition concept for future high compression ratio turbocharged spark-ignition engines”. Applied Energy 248, 2019, pp. 576–588 (cited in pp. 114, 116, 120).

[154] C. P. Borges, J. C. Sobczak, T. R. Silberg, M. Uriona-Maldonado, and C. R. Vaz. “A systems modeling approach to estimate biogas potential from biomass sources in Brazil”. Renewable and Sustainable Energy Reviews 138, 2021, p. 110518 (cited in p. 115).

[155] C. K. Law and O. C. Kwon. “Effects of hydrocarbon substitution on atmospheric hydrogen-air flame propagation”. International Journal of Hydrogen Energy 29 (8), 2004, pp. 867–879 (cited in p. 115).

[156] Y. Li, M. Bi, B. Li, Y. Zhou, and W. Gao. "Effects of hydrogen and initial pressure on flame characteristics and explosion pressure of methane/hydrogen fuels". Fuel 233 (December 2017), 2018, pp. 269–282 (cited in p. 115).

[157] E. Salzano, F. Cammarota, A. Di Benedetto, and V. Di Sarli. "Explosion behavior of hydrogen-methane/air mixtures". Journal of Loss Prevention in the Process Industries 25 (3), 2012, pp. 443–447 (cited in p. 115).

[158] V. Di Sarli, A. Di Benedetto, E. J. Long, and G. K. Hargrave. "Time-Resolved Particle Image Velocimetry of dynamic interactions between hydrogen-enriched methane/air premixed flames and toroidal vortex structures". International Journal of Hydrogen Energy 37 (21), 2012, pp. 16201–16213 (cited in p. 115).

[159] M. Sjeric, D. Kozarac, and M. Bogensperger. "Implementation of a single zone k-ϵ turbulence model in a multi zone combustion model". SAE Technical Papers, 2012 (cited in p. 115).

[160] C. Borgnakke, V. S. Arpaci, and R. J. Tabaczynski. "A model for the instantaneous heat transfer and turbulence in a spark ignition engine". SAE Technical Papers, 1980 (cited in p. 115).

[161] R. D. Matthews and Y. W. Chin. "A fractal-based SI engine model: Comparisons of predictions with experimental data". SAE Technical Papers, 1991 (cited in p. 115).

[162] S. G. Poulos and J. B. Heywood. "The effect of chamber geometry on spark-ignition engine combustion". SAE Technical Papers, 1983 (cited in p. 115).

[163] F. Bozza, A. Gimelli, A. Senatore, and A. Caraceni. "A theoretical comparison of various VVA systems for performance and emission improvements of SI-engines". SAE Technical Papers 2001 (724), 2001 (cited in p. 115).

[164] A. J. Torregrosa, A. Broatch, P. Olmeda, and S. Aceros. "Numerical Estimation of Wiebe Function Parameters Using Artificial Neural Networks in SI Engine". SAE Technical Papers (2021), 2021, pp. 1–10 (cited in p. 115).

[165] V. Giglio and A. di Gaeta. "Novel regression models for wiebe parameters aimed at 0D combustion simulation in spark ignition engines". Energy 210, 2020, p. 118442 (cited in p. 115).

[166] F. Lindström, H. E. Ångström, G. Kalghatgi, and C. E. Möller. "An empirical SI combustion model using laminar burning velocity correlations". SAE Technical Papers, 2005 (cited in p. 115).

[167] J. Liu and C. E. Dumitrescu. "Single and double Wiebe function combustion model for a heavy-duty diesel engine retrofitted to natural-gas spark-ignition". Applied Energy 248 (March), 2019, pp. 95–103 (cited in p. 115).

[168] V. De Bellis, E. Severi, S. Fontanesi, and F. Bozza. "Hierarchical 1D/3D Approach for the Development of a Turbulent Combustion Model Applied to a VVA Turbocharged Engine. Part II: Combustion Model". Energy Procedia 45, 2014. ATI 2013 - 68th Conference of the Italian Thermal Machines Engineering Association, pp. 1027–1036 (cited in p. 115).

[169] T. Daniela. "A quasi-dimensional SI combustion model: A bi-fractal approach". Energy Procedia 126, 2017, pp. 931–938 (cited in p. 115).

[170] D. Guijo-Rubio, A. Durán-Rosal, P. Gutiérrez, A. Gómez-Orellana, et al. "Evolutionary artificial neural networks for accurate solar radiation prediction". Energy 210, 2020, p. 118374 (cited in p. 116).

[171] K. M. Reese. "Deep learning artificial neural networks for non-destructive archaeological site dating". Journal of Archaeological Science 132, 2021, p. 105413 (cited in p. 116).

[172] J. M. Flores-Fernández, E. J. Herrera-López, F. Sánchez-Llamas, A. Rojas-Calvillo, et al. "Development of an optimized multi-biomarker panel for the detection of lung cancer based on principal component analysis and artificial neural network modeling". Expert Systems with Applications 39 (12), 2012, pp. 10851–10856 (cited in p. 116).

[173] M. Lapuerta, O. Armas, and J. Hernández. "Diagnosis of DI Diesel combustion from in-cylinder pressure signal by estimation of mean thermodynamic properties of the gas". Applied Thermal Engineering 19 (5), 1999, pp. 513–529 (cited in p. 117).

[174] F. Payri, S. Molina, J. Martín, and O. Armas. "Influence of measurement errors and estimated parameters on combustion diagnosis". Applied Thermal Engineering 26 (2), 2006, pp. 226–236 (cited in p. 117).

[175] J. Benajes, R. Novella, J. Gomez-Soriano, I. Barbery, et al. "Computational assessment towards understanding the energy conversion and combustion process of lean mixtures in passive pre-chamber ignited engines". Applied Thermal Engineering 178, 2020, p. 115501 (cited in pp. 119, 126).

[176] S. Wahiduzzaman, T. Morel, and S. Sheard. "Comparison of measured and predicted combustion characteristics of a four-valve SI engine". SAE Transactions, 1993, pp. 810–819 (cited in p. 120).

[177] M. Mirzaeian, F. Millo, and L. Rolando. "Assessment of the predictive capabilities of a combustion model for a modern downsized turbocharged si engine". SAE Technical Paper, 2016 (cited in p. 120).

[178] Z. Huang, Y. Zhang, K. Zeng, B. Liu, Q. Wang, and D. Jiang. "Measurements of laminar burning velocities for natural gas-hydrogen-air mixtures". Combustion and Flame 146 (1-2), 2006, pp. 302–311 (cited in pp. 121, 122).

[179] Ö. L. Gülder. Correlations of laminar combustion data for alternative SI engine fuels. Tech. rep. SAE Technical Paper, 1984 (cited in p. 121).

[180] V. Di Sarli and A. Di Benedetto. "Laminar burning velocity of hydrogen-methane/air premixed flames". International Journal of Hydrogen Energy 32 (5), 2007, pp. 637–646 (cited in p. 121).

[181] F. Ma, S. Ding, Y. Wang, Y. Wang, J. Wang, and S. Zhao. "Study on combustion behaviors and cycle-by-cycle variations in a turbocharged lean burn natural gas S.I. engine with hydrogen enrichment". International Journal of Hydrogen Energy 33 (23), 2008, pp. 7245–7255 (cited in pp. 121, 133, 146).

[182] F. Perini, F. Paltrinieri, and E. Mattarelli. "A quasi-dimensional combustion model for performance and emissions of SI engines running on hydrogen-methane blends". International Journal of Hydrogen Energy 35 (10), 2010, pp. 4687–4701 (cited in p. 121).

[183] C. Ji, D. Wang, J. Yang, and S. Wang. "A comprehensive study of light hydrocarbon mechanisms performance in predicting methane/hydrogen/air laminar burning velocities". International Journal of Hydrogen Energy 42 (27), 2017, pp. 17260–17274 (cited in pp. 122, 146).

[184] G. P. Smith, D. M. Golden, M. Frenklach, N. W. Moriarty, et al. "Current and future releases of GRI-Mech". GRI-MechTM. Serauskas, Bob. Version GRI 3 (cited in p. 122).

[185] C. Dong, Q. Zhou, X. Zhang, Q. Zhao, T. Xu, and S. Hui. "Experimental study on the laminar flame speed of hydrogen/natural gas/air mixtures". Frontiers of Chemical Engineering in China 4 (4), 2010, pp. 417–422 (cited in p. 122).

[186] S. Ravi and E. L. Petersen. "Laminar flame speed correlations for pure-hydrogen and high-hydrogen content syngas blends with various diluents". International Journal of Hydrogen Energy 37 (24), 2012, pp. 19177–19189 (cited in p. 122).

[187] F. Bozza, A. Gimelli, L. Strazzullo, E. Torella, and C. Cascone. "Steady-state and transient operation simulation of a "downsized" turbocharged SI engine". SAE Technical Paper, 2007 (cited in p. 126).

[188] A. Broatch, R. Novella, J. García-Tíscar, J. Gomez-Soriano, and P. Pal. "Analysis of combustion acoustic phenomena in compression–ignition engines using large eddy simulation". Physics of Fluids 32 (8), 2020, p. 085101 (cited in p. 131).

[189] A. Broatch, R. Novella, J. García-Tíscar, J. Gomez-Soriano, and P. Pal. "Investigation of the effects of turbulence modeling on the prediction of compression-ignition combustion unsteadiness". International Journal of Engine Research, 2021, p. 1468087421990478 (cited in p. 131).

[190] J. Benajes, R. Novella, J. Gomez-Soriano, P. Martinez-Hernandiz, C. Libert, and M. Dabiri. "Performance of the passive pre-chamber ignition concept in a spark-ignition engine for passenger car applications", 2019 (cited in p. 132).

[191] "Experimental study on thermal efficiency and emission characteristics of a lean burn hydrogen enriched natural gas engine". International Journal of Hydrogen Energy 32 (18), 2007, pp. 5067–5075 (cited in pp. 133, 146).

[192] B. Nagalingam, F. Duebel, and K. Schmillen. "Performance study using natural gas, hydrogen-supplemented natural gas and hydrogen in AVL research engine". International Journal of Hydrogen Energy 8 (9), 1983, pp. 715–720 (cited in pp. 135, 146).

[193] G. Lim, S. Lee, C. Park, Y. Choi, and C. Kim. "Knock and emission characteristics of heavy-duty HCNG engine with modified compression ratios". SAE Technical Papers 2, 2013 (cited in p. 135).

[194] S. Singh, S. Mishra, R. Mathai, A. K. Sehgal, and R. Suresh. "Comparative Study of Unregulated Emissions on a Heavy Duty CNG Engine using CNG 'I&' Hydrogen Blended CNG as Fuels". SAE International Journal of Engines 9 (4), 2016, pp. 2292–2300 (cited in p. 139).